Late Pleistocene glacier dynamics of southwestern Montana and adjacent Idaho and paleoclimatic implications
by Donald R Murray

A thesis submitted in partial fulfillment of the requirements for the degree of Master of Science in Earth Sciences
Montana State University
© Copyright by Donald R Murray (1989)

Abstract:
Application of glacial flow theory to reliable reconstructions of paleoglaciers allows calculation of the dynamics of these glaciers. Effective basal shear stresses calculated along the longitudinal profiles of these glaciers can be used to estimate the component of mass flux due to internal deformation. Assuming basal slip to be zero at the point where deformation mass flux is a maximum, minimum net accumulation and ablation gradients can be calculated. Using the continuity equation, minimum mass flux at the ELA can be estimated. Also, net winter accumulation can be calculated by dividing the mass flux at the ELA by the accumulation area. Because local climate, in part, controls the mass balance and dynamics of a glacier, this model provides information on the climatic setting of paleoglaciers.

The model also allows estimation of basal slip as a factor in point estimates of glacial flow. Application of the continuity equation above and below the ELA generates additional estimates of mass flux at discrete points along each glacier. The difference between calculated deformation mass flux and continuity flux at these points yields a first approximation of basal slip, which can be highly variable along the length of a glacier.

The . model was developed on the late Pleistocene Big Timber glacier of west-central Montana and tested on five other paleoglaciers in the Northern Rocky Mountains of southwestern Montana and adjacent Idaho. Sensitivity analysis performed on Big Timber glacier shows that the results are accurate within 20%. Low ablation gradients, ranging from 1.9 to 5.4 mm/m for five of the six glaciers, suggest a cold, dry environment in this region during the late Pleistocene. Calculated average annual net accumulation for these glaciers is 20-75% below modern maximum snowpack values, indicating a drier climate during the full glacial period. Basal sliding accounts for most (> 90%) of the glacial flow near the terminus of each glacier, but is variable along the rest of the glacier. While the mass balance values are minima, they are assumed to be reasonable approximations of the actual values, unless very high basal slip rates occurred along the entire length of each glacier.

LATE PLEISTOCENE GLACIER DYNAMICS OF SOUTHWESTERN MONTANA AND ADJACENT IDAHO AND PALEOCLIMATIC IMPLICATIONS

by

Donald R. Murray

A thesis submitted in partial fulfillment
of the requirements for the degree

of

Master of Science

in

Earth Sciences

MONTANA STATE UNIVERSITY
Bozeman, Montana

December 1989

N378
M9618

APPROVAL

of a thesis submitted by

Donald Richard Murray

This thesis has been read by each member of the thesis committee and has been found to be satisfactory regarding content, English usage, format, citations, bibliographic style, and consistency, and is ready for submission to the College of Graduate Studies.

December 20, 1989
Date

William W. Locke III
Chairperson, Graduate Committee

Approved for the Major Department

December 20 1989
Date

Stephen C. Cook
Head, Major Department

Approved for the College of Graduate Studies

January 8, 1990
Date

Henry L. Parsons
Graduate Dean

STATEMENT OF PERMISSION TO USE

In presenting this thesis in partial fulfillment of the requirements for a master's degree at Montana State University, I agree that the Library shall make it available to borrowers under rules of the Library. Brief quotations from this thesis are allowable without special permission, provided that accurate acknowledgement of source is made.

Permission for extensive quotation from or reproduction of this thesis may be granted by my major professor, or in his absence, by the Dean of Libraries when, in the opinion of either, the proposed use of the material is for scholarly purposes. Any copying or use of the material in this thesis for financial gain shall not be allowed without my written permission.

Signature Donald R Mercy

Date December 19, 1989

ACKNOWLEDGEMENTS

The author wishes to thank the members of his committee, Dr. William W. Locke (Committee Chairman), Dr. Katherine Hansen-Bristow, and Dr. Joseph Ashley, for providing support, guidance and helpful criticism throughout the project. Dr. Locke first suggested the topic and was extremely helpful in nurturing the project as it developed. Thanks are also due to Dr. James McCalpin of Utah State University for use of his unpublished work on glacier dynamics of the Sangre de Cristo Range and for discussion of the methods used in this project. I also wish to thank the Department of Earth Sciences for accepting me into the graduate program and for providing a productive and amiable atmosphere in which to work; my parents, William and Barbara Murray, for encouraging me to do whatever makes me happy; my wife, Diana Shellenberger, for field assistance, copyediting and moral support; and finally Bud Ebbett of Lyndon State College for providing the initial spark of my interest in glaciers and geology. This project was partially funded by GSA Research Grant 4051-88 and the D.L. Smith Scholarship through the Department of Earth Sciences.

TABLE OF CONTENTS

TABLE OF CONTENTS -- continued

TABLE OF CONTENTS -- continued

LIST OF TABLES

LIST OF TABLES -- continued

LIST OF FIGURES

LIST OF FIGURES -- continued

LIST OF FIGURES -- continued

ABSTRACT

Application of glacial flow theory to reliable reconstructions of paleoglaciers allows calculation of the dynamics of these glaciers. Effective basal shear stresses calculated along the longitudinal profiles of these glaciers can be used to estimate the component of mass flux due to internal deformation. Assuming basal slip to be zero at the point where deformation mass flux is a maximum, minimum net accumulation and ablation gradients can be calculated. Using the continuity equation, minimum mass flux at the ELA can be estimated. Also, net winter accumulation can be calculated by dividing the mass flux at the ELA by the accumulation area. Because local climate, in part, controls the mass balance and dynamics of a glacier, this model provides information on the climatic setting of paleoglaciers.

The model also allows estimation of basal slip as a factor in point estimates of glacial flow. Application of the continuity equation above and below the ELA generates additional estimates of mass flux at discrete points along each glacier. The difference between calculated deformation mass flux and continuity flux at these points yields a first approximation of basal slip, which can be highly variable along the length of a glacier.

The model was developed on the late Pleistocene Big Timber glacier of west-central Montana and tested on five other paleoglaciers in the Northern Rocky Mountains of southwestern Montana and adjacent Idaho. Sensitivity analysis performed on Big Timber glacier shows that the results are accurate within 20%. Low ablation gradients, ranging from 1.9 to 5.4 mm/m for five of the six glaciers, suggest a cold, dry environment in this region during the late Pleistocene. Calculated average annual net accumulation for these glaciers is 20-75% below modern maximum snowpack values, indicating a drier climate during the full glacial period. Basal sliding accounts for most (> 90%) of the glacial flow near the terminus of each glacier, but is variable along the rest of the glacier. While the mass balance values are minima, they are assumed to be reasonable approximations of the actual values, unless very high basal slip rates occurred along the entire length of each glacier.

INTRODUCTION

The Problem

There is an intimate relationship between climate and glaciation (Fig. 1), such that the dynamics (thickness, rate of flow and length) of a glacier are controlled to a large extent by changes in climate (Meier, 1965; Andrews, 1975). Climatic changes during the late Pleistocene (79,000 to 10,000 years ago) have been characterized by several global glacial advances and retreats. Evidence that late Pleistocene glaciers existed in some valleys of the Northern Rocky Mountains, which do not have glaciers at present, suggests that the paleoclimate must have been different from the present. The existence of glaciers does not, however, provide an actual measure of temperature or precipitation, but certain features of glaciers may be used as proxies to these climatic variables. Because the dynamics of a glacier are controlled in part by climate, reconstructed dynamics of paleoglaciers can be used as proxies to climate. In this study, a model is developed to interpret the ice dynamics of paleoglaciers. Although this project concentrates on the development of the model, the application of this model to six paleoglaciers that existed in southwestern Montana and adjacent Idaho during the last glacial maximum (20,000 years ago) suggests the magnitude and direction of late Quaternary changes in precipitation.

Changes in climate affect the mass balance of a glacier, which is a measure of the balance between mass gain (accumulation) and mass loss (ablation) on a glacier. On alpine glaciers, accumulation occurs mainly as snowfall while ablation takes place mainly through melt (Sugden and John, 1976). Changes in mass balance cause a dynamic response in the glacier. An increase in thickness generally causes an increase in the velocity and mass flux, which cause the glacier to advance (Nye, 1960; Meier, 1965). Thus, mass flux is an indicator of the mass balance of the glacier. For an ideal steady state glacier (one that is neither advancing or retreating), net accumulation is equal to net ablation (gain = loss). The calculated mass balance (i.e. net accumulation) of a steady state paleoglacier could be used as a crude proxy indicator of the paleoprecipitation on that glacier.

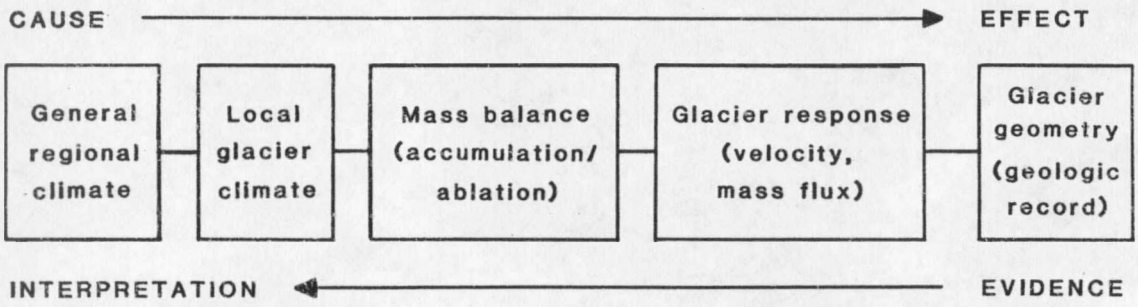

Figure 1. General relationships between climate, glacier response and geologic evidence of an individual glacier (left to right) (after Meier, 1965; Andrews, 1975). This study uses the reverse approach by interpreting mass balance and climate from the geologic record.

Working backwards through the pattern of study usually applied to climate-glacier relationships (Fig. 1), it is feasible to calculate the mass balance of paleoglaciers if the dynamics of these glaciers can be reconstructed (Haeberli and Penz, 1985; McCalpin, 1986). In

the Northern Rocky Mountains, many alpine paleoglaciers left clear evidence of their maximum areal extent in the form of moraines and trimlines. This evidence allows reconstruction of the former glacier shape and thickness. Ice velocity and mass flux can be estimated by applying ice flow theory to the reconstructed paleoglacier geometry. Mass flux through the equilibrium-line altitude of the paleoglacier provides an estimate of mass balance (net accumulation and net ablation). As a result, reconstruction of paleoglacier dynamics can be used to provide an approximation of paleoprecipitation (accumulation) on the glacier.

Previous Work

Only a few studies have used glacial mass balance as inferred from the ice dynamics of paleoglaciers to model paleoclimate. Haeberli and Penz (1985) applied this method to late Pleistocene paleoglaciers in the Alps. Although their methods allowed for only low precision, their estimates showed the Alps to be cold and dry during the last glacial maximum. McCalpin (1986) examined the ice flow dynamics and mass balances of paleoglaciers in the Sangre de Cristo Mountains of south-central Colorado and found that the calculated balances depended greatly on the flow regimes (extending, compressing, or uniform) of the glaciers. Using his method, only balances calculated in uniform flow regimes could be considered valid. Leonard and others (1986) used a similar method to model the climate of the Colorado Front Range during the late Pleistocene. Their

results show that area to be much drier during the glacial maximum than was previously thought.

In each of these ice dynamics studies, the method was applied to all the valleys within each study area. In some cases, irregularities in the geometries of the paleoglaciers (icefalls, stepped valleys) would have produced either overestimates or underestimates of mass balance (McCalpin, 1986). It is suggested that when using ice flow theory to model paleoglaciers, restrictions should be placed on the valley selection (applying the valleys to the method rather than the method to the valleys), thereby ensuring the quality of the results.

Theoretical Considerations

Glacier Dynamics

The geometry of a glacier is a response to the flow behavior of ice over the underlying topography. As such, if the geometry of the glacier is known, ice flow laws can be applied to this geometry to calculate values of velocity and mass flux (Nye, 1952; Paterson, 1981).

Equilibrium-Line Altitude (ELA). The equilibrium-line altitude (ELA) is an important descriptor of any glacial system because it is the line where mass balance changes from net accumulation to net ablation. On a steady state glacier (Fig. 2), the net accumulation, the net ablation, and the mass flux (velocity x cross-sectional area) through the ELA are all equal over a given period of time (Andrews, 1975). In this steady state system, net mass balance is zero. The mass flux through the ELA is somewhat less than the total mass

exchange (where total accumulation = total ablation) on the glacier because there is seasonal accumulation below the ELA and seasonal ablation above the ELA. However, the mass flux at the ELA is equal to the net mass exchange, and balances the net accumulation above the ELA and the net ablation below the ELA. Once the ELA of a paleoglacier is located, the net mass exchange (therefore net accumulation and net ablation) can be determined by calculating the glacier velocity and multiplying it by the cross-sectional area at the ELA.

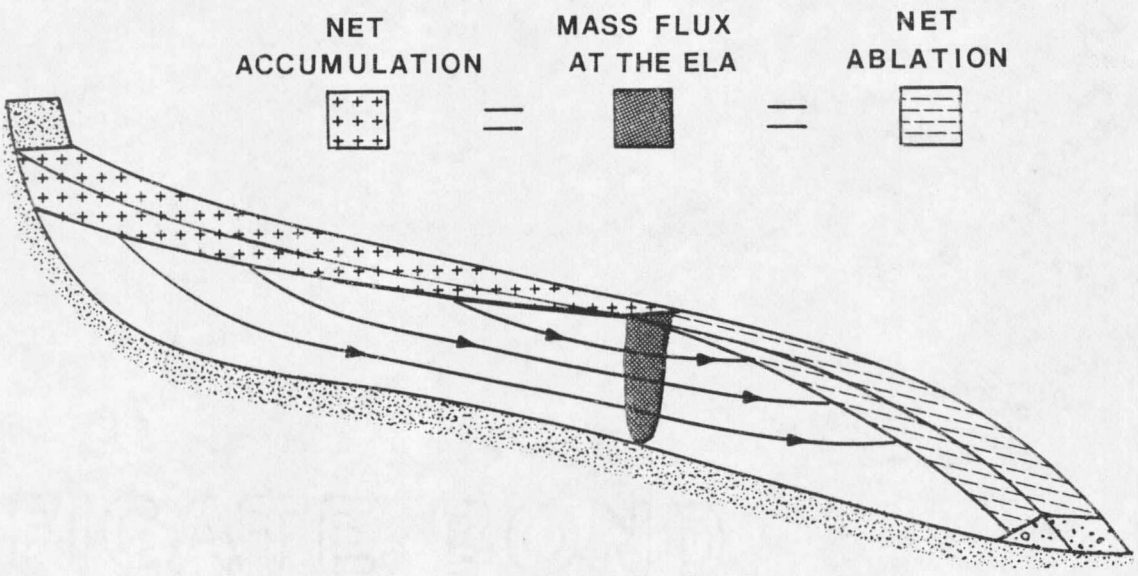

Figure 2. Mass exchange on a steady state glacier where net accumulation, net ablation and mass flux at the ELA are all equal.

Glacier Flow Velocities. Glacier movement can be broken down into components of ice deformation and basal sliding (Fig. 3). When ice is under pressure (stress), deformation takes place along internal planes of ice crystals. From laboratory experiments, Glen (1952) showed that the relationship of the strain rate (rate of deformation)

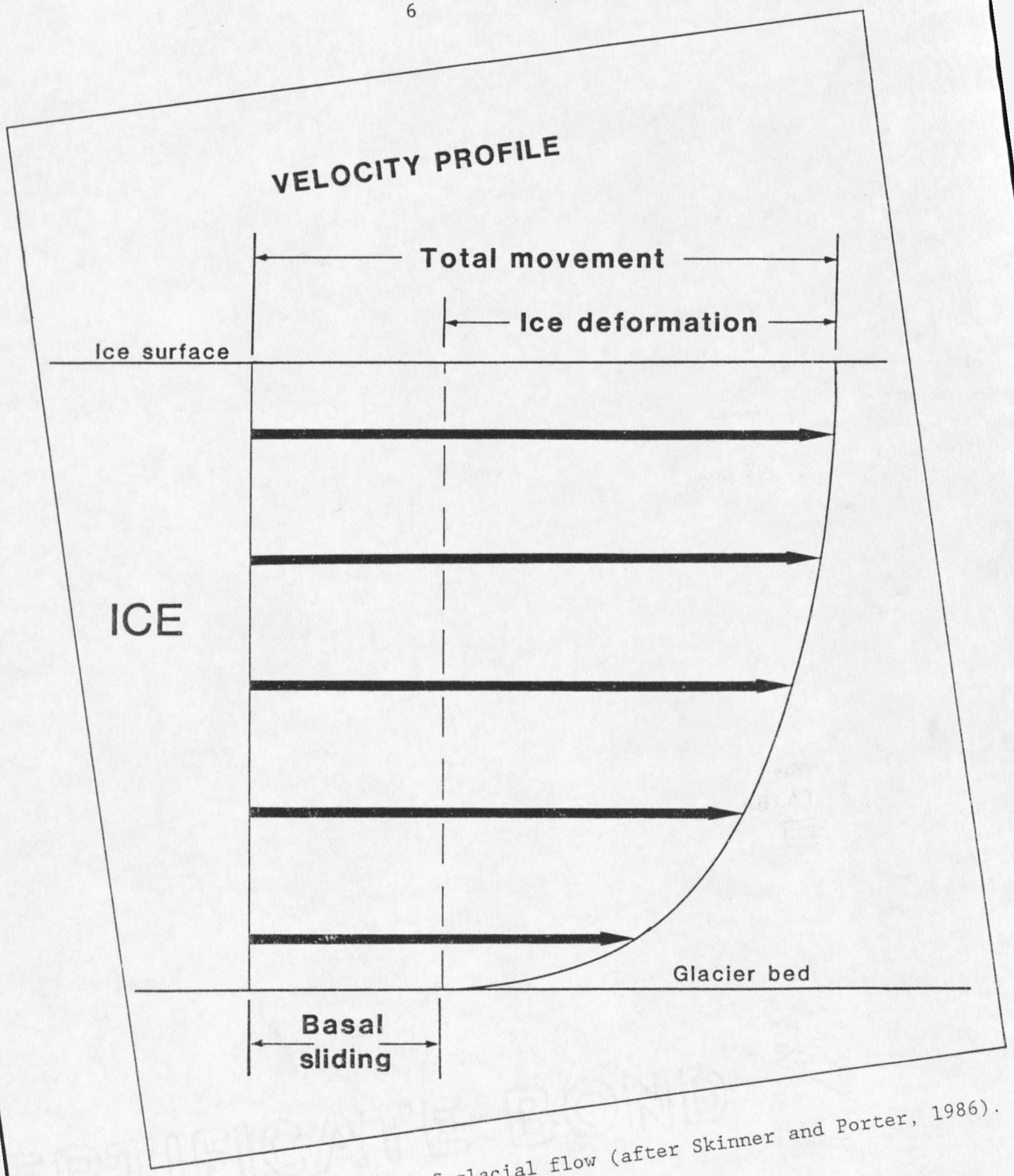

Figure 3. Components of glacial flow (after Skinner and Porter, 1986).

($\dot{\varepsilon}$) to shear stress (τ) could be expressed as:

$$\dot{\varepsilon} = A\tau^n \qquad (1)$$

where A is a temperature dependent constant and n is the slope of the strain rate curve. This is referred to as Glen's flow law. Laboratory and field experiments have shown that a value of n = 3 is appropriate for glaciers (Paterson, 1981). Shear stress is a function of the glacier thickness and surface slope and has been found to vary from about 0.5 to 1.5 bars for modern glaciers (Nye, 1952). Estimates of the basal shear stresses of paleoglaciers (Mathews, 1967; Pierce, 1979) have indicated that this range is also valid for former glaciers. By integrating the strain rate function over small increments of glacial thickness (Nye, 1952; Paterson, 1981), the velocity at the centerline due to ice deformation can be determined (see Methods). Using this integral, deformation velocity varies as the fourth power of the glacier thickness so accurate estimation of thickness is needed. While Glen's flow law provides a method of determining the deformation velocity, this velocity is only part of the total flow through a cross-section.

The other component of glacial flow through a cross-section occurs from the glacier sliding over its bed (Fig. 3). Sliding velocities in modern glaciers have been directly observed in boreholes or have been determined by subtracting the calculated velocity due to deformation from the observed surface velocity (Paterson, 1981). The amount of basal sliding (basal slip) has been measured to account for 3-90% of total velocity on modern glaciers (Andrews, 1975; Paterson, 1981). Several models have been developed (summarized in Weertman,

1979; Raymond, 1980; Paterson, 1981) to explain basal slip, but there has been little agreement between observations and theory. For paleoglaciers, actual surface velocity cannot be compared with calculated deformation (creep) velocity, therefore, estimation of basal slip on these glaciers presents a problem.

Studies using ice dynamics to model mass balance (Haeberli and Penz, 1985; Leonard and others, 1986; McCalpin, 1986, Holmlund, 1988) usually assumed a constant basal slip, yet this did not consider the fact that slip can vary along the length of the glacier. Holmlund (1988) used an average value of 50% slip to calculate the mass balance on the modern Storglaciaren in Sweden, but actual measurements showed that basal slip locally accounted for 80-90% of the motion. Because slip varies along the length of a glacier, local calculations of slip must be made for an accurate assessment of the local flow regime.

Mass Balance Gradients. Mass balance provides a key to the activity (velocity, mass flux) of a glacier. Accumulation and ablation gradients show the relationship of net accumulation and net ablation, respectively, to elevation (Fig. 4), and as such, provide a measure of a glacier's activity (Andrews, 1975). These gradients are expressed in terms of change of net thickness (mm) of water accumulated or melted with elevation (m) above or below the ELA (thus mm/m).

Both ablation and accumulation tend to change linearly with elevation, therefore average gradients are reasonable descriptors (Andrews, 1975). High ablation gradients (> 10 mm/m) are typical of glaciers in maritime environments where glacier activity is great due

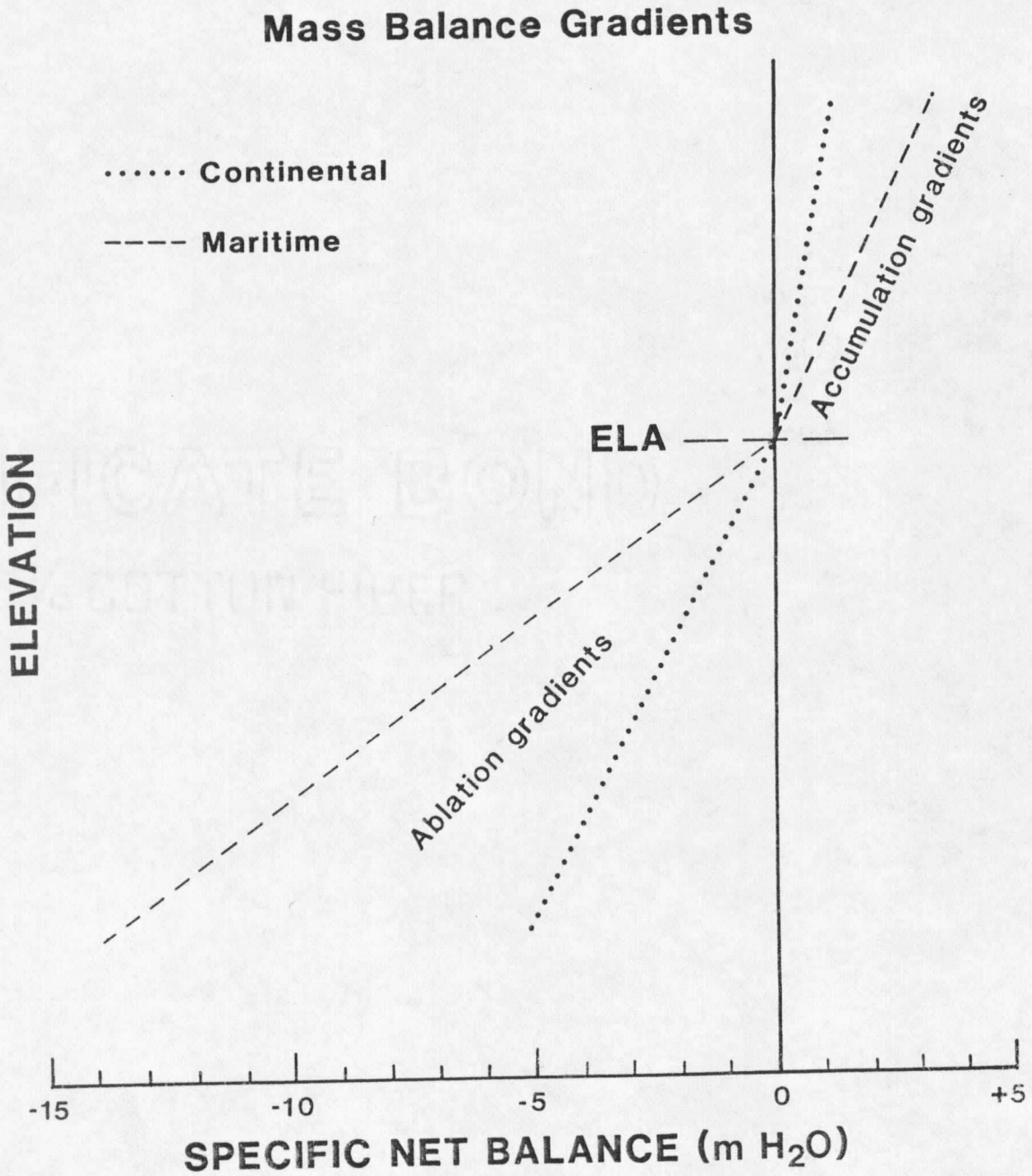

Figure 4. Generalized mass balance gradients for maritime and continental glaciers.

to the increased accumulation. Ablation gradients decrease inland toward more continental environments, to values of 2-7 mm/m (Fig. 4) (Meier and others, 1971; Andrews, 1975). Ablation gradients also decrease in value from temperate to polar climates. An exception to this trend is the occurrence of high gradients on small cirque glaciers in the Rocky Mountains of Wyoming and Montana. This exception can be accounted for by the local microclimates of small niche glaciers like these that produce large amounts of snow accumulation from wind drifting and orographic precipitation (Meier and others, 1971). On moderate sized glaciers, however, ablation gradients should be more indicative of regional climate (Meier and others, 1971; Andrews, 1975).

On modern glaciers, mass balance is directly measured on the glacier surface or can be determined using photogrammetric, hydrologic, or reconnaissance methods (Paterson, 1981). Balance gradients are determined using the measured mass balance and the areal distribution of the glacier with elevation. On paleoglaciers, these methods cannot be employed because the glacier no longer exists. However, if net accumulation and net ablation can be estimated by calculating net mass exchange at the ELA using reconstructed ice dynamics, average net balance gradients can then be determined. These gradients can be used to determine the annual net accumulation or ablation above or below a point on the glacier. The gradients can also be used as proxies to climate by comparison with modern analogs.

The Study Area

Regional Setting

The mountains of southwestern Montana and adjacent Idaho (Fig. 5) show extensive evidence of late Pleistocene glaciation (Alden, 1953; Porter and others, 1983). The large number of glaciated valleys provides an opportunity to select only those valleys that comply with the criteria in the model, including valleys with well defined glacial features and constant or slowly varying gradients (see Methods). The study area consists generally of northwest-southeast trending mountain ranges separated by broad valleys. The region is bounded on the east by the flat terrain of the Great Plains and on the west by the Salmon River Mountains of central Idaho. The relatively low, flat area of the Snake River Plain lies to the south. During the late Pleistocene, the region was bounded to the north by the Laurentide and Cordilleran ice sheets (Porter and others, 1983) and to the southeast by the Yellowstone ice cap (Pierce, 1979) (Fig. 6). The presence of these ice sheets significantly altered the regional topography during the last glacial maximum.

Six valleys (Fig. 6) were used to model paleoglacier dynamics and the paleoenvironment in this area. Big Timber Canyon (#1) in the Crazy Mountains was used to develop and refine the model. Four valleys (#3-6; Mill Creek, Stroud Creek, Everson Creek, and Meadow Lake) in the Lemhi Range were selected to test the local variability of the model. One other valley (#2; Miner Lakes) in the Beaverhead Range was also studied to test the regional applicability of the

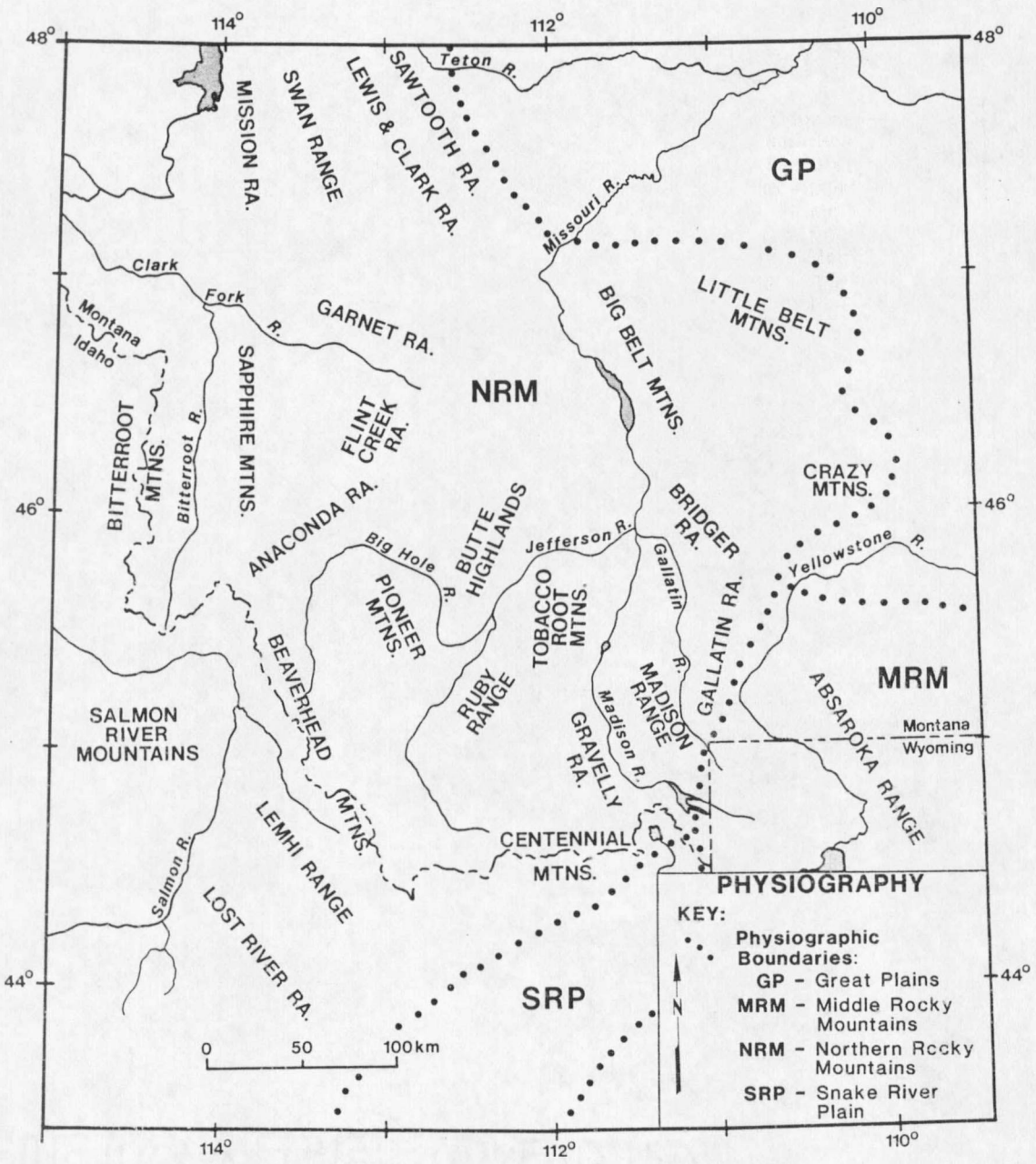

Figure 5. Location and physiography of the study area.

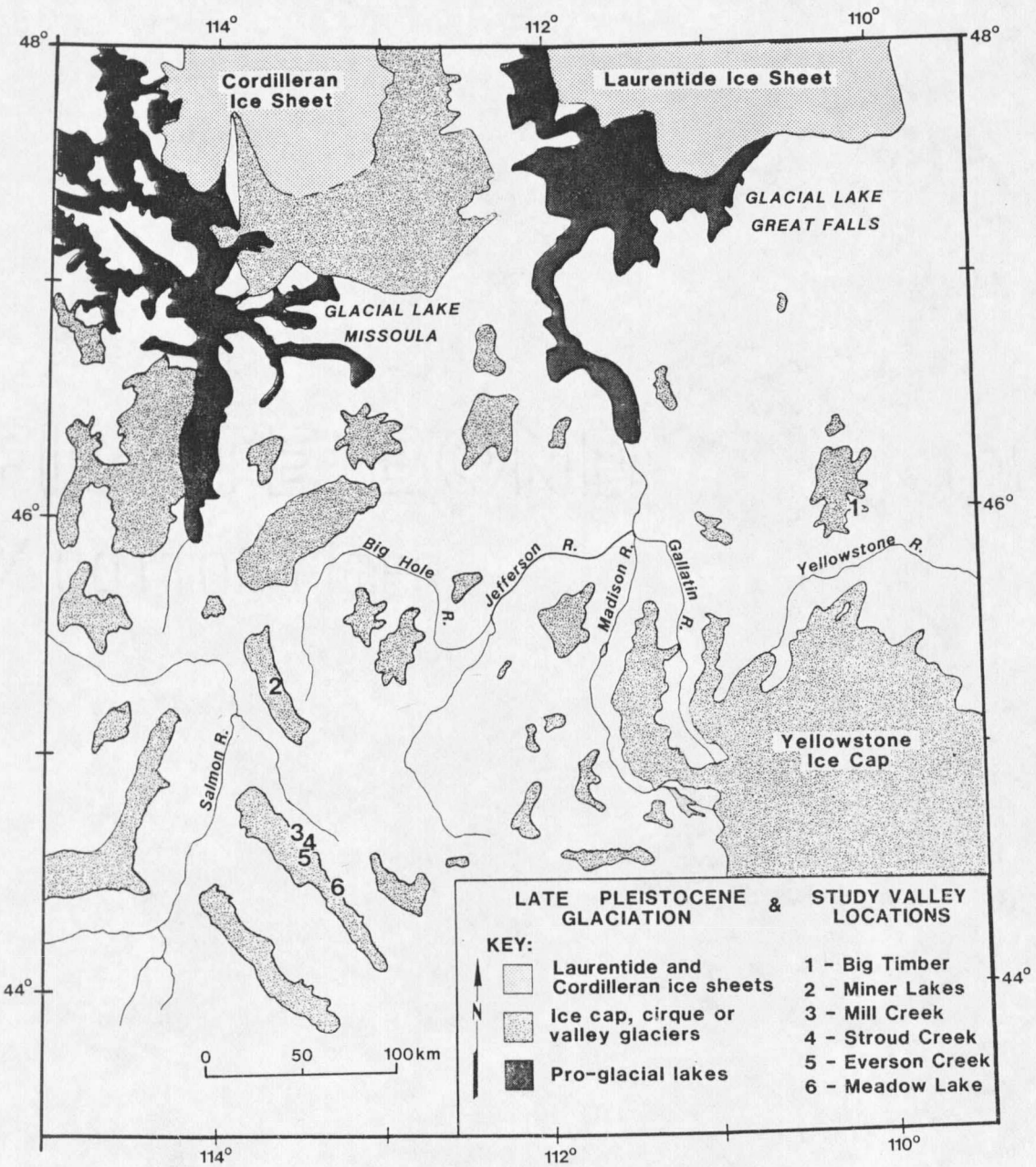

Figure 6. General areas of western Montana and adjacent Idaho covered by ice during the last glacial maximum (Taylor and Ashley, 1986; Waitt and Thorson, 1983; Fullerton and Colton, 1986) and location of the study valleys.

model. The model could be applied to many other valleys in this area, but that was not the purpose of this study.

Geology

The bedrock geology of the mountains in the area ranges from Tertiary volcanic to Precambrian metamorphic rocks (Ross and others, 1955). Because the model used in this study is only dependent on the valley cross-sectional shape, and the U-shape of a glacial valley is independent of bedrock type (Graf, 1970), differences in lithology from valley to valley should not have affected the results of this study. Varying lithologies along the axis of a glacier could produce irregularities in the profile of the glacier (Flint, 1971), however, stepped valleys were not used in this study because of the problems in calculating mass flux created by extensional and compressional flow.

Present Climate

The varied topography of the study area makes use of the traditional climatic classifications (e.g. Köppen) using mean temperature and precipitation almost impossible. Temperature and precipitation vary over short distances because of the terrain (Harding, 1982) and create a patchwork of climate types which are largely a function of elevation. However, general trends in air mass domination and moisture sources can be determined.

Mitchell (1969) classifies the climate of this region using equivalent potential temperature (the temperature that a parcel of air would attain if it were allowed to rise pseudo-adiabatically until it has lost all its moisture and then allowed to descend back to its

original pressure (Blair and Fite, 1965)) to distinguish changes in air mass domination over the western United States. Mitchell's (1969) findings show the present study area to be dominated by moist Pacific air masses in the winter (Fig. 7) and drier interior continental air masses in the summer.

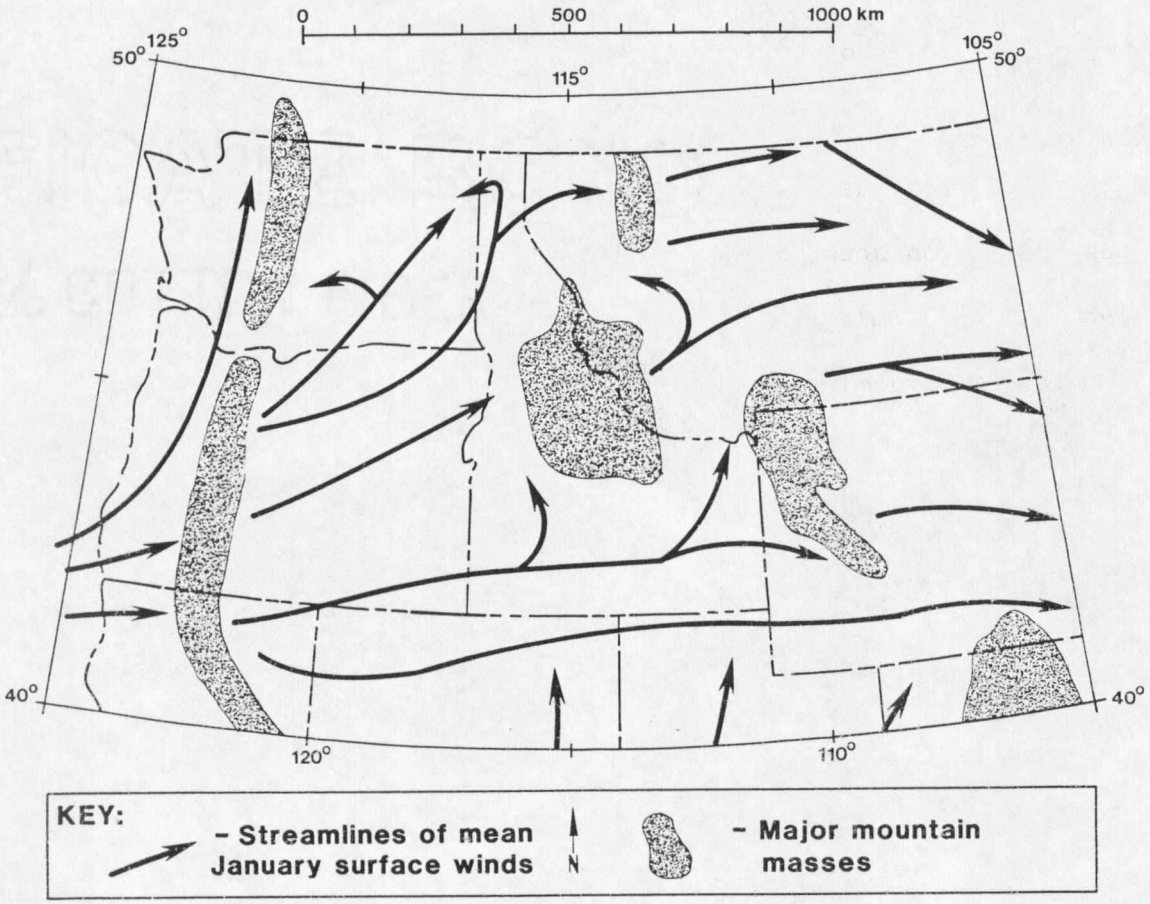

Figure 7. Streamlines of mean January surface winds over the western United States (after Mitchell, 1969).

Harding (1982) notes that the southeastern part of this study area is affected by strong upslope winds from the east during May and June accounting for precipitation maximums at this time (see Bozeman; Fig. 8). An analysis of winter precipitation patterns over western

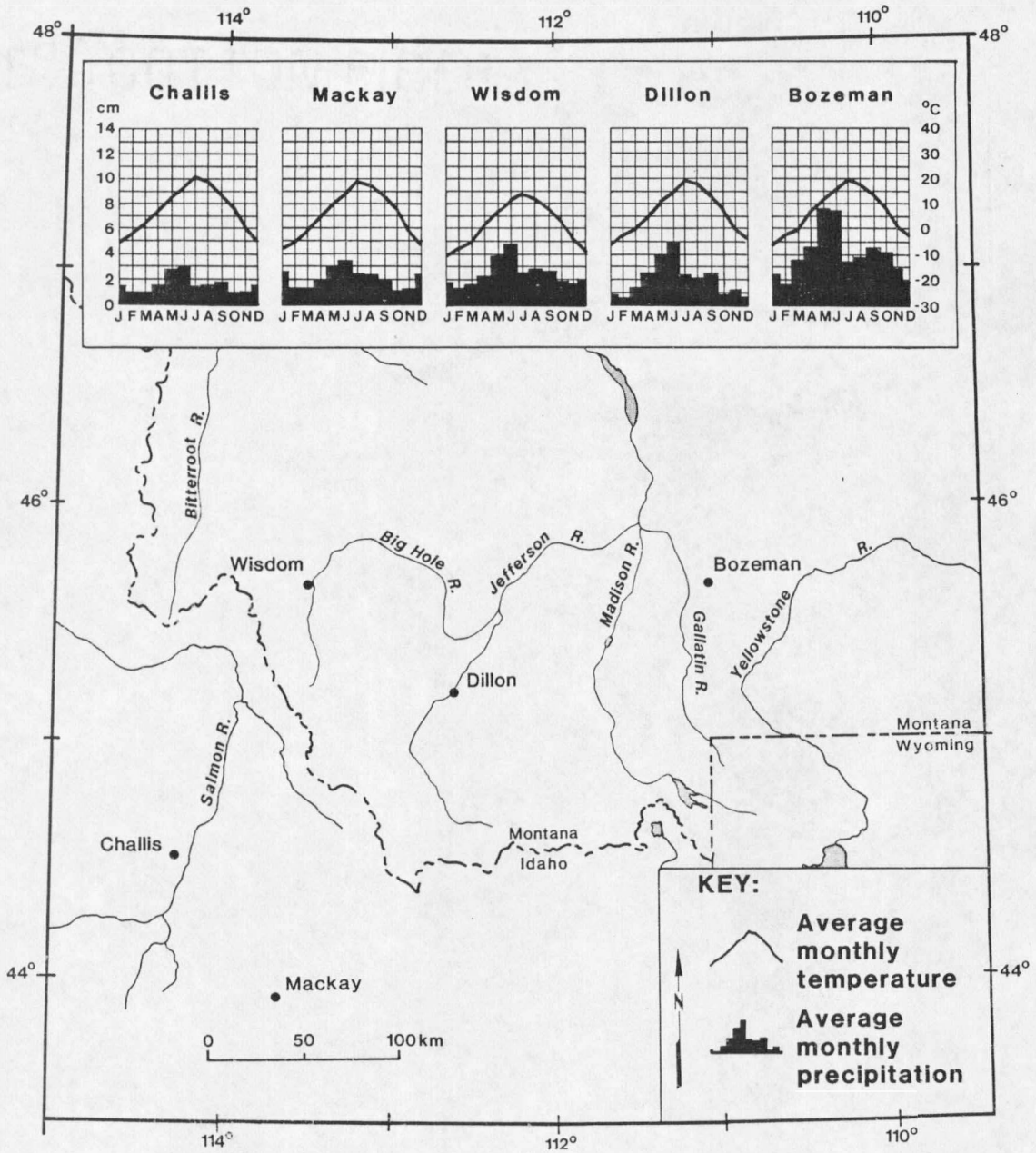

Figure 8. Climographs and locations of selected cities within the study area (data from NOAA, 1985a, 1985b).

Montana by Locke (1989) showed a dominance of Pacific moisture to the northwest with decreasing precipitation to the southeast. Locke (1989) also found a secondary source of moisture from the Gulf of Mexico into the southeastern corner of the study area, which agrees with Harding's (1982) observations.

Mountain ranges have an effect on the paths that storms follow (Price, 1981; Barry, 1981). In the study area, winter storms are steered around the central Idaho uplands allowing an influx of moisture along the Snake River Plain to the south (Fig. 7). Mackay Ranger Station, Idaho, shows a secondary maximum of precipitation in December-January (Fig. 8) which might be accounted for by its position on the northern boundary of the Snake River Plain (Fig. 5).

Mountains also affect the local, as well as regional, precipitation patterns. Precipitation usually increases with increasing elevation due to the orographic effects of mountains, thus precipitation differences occur between valleys and mountains. Bozeman, Montana (Fig. 8) has a 12 cm higher annual average precipitation than Belgrade 13 km to the west because of the orographic effects of the Bridger Range (Harding, 1982). The effect of elevation on precipitation is also noticeable in snowpack records. Plots of maximum winter snowpack versus elevation for the Lemhi, Beaverhead and Crazy Mountains are shown in Figure 9. In addition to the increase of precipitation with elevation, these gradients also show that precipitation amounts at a given elevation are lower in the western portion of the study area (Lemhi Range) and increase to the east.

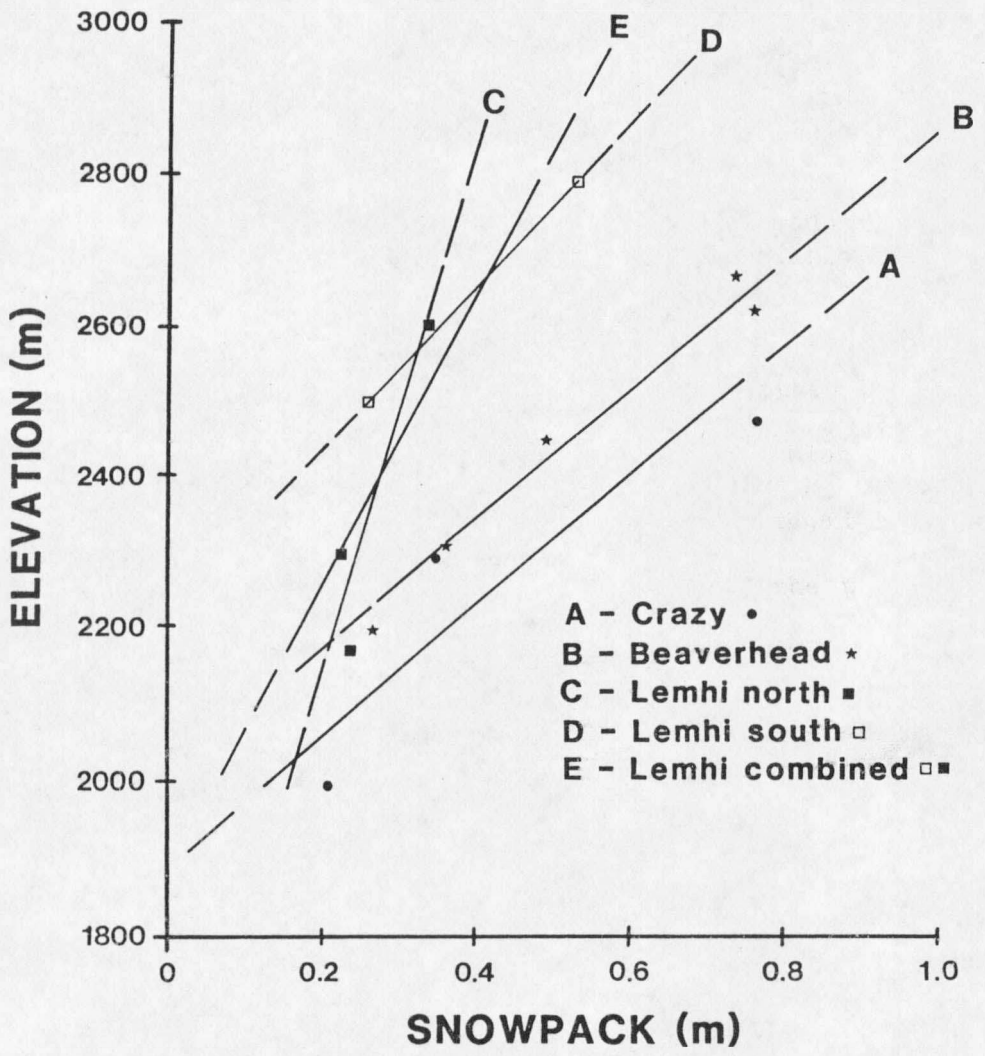

Figure 9. Modern snow accumulation gradients for the mountain ranges of the study valleys (data from Soil Conservation Service, 1986a, 1986b).

Present climates supporting alpine glaciers within the studied areas exist only in the Crazy Mountains of Montana. Glacial climates do exist outside the study area: in the Beartooth Mountains to the southeast, the Salmon River Mountains of Idaho to the west, and in several of the mountain ranges (Mission, Swan, Flathead) to the north (Field, 1975; Graf, 1976).

Late-Pleistocene Climate

During the late Pleistocene, the Cordilleran and Laurentide ice sheets that lay to the north of the study area (Fig. 6) were up to 1500 m thick in Montana (Waitt and Thorson, 1983). The presence of this ice not only altered the topography, but probably the temperature gradients as well, which in turn, modified regional windflow and precipitation patterns (Manabe and Broccoli, 1985; Kutzbach and Wright, 1985; Locke and Kemph, 1987).

General Circulation Models (GCMs) (Kutzbach and Wright, 1985; Manabe and Broccoli, 1985) show a split jet stream over the Laurentide ice sheet over North America during the last glacial maximum. This split left most of the study area in a zone of weak westerlies with a slight easterly flow on the eastern edge. Such a wind flow pattern would suggest a Pacific moisture source for most of the area, with the possibility of a low level Gulf of Mexico source for the eastern edge. The paleoprecipitation patterns determined by Locke and Kemph (1987) show a trend of increasing moisture to the north and west over western Montana, agreeing with a dominant Pacific moisture source. Their data also suggest that the Snake River Plain and Gulf of Mexico were locally important sources of moisture.

Summer temperatures in the Northern Rocky Mountains during the last glacial maximum have been estimated to be at least 10^{o} C lower than present (Porter and others, 1983; Barry, 1983; Kutzbach and Wright, 1985; Manabe and Broccoli, 1985). A strong temperature gradient is interpreted by the GCMs (Kutzbach and Wright, 1985; Manabe and Broccoli, 1985) along the edge of the ice sheets in the Northern

Rocky Mountains. While the paleoclimatic analysis in this study did not address climate, temperature is important in modelling the ice dynamics.

The present study provides estimates of average annual net accumulation at each glacier locality in addition to an analysis of the dynamics of each paleoglacier. While the sample size in this study is too small to provide accurate regional estimates of paleoprecipitation patterns, it does provide independent spot checks on other paleoclimatic studies in this area (Kutzbach and Wright, 1985; Manabe and Broccoli, 1985; Locke and Kemph, 1987). The results of this study are also compared with modern precipitation data for each locality.

METHODS

This chapter details the methods, and underlying assumptions, employed in this study. These methods were tested and refined using the Big Timber Canyon paleoglacier on the east flank of the Crazy Mountains, Montana and the results from that test case are discussed in the next chapter.

A model involving glacier flow theory can be used to determine mass balance parameters using the geologic evidence left by glaciers (Fig. 1). Underlying each of the steps in this model are certain assumptions, detailed in this chapter, that affect the accuracy of the results. Figure 10 shows the flow of the methodology used in this study to reconstruct the glacier dynamics and paleoclimate. Basically, the following steps were taken during the reconstructions: 1) selection of a study valley according to specific criteria, 2) reconstruction of the glacier profile and areal extent, 3) calculation of average effective basal shear stress along the longitudinal profile, 4) calculation of mass flux from ice flow equations, 5) calculation of mass balance gradients from the calculated mass flux at the point of highest ice deformation and through the equilibrium-line altitude (ELA), and 6) climatic interpretation of the results by comparison to modern analogs. To ensure the accuracy of the results, a sensitivity analysis was performed during steps 3, 4, and 5 by varying parameters such as glacier thickness and slope (see Results).

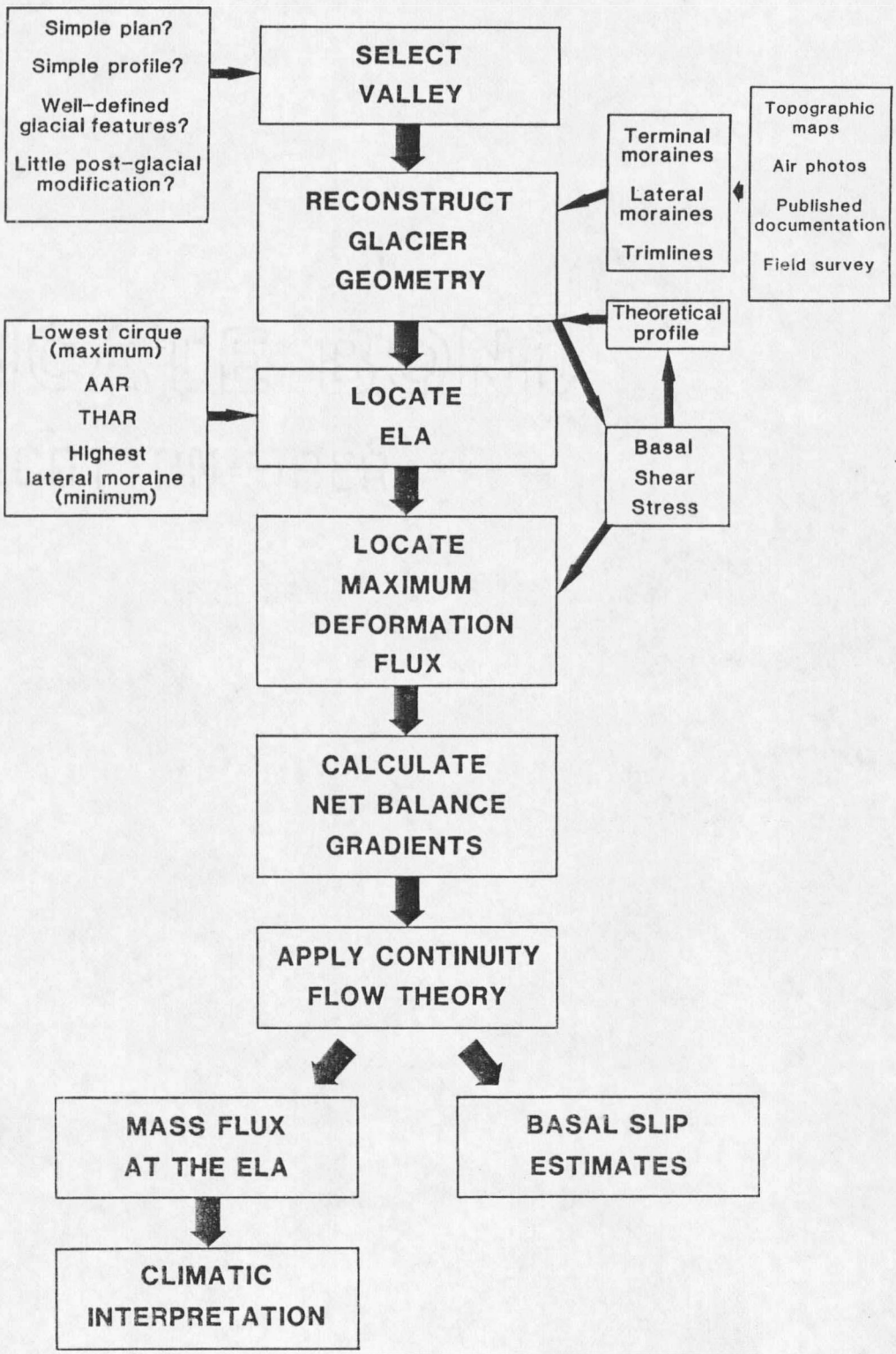

Figure 10. Flowchart of the methodology used in this study.

Valley Selection

In previous studies (Pierce, 1979; Haeberli and Penz, 1985; Leonard and others, 1986; McCalpin, 1986), all valleys in one area were used because the ice dynamics modelling was secondary to other studies of the glacial geology in those areas. The accuracy of their results was diminished because the flow law of ice is sensitive to changes in glacier thickness and slope, which are in part controlled by the underlying topography. The topography of most valleys in any area is conducive to creating changes in ice slope and thickness over short distances and creates problems when using glacial flow theory in ice dynamics modelling.

In an effort to minimize the effects of topographically induced changes in ice thickness and surface slope, criteria were established for selecting valleys that would be suitable to the method. Valleys with stepped longitudinal profiles and many tributary glaciers were not used in order to minimize landform-induced extensional and compressive flow. Areas where extensional and compressive flow occur may have had actual velocities differing from those calculated by Glen's flow law (Pierce, 1979; Paterson, 1981). Mountain ranges with small ice caps were not used because of the difficulties in determining the boundaries of the source region of ice flowing into the valley glaciers. Some methods used to determine the location of the ELA are dependent on the areal extent of the glacier, and valleys with well defined depositional (moraines) and erosional (trimlines, hanging valleys) glacial features were selected to enhance the accuracy of the reconstructions of the geometries of the

paleoglaciers. Valleys that had minimal mass movement and alluvial valley fill since the glaciers retreated were best suited to this study because the accuracy of thickness and valley shape values was increased if the glacially eroded surface was well exposed. By using these selection criteria, the accuracy of the reconstructions was enhanced, and the final output from the model was as accurate and precise as possible.

Glacier Geometry

The areal extent of each paleoglacier was determined from USGS topographic maps (scales 1:24000 and 1:62500), aerial photographs (Appendix A), and published documentation (Alden, 1932; Aten, 1974; Knoll, 1977; Ruppel, 1980; Ruppel and Lopez; 1981; Richmond; 1986). Field checking of the geologic evidence of glaciation (terminal and lateral moraines, truncated spurs, hanging tributary valleys and glacial trimlines) was performed on all but two of the valleys during the summer of 1988. There was good correlation between the field checked features and the features observed on the topographic maps and air photographs. In the valleys that were not field checked (Stroud and Everson Creeks, Lemhi Range), glacial geologic evidence was well-preserved; therefore it was assumed that field checking would not significantly alter the results.

Because multiple terminal moraines were present in most of the valleys, the crests of the largest, well-defined, morphologically fresh moraines were used as the outer limit of each paleoglacier. Published documentation (when available for a particular site) usually

correlated such moraines with the Pinedale-equivalent maxima. While the ages of the early and late Pinedale moraines vary by as much as a factor of three (Porter and others, 1983), differences in the areal extent of the glaciations are minimal. Terminal moraines from the late Pinedale maximum (20,000 years ago) are always present (Porter and others, 1983; Richmond, 1986) in the glaciated valleys of the Northern Rockies. Because the early and late Pinedale terminal moraines are usually indistinguishable, the use of either moraine should produce similar results in determining the glacier length.

Although the glacier length may have been the same, climatic differences between the two periods of glaciation may have been substantial. For a given glacier length and valley shape, a glacier in a warm/wet (e.g. maritime) climate should be thicker than one in a cold/dry (e.g. continental) climate, because more mass is exchanged on the glacier (Fig. 11). Any significant difference in climate (i.e. warm/wet versus cold/dry) using the terminal moraines in this study should be reflected in the number of lateral moraines that grade into these terminal moraines (Table 1). If only one set of lateral moraines graded into the terminal moraine, then that set was assumed to represent the late Pinedale ice margin. If two sets of lateral moraines graded into the terminal moraine, the lower (in elevation) of the two sets was used to represent the late Pinedale ice margin.

The longitudinal profiles of both the bedrock and the centerline ice elevation along the axis of the each glacier were drawn based on the reconstruction of the areal extent. In the upper reaches of the valleys, depositional and erosional features were not as prevalent as

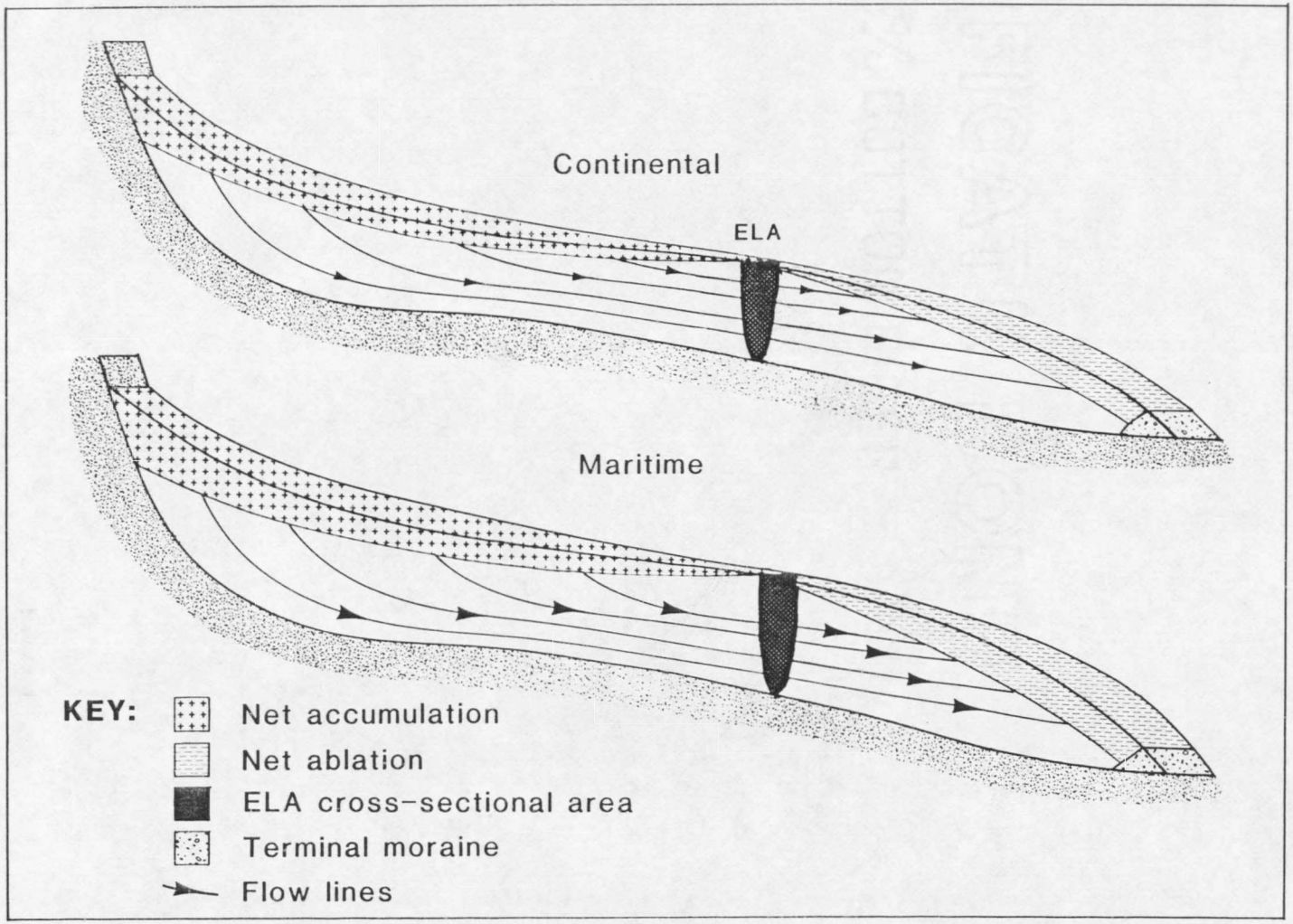

Figure 11. Comparison of the shapes of maritime and continental glaciers for a given valley length.

Table 1. Analysis of the number of lateral moraines that should exist in a valley, given differences in climate between two successive glaciations.

Early Pinedale	Late Pinedale	Number of ice marginal features
Warm and wet	Warm and wet	1
Warm and wet	Cold and dry	2
Cold and dry	Warm and wet	1
Cold and dry	Cold and dry	1

in the lower reaches and reconstruction of the ice surface contours presented a problem. Theoretical glacier profiles were determined using a model (Schilling and Hollin, 1981) which calculates ice surface elevations using theoretical average effective basal shear stresses (see next section). Values for the ice surface elevations from the theoretical profile that best fit the actual profile were used to reconstruct the ice surface contours in the upper reaches of the valley where geologic evidence of glaciation was lacking.

In the lower reaches of the valley, centerline ice surface elevations were assumed to be equivalent to the elevations of the ice margins. Comparison of the surface contours of several modern glaciers in Alaska which are similar in plan form to the paleoglaciers used in this study (American Geographical Society, 1960) showed a mean difference of only + 3.9 m between the ice centerline and ice marginal elevations below the equilibrium line (Fig. 12). Because of this minimal variance, no correction factor was added to the ice surface elevations below the equilibrium line. Ice centerline elevations are lower than the ice margin above the equilibrium line of modern glaciers (Fig. 12). Because the theoretical ice elevations were lower

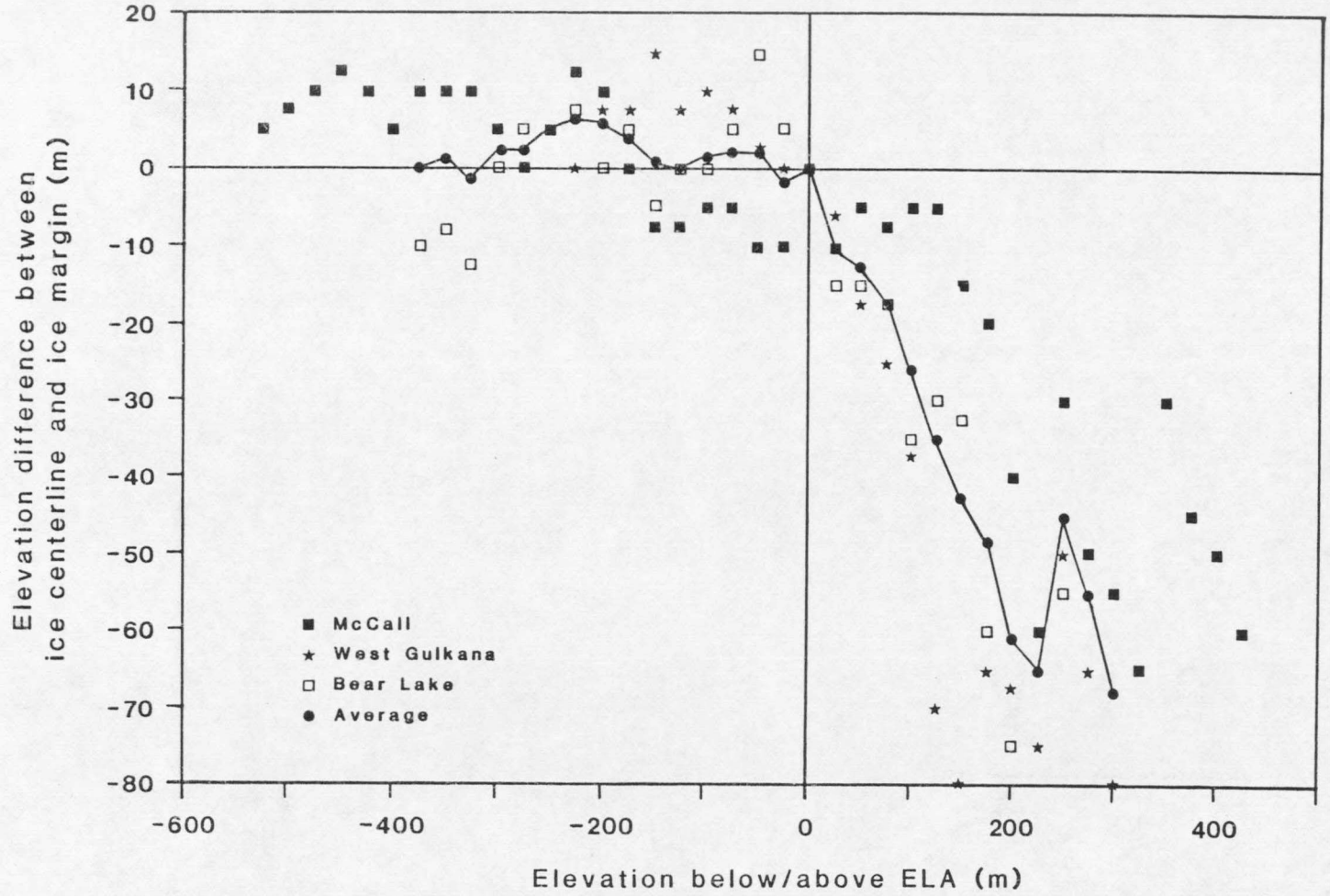

Figure 12. Comparison of the difference in elevation between the ice centerline and the ice margins against elevation above or below the ELA on modern glaciers (data from American Geographical Society, 1960).

than the ice marginal features on the upper portions of many of the paleoglaciers in this study (see Appendices F-J), the theoretical ice elevations were assumed to be appropriate values of ice centerline elevation and were used for calculations of ice thickness, velocity and mass flux.

Ice thicknesses were calculated from the difference of ice surface elevation and bedrock elevation. One of the underlying assumptions was that the valley floor elevation has changed little since late Pleistocene time. Because there have been subsequent glaciations (as evidenced by recessional and re-advance moraines up-valley from the end moraines in most valleys), additional scouring of the bedrock has occurred in the upper reaches since maximum late Pinedale ice extent. The calculated ice thicknesses in this part of each valley were thus maximum values. In the lower reaches of the valley, re-advance and recessional till and post-glacial fill made the estimated ice thickness values a minimum. Where the present stream runs along bedrock (usually in the upper portions of the valleys), fill did not present a problem in estimating ice thicknesses.

Basal Shear Stresses

Calculation of basal shear stress along the ice centerline provides a check on the accuracy of the reconstructed longitudinal profile. Ice thickness and surface slope, which are determined from the shape of a reconstructed glacier, are used to calculate basal shear stress (Pierce, 1979). On most modern glaciers (Paterson, 1981) and well-studied paleoglaciers (Mathews, 1967; Pierce, 1979), average

effective basal shear stresses range from 0.5 to 1.5 bars. Excessively high (> 1.5 bars) or low (< 0.5 bar) shear stresses could imply an error in reconstruction. While these values are not impossible to attain, Mathews (1967) explained that the dynamics of a glacier provide adjustments of slope and/or thickness over time which will yield values in the normal range. The profiles used in reconstructions are time-averaged (steady state) so the values of average effective basal shear stress should also lie in this narrow range.

For a valley glacier, the average basal shear stress (τ_b) can be calculated from the relation:

$$\tau_b = \rho g H \, F \sin \alpha \qquad (2)$$

(Paterson, 1981) where ρ = specific gravity of ice (910 kg m^{-3}); g = acceleration due to gravity (9.81 m s^{-2}); H = centerline ice thickness (m); F = shape factor to account for drag on the valley sides (dimensionless) (Nye, 1965b); and α = ice surface slope (dimensionless). The shape factor (F) is a function of the glacier half-width divided by the glacier thickness (W) (Fig. 13). Ice thickness, surface slope and valley shape were determined from the reconstructed geometry of the paleoglacier.

In strongly extending or compressing flow, longitudinal or transverse normal gradients can add to the total, or effective, shear stress (Pierce, 1979; Paterson, 1981). In this study, basal shear stress calculated from equation 2 was used as the average effective basal shear stress. With uniform flow, effective basal shear stress and total basal shear stress are the same, and most compressing and

extending flow regimes should have been eliminated in this study by the valley selection criteria.

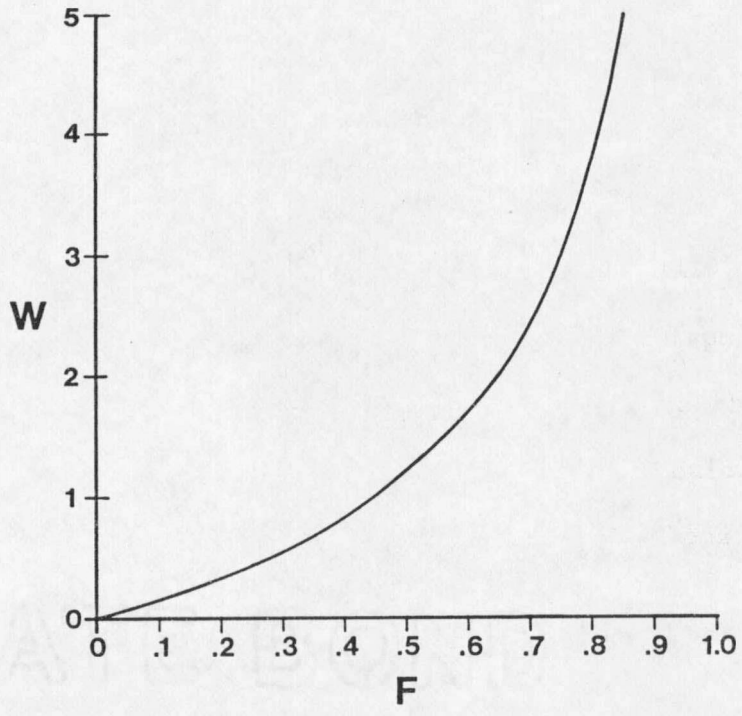

Figure 13. Values of the shape factor (F) for varying parabolic glacier cross-sectional shapes, represented by W values (W = glacier half width/glacier centerline thickness) (after Nye, 1965b).

A theoretical profile of each glacier was calculated using the relation:

$$e_{i+1} = e_i + \frac{\tau_b}{F\rho g} \frac{x}{H_i} \qquad (3)$$

which is derived from equation 2 (Schilling and Hollin, 1981). Here e_i and e_{i+1} are the ice surface elevations at steps x_i and x_{i+1} respectively (Fig. 14), and the other variables are the same as in equation 2. This iterative approach is used to calculate glacier thickness (H) at 1000 ft (305 m) intervals (x) along each glacier

profile. This step length was used for simplicity (1000 ft = 1/2" on a 1:24000 map) and because no appreciable difference in the ice thickness was determined using a shorter step length. When $H_i = 0$ (at the terminus), e_{i+1} had to be chosen arbitrarily. In this study, the elevation of the lateral moraine at an arbitrary point up valley from the terminus was used as the ice elevation for the first step. The first step was chosen at a point where post-glacial fill did not create errors in thickness calculations. Profiles using various average effective basal shear stresses between 0.5 to 1.5 bars were computed for each valley and compared with the geomorphic evidence. The theoretical (using a constant τ_b) profile, which had the least difference in ice thickness from the morphologic profile, was used to estimate ice surface elevations in those regions where geomorphic evidence was absent.

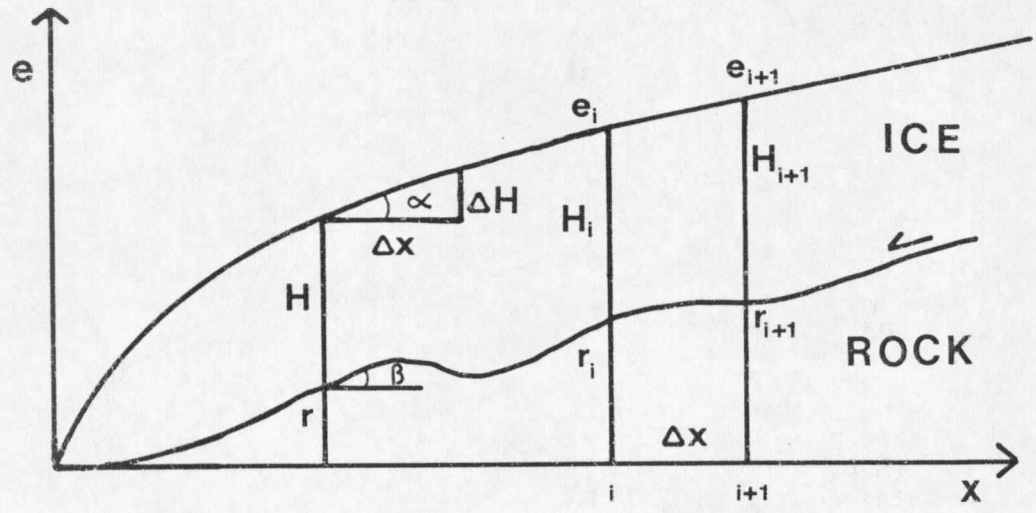

Figure 14. Variables used in the iterative scheme for calculating theoretical glacier longitudinal profiles (after Schilling and Hollin, 1981).

Location of the ELA

Once the glacial extent and longitudinal profile were determined, the location of the equilibrium-line altitude (ELA) was determined. Several methods for determining the ELAs of paleoglaciers have been developed and employed (Andrews, 1975; Porter, 1975; Meierding, 1982; Leonard, 1985; Locke and Kemph, 1987). The paleo-ELAs for the glaciers in this study were estimated from 1) highest lateral moraines, 2) lowest cirque floor elevation, 3) toe-headwall altitude ratio (THAR) and 4) accumulation area ratio (AAR). Meierding (1982) tested the accuracy of each of these methods in the Colorado Front Range. He found that the root mean square error of the methods ranged from 80 m for accumulation area ratio (AAR) and toe-headwall altitude ratio (THAR) to 109 m for cirque floor altitudes to 148 m for highest lateral moraines. Accuracy of the location of the paleo-ELA was important because calculations of net mass exchange could only be made at that point.

Lateral Moraines

Lateral moraines develop in the ablation zone where ice flows outward towards the margins of the glacier and deposits debris. Because ice flow lines are descending in the accumulation area (Figs. 2,11), the highest point on the lateral moraine would indicate a change from descending to ascending flow and would therefore be an approximation of the location of the ELA (Andrews, 1975; Meierding, 1982). Although lateral moraines were well developed in the lower reaches of many of the valleys, they have been subject to erosion and

mass wasting since the ice retreated. If the ELA was on a portion of the glacier that was confined within the walls of a canyon, the lateral moraines that developed on this part of the glacier would have been supported by the ice. When the glacier retreated, the lateral moraines would have slumped to the bottom of the valley and the moraines would not have been preserved. The portion of the moraine that was preserved thus represents a minimum estimate of ELA.

Lowest Cirque Elevation

Cirque floor elevations are widely used as a measure of the ELA of former cirque glaciers (Andrews, 1975; Meierding, 1982). Meierding (1982) showed that although this method is rapid, it is also highly subjective because cirque floors are not always easily identifiable. Andrews (1975) pointed out that this method is better for a regional approximation of ELA if a trend surface connecting the lowest north facing cirques is constructed. Also, valley glaciers extend well outside the cirques, thus ELAs using this method on valley glaciers should provide a maximum estimate. Most of the valleys used in this study have well-defined cirques, and the elevation of the lowest of these was used as a maximum estimate of the ELA.

Toe-Headwall Altitude Ratio (THAR)

An empirical relation between the highest and lowest ice limits is used extensively for the rapid determination of the ELA. Highest ice limits were determined from the highest elevation of ice on the reconstructed glaciers. Because the bedrock surface at the termini of the paleoglaciers was covered with till and outwash deposits, the

terminal elevation was determined by extrapolating elevations from surrounding pediments to the glacier front wherever possible. If this was not possible, the elevation of the valley floor on the upstream side of the terminal moraine was used. Meierding (1982) found toe-headwall altitude ratios of .35 and .40 produced the best results. A THAR of .40 was used in this study because ELAs using a value of .35 were lower than the highest lateral moraine in all valleys.

Accumulation-Area Ratios (AAR)

Studies of modern glaciers have shown that the accumulation area of a glacier is about .65 of the total glacial area, however, this percentage may vary between .60 and .70 (Andrews, 1975). Several studies of paleoglaciers have used the .65 value (Porter, 1975; Meierding, 1982; Leonard, 1984) to estimate the ELA. Meierding (1982) calculated ELAs using values ranging from .50 to .75 and found .65 to have the least error. In this study, the area between successive 200 ft (61 m) and/or 400 ft (122 m) contours (depending on map contour interval) was measured and a cumulative total was plotted against elevation for each glacier. The ELA using an AAR value of .65 was determined for each paleoglacier using this graph.

Estimated ELAs

The final ELA for each paleoglacier was estimated using a combination of those methods that agreed most closely in each valley. The highest lateral moraine elevation provided a minimum value for the ELA and was used if the THAR and AAR provided lower values. Similarly, lowest cirque floor elevation is a maximum of ELA, so the

final ELA must be less than or equal to that value. By nature, THAR and AAR are the least subject to modification after deglaciation, and they are considered to produce the best estimates of ELA (Meierding, 1982). If the ELAs calculated using THAR and AAR lie between the highest lateral moraine and the lowest cirque floor, an average of THAR and AAR was used as the final ELA.

Glacier Flow

Mass flux through a cross-section of a glacier was calculated by multiplying the average velocity by the cross-sectional area. The cross-sectional area was measured from the topographic maps, but the average velocity had to be estimated using glacial flow theory. As stated previously, glacier movement can be broken down into components of ice deformation and basal sliding, and the contribution of each to total flow had to be determined.

Ice Deformation

By integrating Glen's flow law of ice over small increments of glacial thickness, Nye (1952) was able to calculate a vertical profile of the velocity due to deformation within a glacier cross-section. Assuming that the basal velocity is zero, the centerline surface velocity due to ice deformation (u_c) can be determined by:

$$u_c = 2A(\tau_b)^n(H)/(n+1) \qquad (4)$$

where: A = temperature-dependent constant of the flow law ($0.167\ \text{bar}^{-3}\ \text{a}^{-1}$ at 0°C; Paterson, 1981)

H = ice thickness at the centerline (m)

τ_b = average effective basal shear stress (bar; calculated from equation 2)

n = exponential constant of the flow law ($n \approx 3$ for valley glaciers; Paterson, 1981)

By substituting equation 2 for τ_b, equation 4 becomes:

$$u_c = 2A(\rho g)^n(\sin^n\alpha)(H)^{n+1}/(n+1) \quad (5)$$

and on valley glaciers (with n = 3), u_c is proportional to the fourth power of thickness and the third power of surface slope. Therefore, estimation of thickness and surface slope must be as precise as possible. Longitudinal variations in velocity were minimized by averaging ice surface slope over 8-20(H) (Raymond, 1980). Local values of H are used in this study because they are the same as the average values in most cases.

The constant A is a function of the ice temperature and thus should vary through the glacier thickness and length (i.e., with elevation). In a temperate or subpolar glacier, the basal temperature should be at the pressure melting point, approximately 0°C. Because most of the motion due to ice deformation occurs near the base of the glacier (Nye, 1952; also Fig. 3), and because the temperature in this region should be near the pressure melting point (0 to -1°C), A was assumed constant in this study.

Basal Slip

The other component of glacier flow is from basal sliding. This has been measured to account for 3-90% of total velocity on modern glaciers (Andrews, 1975; Paterson, 1981). As discussed in the previous chapter, the component of basal sliding (referred to in this

study as basal slip) on paleoglaciers cannot be determined by subtracting calculated deformation velocity from measured surface velocity because the surface velocity cannot be measured on a vanished glacier. As a result, estimation of basal slip on paleoglaciers presented a problem. Previous studies (Haeberli and Penz, 1985, Leonard and others, 1986, McCalpin, 1986) assumed a constant percentage of slip along the entire length of the glacier.

Basal slip may occur to varying degrees along a glacier depending on the thermal and moisture regime. Even subfreezing conditions do not prevent basal sliding (Echelmeyer and Zhongxiang, 1987), although sliding velocities account for very small portions of the total velocity under those conditions. Therefore, the assumption of a constant sliding velocity at all points on the glacier (Haeberli and Penz; 1985; Leonard and others; 1986; Holmlund, 1988) is not likely to provide an accurate estimation of slip.

If the total flux on a glacier changes slowly with distance (Pierce, 1979; Raymond, 1980), highest deformation flux should be offset by lowest slip flux. Highest deformation flux occurs at the point of highest average effective basal shear stress, therefore this should also be the point of least slip. Although basal sliding should be at a minimum here, its actual percentage of total velocity cannot be determined for a paleoglacier. The assumption of zero basal slip at this point introduces the smallest possible bias to all velocity and discharge estimates, which are calculated relative to the point of highest average effective basal shear stress. Variations in basal

slip along the length of the paleoglacier can also be calculated, although these estimates will also be minima.

Because basal shear stresses may vary due to extensive and compressive flow arising from irregularities in the bedrock slope, the above approach will not work in a multi-stepped glacial valley. In this study, valleys with gentle, constantly sloping floors were used to avoid compression and extension problems. Therefore, the place where the highest average effective basal shear stress occurred was a reasonable approximation of the place where slip was at a minimum.

Average Velocity

Assuming no slip at the point of maximum average effective basal shear stress, ice surface centerline velocity (u_c) was determined using equation 4. Frictional drag on the valley floor and walls causes the average velocity of a glacier through a cross-section to be less than the centerline velocity. Nye (1965b) calculated that the ratios of average velocity through a cross-section ($\bar{u}$) to the surface centerline velocity (u_c) for glacial channels of varying parabolic shapes average $\bar{u}/u_c = 0.63$. This ratio assumes no basal sliding and therefore produces a minimum estimate of average velocity. With very high values of slip, this ratio can increase as much as 15 percent (Raymond, 1980). The calculation of u_c from equation 4 also assumes no slip; therefore a value of $.63u_c$ should be representative of the average deformation velocity ($\bar{u}$) through the cross-section.

The deformation mass flux at the point where average effective basal shear stress was a maximum was calculated by multiplying $\bar{u}$ by the cross-sectional area at that point. If the highest effective

basal shear stress occurred at the ELA, then the value derived by this method was also a minimum approximation of net mass exchange (mass balance). If the point of highest average effective basal shear stress occurred elsewhere on the glacier, net mass balance gradients were calculated for the glacier, and the mass flux at the ELA was extrapolated from this point.

Ablation/Accumulation Gradients

Net balance (accumulation and ablation) gradients define the specific net balance (average annual net gain or loss of mass) at elevations above and below the ELA, respectively. As such, the net accumulation or ablation above or below any point on a glacier can be determined by multiplying the gradients by the surface area (Fig. 15). Conversely, if the net accumulation or ablation and the surface area are known, then accumulation and ablation gradients can be calculated.

In a steady state glacier system, the mass flux at any point on the glacier is equal to the net mass gain (net accumulation - net ablation) upstream from that point. Ideally, mass flux on a glacier increases from zero at the headwall to a maximum at the ELA and then decreases in the ablation zone to zero at the terminus (Raymond, 1980). In this study, the calculated mass flux at the point of maximum deformation flux (minimum slip flux) provided a minimum estimate of the net accumulation above that point on the glacier. The surface area was determined in the reconstruction; thus net balance gradients were calculated to match the net accumulation above and the mass flux at the point of maximum deformation flux. In this study,

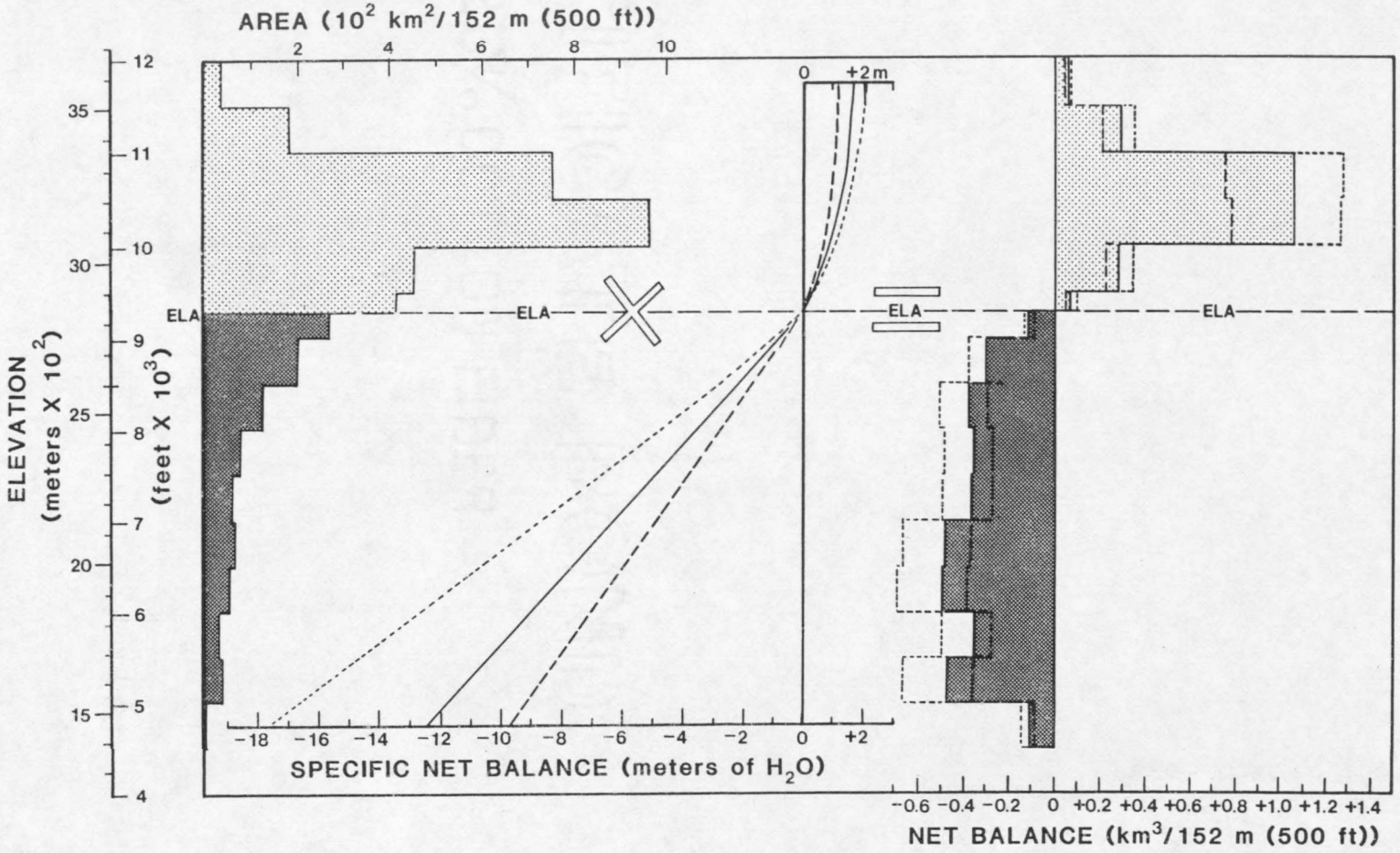

Figure 15. Mass balance of the late Pleistocene Yellowstone ice cap (Pierce, 1979). The reconstructed surface area (left) and the estimated mass flux at the ELA allow the calculation of average mass balance gradients (center), thus specific (center) and net (right) mass balance.

the point of maximum deformation flux occurred at or above the ELA, so accumulation gradients were used to produce the match. If the point of maximum deformation flux occurred below the ELA, ablation gradients would be used.

When the point of maximum deformation flux occurred at the ELA, the calculated mass flux provided a minimum estimate of the net mass exchange. Accumulation and ablation gradients that produced net accumulation and net ablation equal to the net mass exchange were then calculated (Fig. 15). When the point of maximum deformation flux occurred above the ELA, the calculated accumulation gradients produced an estimate of net accumulation above the ELA (net mass exchange) as well as the net accumulation above the point of minimum slip, because the gradients were calculated relative to the ELA. Ablation gradients that produced net ablation equal to the net mass exchange were then calculated.

The gradients also allowed an estimation of basal slip at discrete points along the glacier. From the continuity equation (Fig. 16), the difference between the mass flux at one cross-section (Q_1) and a down-ice cross-section (Q_2) is equal to the amount of mass (A) that is ablated (-) or accumulated (+) over the glacier surface area between these two cross-sections such that:

$$Q_1 + A = Q_2 \tag{6}$$

or

$$D_1 + S_1 + A = D_2 + S_2 \tag{7}$$

Average ice velocities from deformation ($\bar{u}$) were calculated at discrete points along the glacier, and when multiplied by the cross-

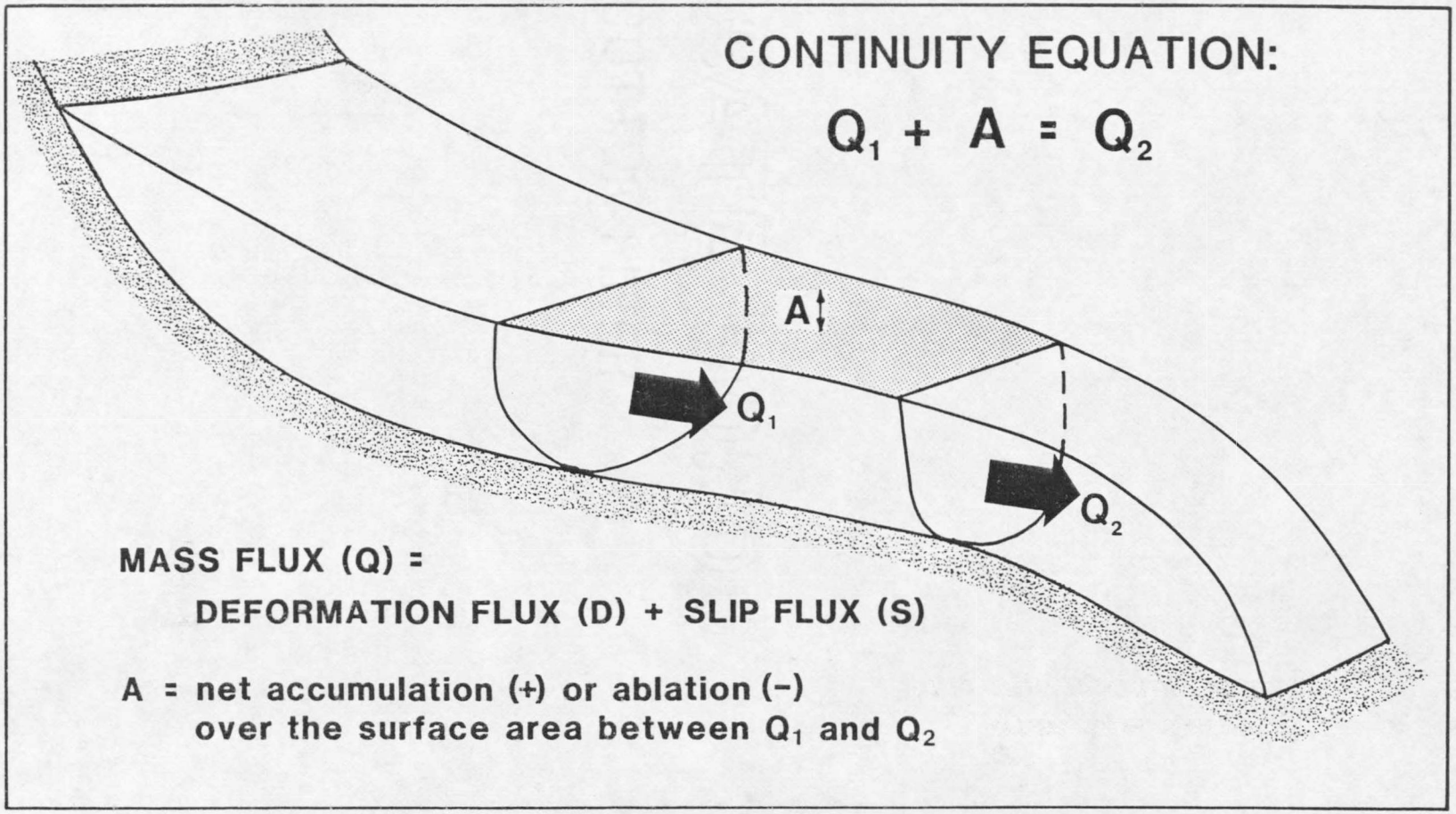

Figure 16. Continuity theory.

sectional area normal to the glacier surface at those points, provided estimates of the mass flux caused by deformation (D). Starting with the point of maximum deformation flux as D_1, deformation mass flux was calculated at the next point downstream (D_2), either the ELA or the next 200 ft (61 m) or 400 ft (122 m) contour, depending on the topographic map contour interval. The mass balance gradient between these two points determined the amount of mass (A) gained (+) or lost (-) on the glacier surface between them. At the point of maximum deformation flux (D_1), S_1 was assumed to be equal to zero, and equation 7 reduced to:

$$S_2 = D_1 + A - D_2 \qquad (8)$$

Equation 8 provided a first approximation of the slip flux component (S_2) of Q_2. This method was continued up and down the glacier using the continuity flux as Q_1 to provide basal slip estimates along the glacier's length.

Paleoclimatic Interpretation

The mass balance gradients provided an estimation of climate because they are indicative of the precipitation and temperature regimes in which the glacier exists. High ablation gradients (> 10 mm/m) are typical of maritime climates where large amounts of precipitation are offset by the moderate temperatures that induce melting (Meier and others, 1971). As the climate becomes more continental, there is less precipitation. Haeberli and Penz (1985) compared their calculated balance gradients with modern analogs and determined that the climate of the European Alps was cold and dry

during the last glacial maximum. Leonard and others (1986) concluded that the Colorado Front Range was also cold and dry by comparing their calculated gradient with modern analogs. The calculated ablation gradients in this study were also compared to modern gradients.

Another paleoclimatic variable that was determined from this study was net accumulation, which was equal to the net mass exchange. This value was divided by the accumulation area to provide an estimate of the average annual net accumulation over the accumulation area. These estimates were then compared with modern accumulation data.

Average annual precipitation data were not available for all the mountain locations in this study. Climatological reporting stations are usually situated in the valleys (NOAA, 1985a, 1985b) and precipitation data from these stations do not reflect the precipitation received at higher elevations. Modern snowpack records are available from snow courses in the mountain ranges in the study area (Soil Conservation Survey, 1986a, 1986b), providing an estimate of winter precipitation at each site.

Total water content of the snowpack is measured on or about the first of each month at these sites. The data are averaged over 25 years (1961-1985) and the maximum average snowpack was used in this study to represent the net winter accumulation at each site. Because these values represent accumulated snowpack, they may underestimate total winter precipitation. Early season snow may melt rather than accumulate and would not be included in later measurements. The maximum snowfall does not necessarily fall on the first of the month either, thus measured maximum snowpack may be less than the total

average annual snowfall in any given year. However, although the values may be minima, they are still the best available precipitation data for the mountain areas in this study.

Linear approximations of increasing snowfall with elevation have been used by others (Porter and others, 1983; Leonard, 1984; Locke, 1989) to approximate snowfall at high elevations where snow course data are not available. In reality, the relationship is non-linear at high elevations. The exact relationship can only be defined with adequate measurements and is only valid for a restricted geographic area (Locke, 1989). Because there are not enough data to define the exact relationship, linear gradients were used to approximate modern net winter precipitation.

Plots of net winter accumulation versus elevation were made for the Lemhi, Beaverhead and Crazy mountains (see Introduction, Fig. 8). The closest stations to each of the study valleys were chosen to represent the actual altitudinal distribution of total winter accumulation. Wherever possible, only stations that were on the same side of the range crest were used. An exception to this was the Crazy Mountains because no snow course data were available for the east side of the range where Big Timber Canyon is located. Data from the northwest end of the range was used instead. The Lemhi Range was divided into a northern and southern gradient to represent the difference between Mill, Stroud and Everson Creeks (northern) and Meadow Lake (southern). An average gradient using all the Lemhi stations was also determined. Calculated average annual net accumulation for each glacier was then compared with extrapolated

precipitation values from the gradients. Thus, differences between late Pleistocene and modern precipitation at all of the sites were assessed in this study.

RESULTS

Case Study - Big Timber Canyon

Valley Selection

Big Timber Canyon in the Crazy Mountains of Montana (Fig. 4) was used to develop and refine the methods presented in the previous chapter. This glacially sculpted U-shaped valley (Fig. 17,18) was chosen because it has a straight channel, few tributary cirques, well-marked trimlines and a nearly constant, gentle gradient. Glacially eroded bedrock is prevalent in the upper reaches of the valley while in the lower reaches of the valley, some valley fill is present (Fig. 18b). Big Timber Canyon meets most of the valley selection criteria and provides a good place to test the reconstruction of paleoglacier dynamics using glacial flow theory.

Glacier Geometry

The geologic evidence left by the Big Timber glacier (Fig. 18b) was determined from USGS topographic maps (scale 1:24000), aerial photographs (Appendix A), published documentation (Alden, 1932; Aten, 1974) and field survey. Trimline and moraine crest positions (Fig. 18b) were located using the air photos and plotted on the topographic maps. These features were used as the boundaries of the ice mass. The areal extent of till deposits (Fig. 18b) was determined from Aten's (1974) map. Some modifications of the extent were made using the air photos. Till blanket (Fig. 18b) refers to areas of

thick (> 3 m) till deposits (mostly moraines), whereas areas assumed to be overlain by a thin covering of till are labeled as till veneer. Areas covered by post-glacial fill (alluvium), landslide and talus deposits were also identified because those areas indicate regions where the valley shape has been modified since the glacier retreated.

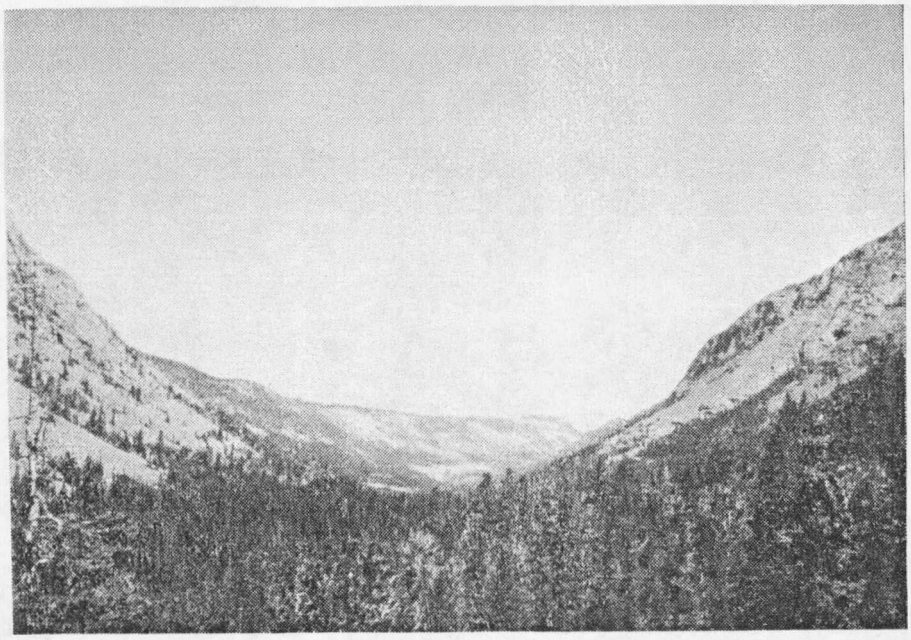

Figure 17. Photo looking down Big Timber Canyon showing the transition from a V-shaped to a U-shaped valley.

Only deposits from the Pinedale I advance identified by Aten (1974) were used in this reconstruction because that advance was the last major glaciation of the valley and those features are best preserved. Because only one maximum Pinedale moraine was identified (Aten, 1974), it was thought to correlate with the last glacial maximum, approximately 20,000 years ago (Porter and others, 1983; Richmond, 1986). Prior glaciation limits have been obscured by this

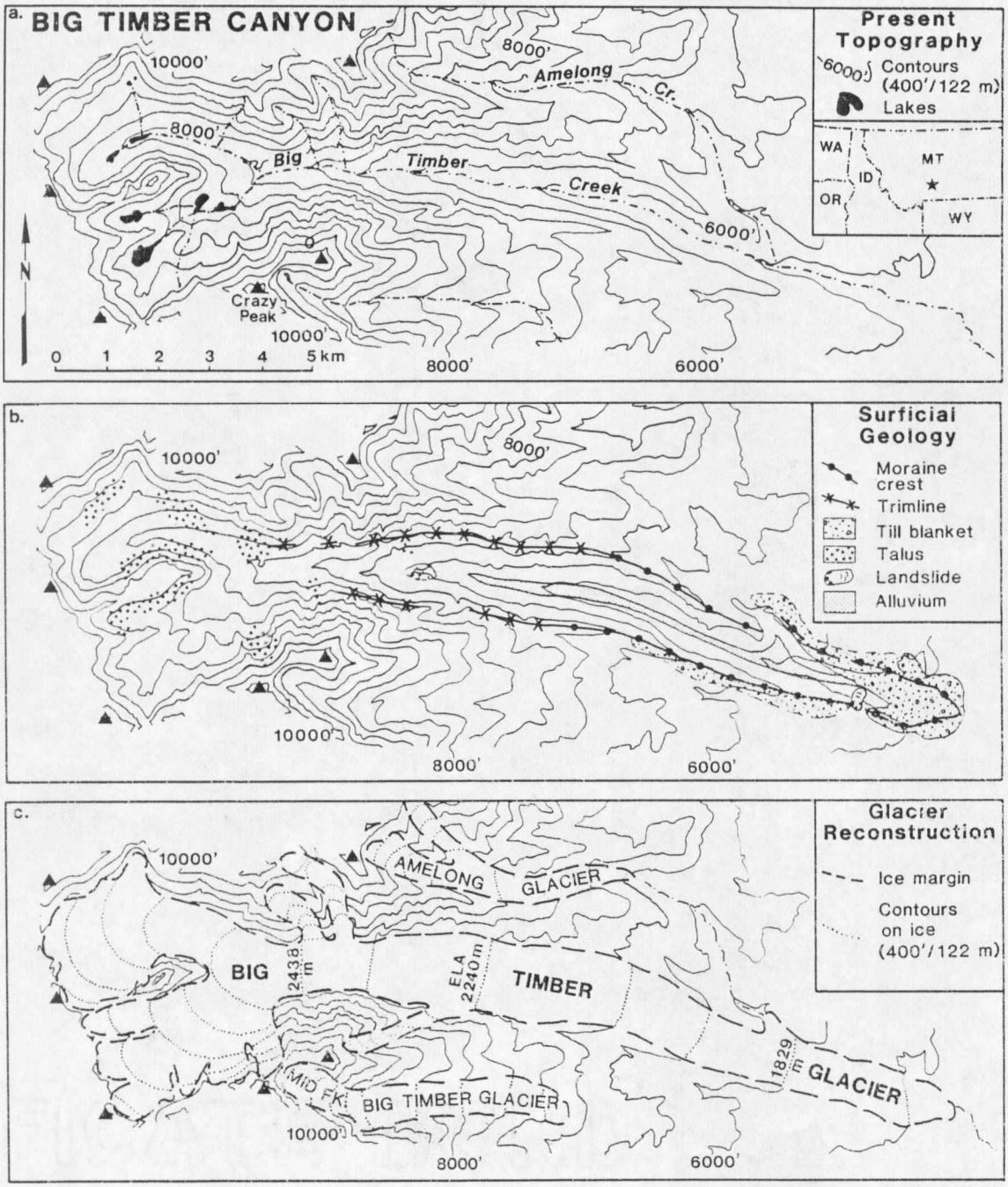

Figure 18. Map of Big Timber Canyon. Topography (a) and surficial geology (b) were used to reconstruct the glacier surface (c).

advance and subsequent glaciations were minor. Ice from both Bull Lake and Pinedale I advances filled the valley to approximately the same elevation (Aten, 1974); thus distinction between the trimlines of each advance was not possible from the air photos. Only one set of trimlines was distinguishable from the the field survey as well. Because these trimlines graded into the Pinedale I moraine crests along the valley sides (Fig. 18b), the trimlines were assumed to be the same age as the moraines. The areal extent of the paleoglacier during the last glacial maximum was determined (Fig. 18c) using these geomorphic features.

Based on the reconstruction of the areal extent (Fig. 18c), the longitudinal profile of the glacier surface was drawn along the axis of the valley (Fig. 19). Ice surface elevations were determined from the reconstructed topography (Fig. 18c), and bedrock elevations were taken from the topographic maps. Ice thicknesses near the terminus are minimum values because the bedrock in this part of the valley is covered by post-glacial fill (Fig. 18b). In the upper reaches of the valley, the stream runs along bedrock and calculated values of ice thickness on this part of the glacier are accurate.

The reconstructed geometry (Figs. 18c,19) shows that the glacier was approximately 18 km long. Approximately 14 km up the valley from the terminus, the main glacier split into two branches, both of which headed in mainly northeast-facing cirques. Three small cirques fed the main glacier between 10 and 13 km from the terminus. Maximum thicknesses were reached between 9 and 10 km up the valley from the

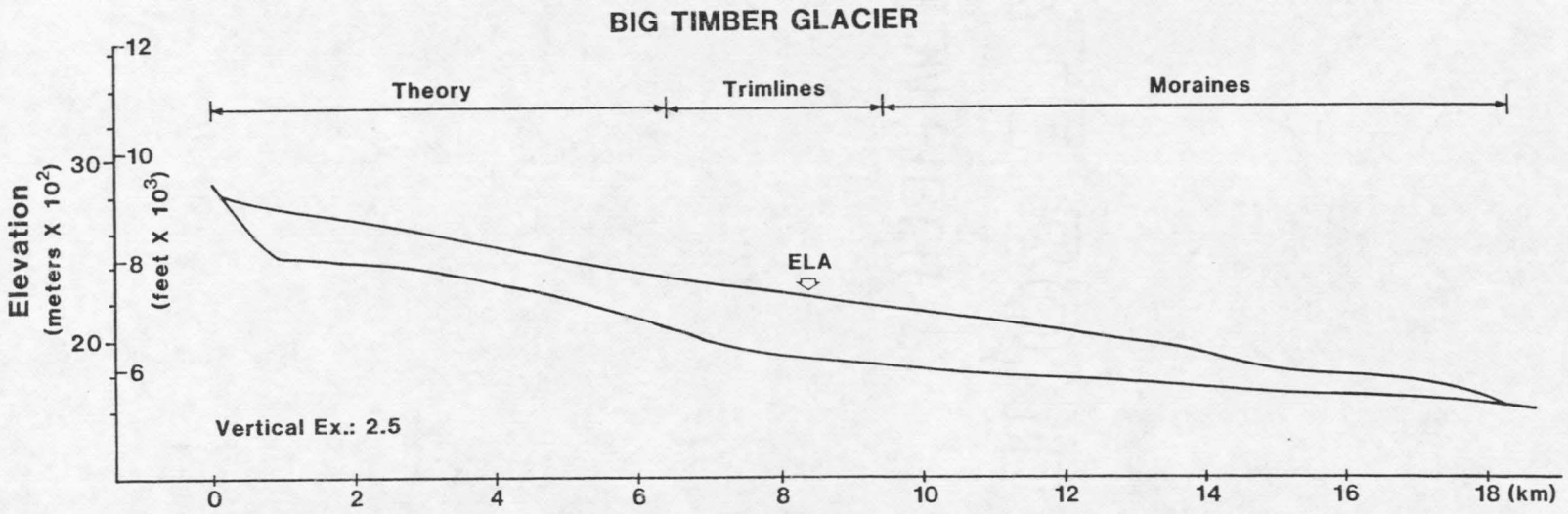

Figure 19. Longitudinal profile of Big Timber glacier.

terminus (Fig. 19, Table 2), where the glacier was 325-350 meters thick.

Basal Shear Stresses

Average effective basal shear stresses (τ_b) at the ice centerline (Table 2, Fig. 20) were calculated at 1000 ft (305 m) increments from the terminus to approximately 14.3 km up the valley, where ice marginal features became obscured. Local ice surface slopes averaged over 2000 ft (610 m) were originally used in calculating τ_b, but wide fluctuations in shear stress from step to step occurred (Fig. 20). These fluctuations in shear stress would cause fluctuations in deformation velocity from step to step also (equation 4), yet total flux on a glacier changes slowly with distance. Raymond (1980) showed that using surface slopes averaged over 8-20(H) to calculate τ_b provided better agreement with longitudinal variations in velocity than using local slopes. The shape factor (F) is also averaged over the same distance. On Big Timber glacier, ice surface slopes and shape factors averaged over 8-20(H) (8000 ft in most cases) were used to calculate the average effective basal shear stresses (Fig. 20).

Values for τ_b under the Big Timber glacier where ice marginal features are well defined (4.0 - 12.0 km from the terminus) range from 0.88 to 1.15 bars (Table 2), well within the range of the expected values. Highest average effective basal shear stresses occur 9.0-12.0 km up the valley (highest = 1.15 bars, 10.1 km), and coincide with the thickest part of the glacier (Fig. 19), illustrating the relationship of average effective basal shear stress to thickness. In the lowest reaches of the glacier (0 - 4.0 km from the terminus),

Table 2. Big Timber paleoglacier morphology and rheology interpreted from topographic maps and comparison with theoretical values.

Step No.	Distance from Terminus (km)	Bedrock Elevation (m)	Ice Elevation (m)	Ice Thickness (m)	Shape Factor	Calc. τ_b[1] (bar)	Theoretical Ice Elevation[2] (m)	Diff. (Theo.-Calc.) (m)
1	0.3	1628	1664	37	0.84			
3	0.9	1646	1725	79	0.85	0.51		
5	1.5	1658	1768	110	0.83	0.49		
7	2.1	1670	1780	110	0.78	0.31		
9	2.7	1682	1804	122	0.79	0.34		
11	3.4	1695	1823	128	0.77	0.51		
13	4.0	1707	1865	158	0.82	0.71		
15	4.6	1722	1920	198	0.69	0.88	1927	+ 7
17	5.2	1737	1963	226	0.68	0.98	1974	+ 11
19	5.8	1752	1999	247	0.69	1.01	2015	+ 16
21	6.4	1767	2042	274	0.68	1.00	2052	+ 10
23	7.0	1786	2082	296	0.68	1.00	2087	+ 5
25	7.6	1804	2109	305	0.69	1.00	2120	+ 11
27	8.2	1825	2134	308	0.69	1.01	2151	+ 17
29	8.8	1847	2170	323	0.69	1.02	2181	+ 11
31	9.4	1877	2207	329	0.67	1.12	2211	+ 5
33	10.1	1889	2240	351	0.67	1.15	2241	+ 1
35	10.7	1926	2268	341	0.66	1.10	2270	+ 2
37	11.3	1965					2301	
39	11.9	2060	2341	280	0.63	1.08	2335	- 6
41	12.5	2133	2390	256	0.63	1.04	2376	- 14
43	13.1	2200					2422	
45	13.7	2258	2487	229	0.67	1.08	2470	- 17
47	14.3	2316	2536	219	0.68	1.07	2521	- 15
49	14.9	2359	2585	226			2570	- 15
51	15.5	2389					2616	
53	16.2	2426					2660	
55	16.8	2447					2701	
57	17.4	2462					2739	
59	18.0	2731					2780	

[1]Calculated from Equation (2).
[2]Calculated from Equation (3) assuming τ_b = 1.0 bar.

unusually low values of shear stress (0.31 - 0.51 bar) occurred. The addition of melt water to the glacier bed in this region from Amelong Creek (Fig. 18a) could have significantly increased basal sliding. In such a situation, the average effective basal shear stress would be very low and the glacier surface gradient would have been lowered. Also, ice contact features in this part of the valley have been modified by stream erosion and mass wasting since they were deposited. The reconstruction in this part of the valley is tentative and may lead to the low values of average effective basal shear stress.

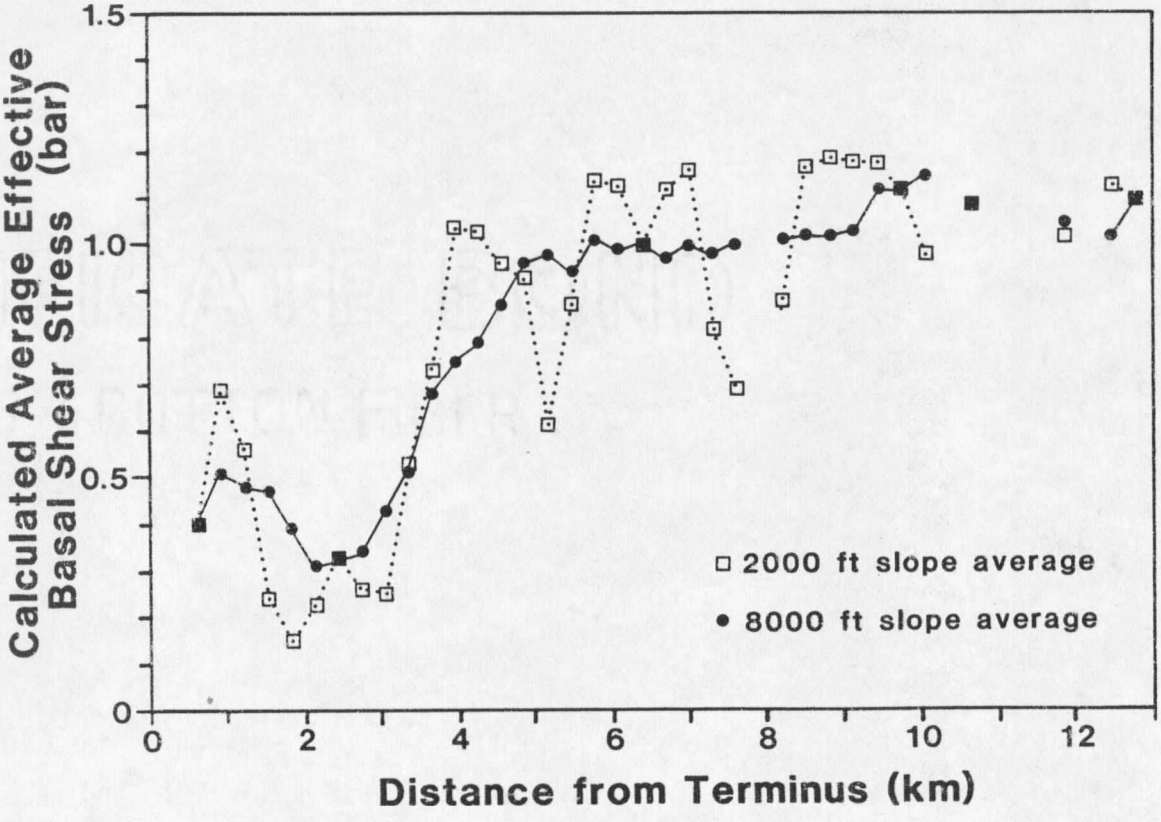

Figure 20. Average basal shear stress along Big Timber glacier with ice surface slope averaged over 2000 and 8000 ft. Gaps indicate places where the geologic evidence of ice thickness was missing.

A computer program (Appendix B) was developed (after Schilling and Hollin, 1981) to calculate the theoretical profile of a glacier using equation 3. Several theoretical longitudinal profiles were calculated for Big Timber glacier using this program. The profile using an average effective basal shear stress of 1.0 bar provided the best agreement with the ice marginal features (Table 2). In the upper reaches of the valley, where geomorphic evidence of glaciation was absent, ice surface elevations and ice thicknesses from the theoretical profile were used to calculate velocity and mass flux.

Location of the ELA

The paleo-ELA of the late Pleistocene Big Timber glacier was estimated using highest lateral moraine elevations, lowest cirque floor elevation, THAR and AAR (Meierding, 1982). Several different ratios were used for THAR (.35, .40, .45) and AAR (.60, .65, .75) to test the correlation between methods. Each method was analyzed for its reliability as related to the Big Timber glacier and the rest of the study. For Big Timber glacier, the ELAs estimated using all the methods ranged from 2163 m to 2452 m with a mean of 2252 m (Table 3).

Table 3. ELAs for Big Timber glacier using each of the methods listed in the text.

Method	Lowest Cirque Elevation	THAR .35	THAR .40	THAR .45	AAR .60	AAR .65	AAR .70	Highest Lateral Moraine
ELA (m)	2432	2163	2241	2318	2170	2231	2286	2170

Lateral Moraines. Lateral moraines in Big Timber Canyon (Fig. 18b) are well developed in the lower reaches of the valley and extend some 8.8 km up the valley. The elevation of the highest of these moraines is 2170 m on the southern edge of the glacier. Above this elevation, the glacier was confined within the walls of the canyon. The lateral moraines that may have developed on this part of the glacier would have slumped after retreat of the ice. Therefore, the portion of the moraine that is preserved in Big Timber Canyon represents a minimum estimate of ELA.

Lowest Cirque Elevation. In the Big Timber valley, there are many well defined cirques. The lowest cirque occurs in the north branch of the main valley at an elevation of 2432 m.

Toe-Headwall Altitude Ratio (THAR). THAR estimates were made using the highest ice limits on the north face of Crazy Peak at an altitude of 3170 m. Because the bedrock surface at the terminus was covered with till (Fig. 18b), the elevation of the toe of the glacier was estimated by extrapolating the elevation of the surrounding sub-alluvial terrace upon which the till was deposited (Aten, 1974). ELAs using THARs of .35, .40, .45 ranged from 2163 to 2318 m (Table 3).

Accumulation Area Ratio (AAR). The area between successive 400 ft (122 m) contours on the glacier surface (Fig. 18c) was measured using a planimeter. A cumulative total of the area from the terminus to headwall was plotted against elevation (Fig. 21). From this graph, ELAs using values of .60, .65 and .70 were determined, ranging from 2170 to 2286 m (Table 3).

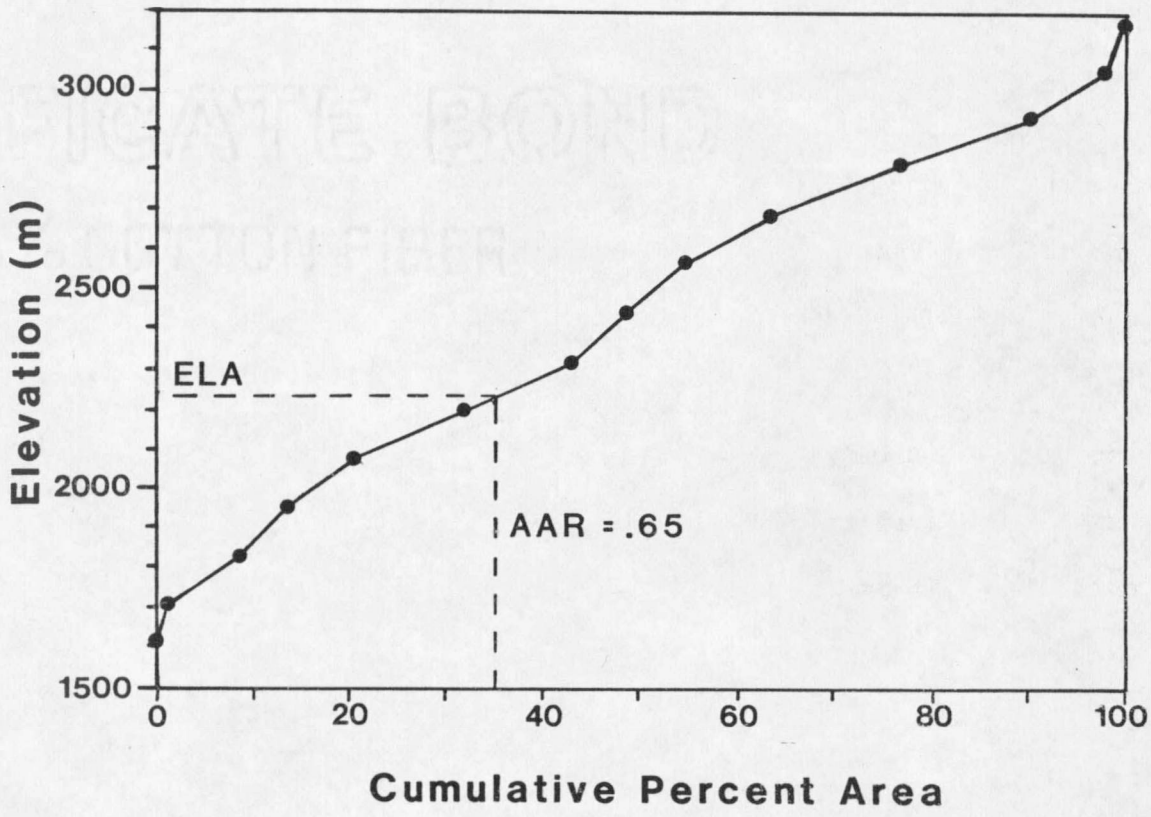

Figure 21. Hypsometric curve of Big Timber glacier used to estimate the ELA using AAR method. ELA using AAR = .65 is shown.

Final ELA. ELAs using a THAR of .35, the highest lateral moraine and an AAR of .70 were within 7 m of each other (Table 3). There was also good agreement between the THAR of .40 and the AAR of .65, both of which Meierding (1982) found to give the best results. Because mass wasting of the lateral moraines would produce a low estimate for the ELA and because Meierding found the latter two methods to produce the best results, an ELA of 2240 m was used. Mass flux through the cross-section perpendicular to the glacier surface at this elevation was used to estimate mass balance.

Glacier Flow

Glacier velocity due to deformation was calculated at discrete points along the paleoglacier using equation 2. On the Big Timber glacier, the highest average effective basal shear stress occurs by coincidence at the ELA (Table 2). Assuming no slip at this location, a calculated average effective basal shear stress of 1.15 bars, and an ice thickness of 351 m, the centerline velocity at the ELA is 44.5 m a^{-1}. This value is well within the range of velocities observed on modern glaciers (Paterson, 1981). Total average annual mass flux through the ELA (u x cross-sectional area) is 8.8 x 10^6 m^3 a^{-1}.

Because basal slip is assumed to be zero at this location, the calculated velocity and mass flux here are minima. Any value of slip can be assumed at this location, however all other values of slip flux elsewhere on the glacier will also increase. If 50% slip is assumed, u_c increases to 89.0 m a^{-1} and the mass flux at the ELA increases to 22.3 x 10^6 m^3 a^{-1} (Continuity Flux 2, Fig. 22). In that case however, slip would have to account for almost all the velocity in the rest of the glacier. This seems unlikely because the glacier was probably frozen to its bed in the cirque regions.

Ablation/Accumulation Gradients

On a steady state glacier such as the Big Timber glacier, the mass that moves through the ELA must be lost in the ablation zone. A specific linear ablation gradient will provide the balance between the net mass exchange and the mass ablated over the glacier surface area below the ELA. The area between successive 400 ft (122 m) contours on the glacier was already determined for locating the ELA using AAR.

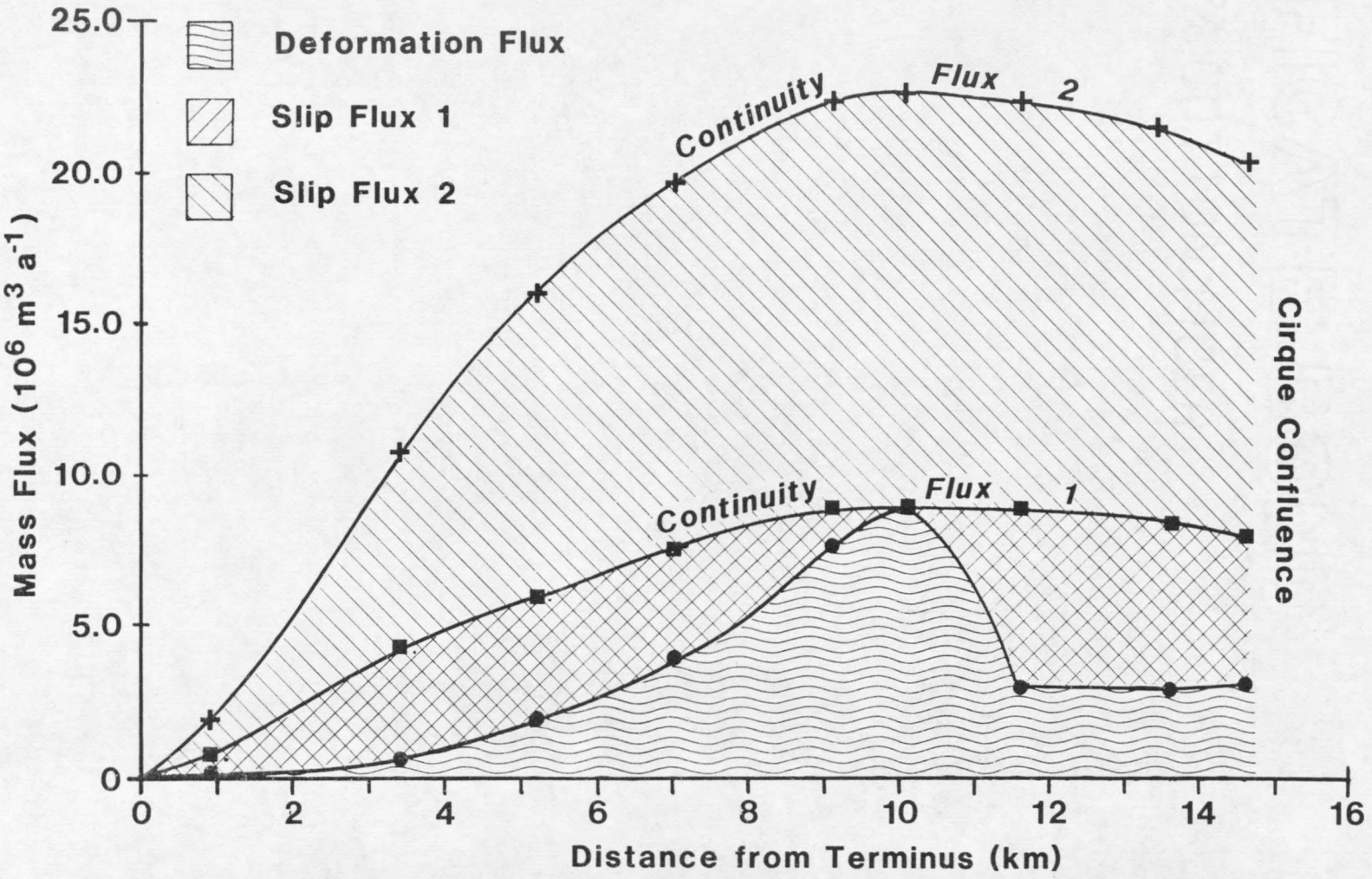

Figure 22. Mass flux on Big Timber glacier. Continuity Flux 1 assumes no slip at the ELA, continuity flux 2 assumes 50% slip at the ELA. Slip flux is the difference between continuity flux and deformation flux.

The midpoint elevation of each of these areas is used as the average elevation of the entire area. A simple program was developed (Appendix D) to calculate the amount of ablation that would occur on the glacier in each contour interval, using the average altitude of the area below the ELA, a specific linear gradient and the surface area (Table 4). Only one gradient (within the limits of resolution) will produce a balance between the net mass flux at the ELA and the amount ablated on the glacier surface (Fig. 23). The accumulation gradient is calculated in a similar manner, using the surface areas above the ELA (Appendix E).

Table 4. Calculation of average annual net ablation on Big Timber glacier using area and elevation.

Mass Flux at ELA = 8.8 X 10^6 m^3 a^{-1} Ablation Gradient = 3.0 mm/m

(1) Elevation Interval (m)	(2) Surface Area (10^6 m^2)	(3) Average Altitude below the ELA (m)	(4) Specific Balance (3) x gradient (m)	(5) Volume Lost (2) x (4) (10^6 m^3)
2195-2240	.98	23	0.069	0.067
2073-2195	3.76	106	0.320	1.203
1951-2073	2.3	228	0.686	1.577
1829-1951	1.6	350	1.052	1.682
1707-1829	2.4	472	1.417	3.402
1615-1707	.47	579	1.737	0.817
			Net Ablation =	8.749

For the Big Timber glacier, an ablation gradient of 3.0 $\pm$ 0.6 mm/m produced the balance between net mass exchange and ablation. An accumulation gradient of 1.0 $\pm$ 0.2 mm/m above the ELA produced a balance between net accumulation and net mass exchange (Fig. 23).

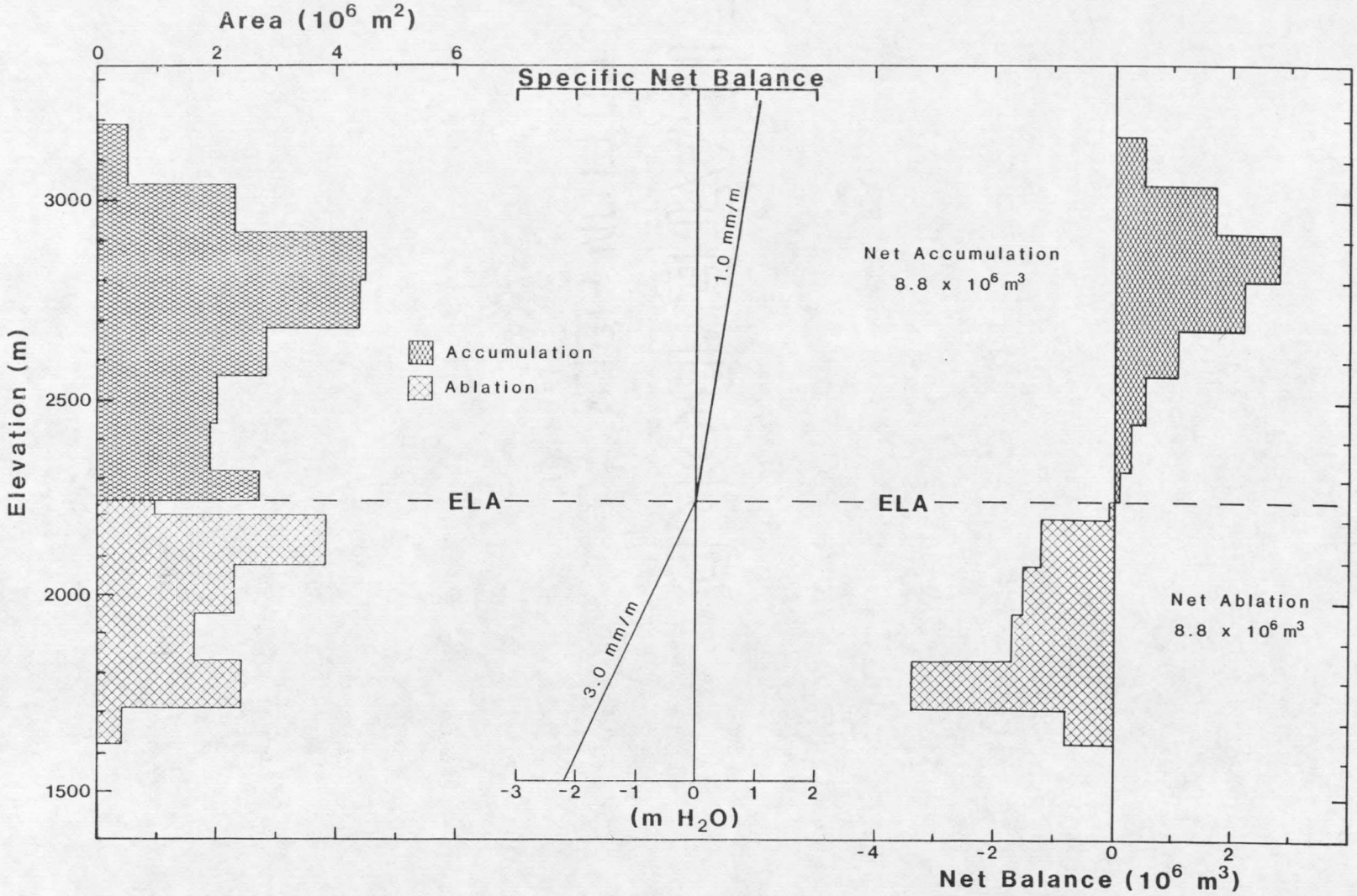

Figure 23. Mass balance of the late Pleistocene Big Timber glacier.

Such a low gradient is typical of cold, low-moisture environments (e.g., McCall Glacier, Brooks Range, Alaska: 2 mm/m; Meier and others, 1971) showing that the Big Timber glacier at its peak was sustained more by low temperatures than by high precipitation.

The accumulation and ablation gradients also allow an estimation of basal slip around the point of assumed no-slip as outlined in the previous chapter. Table 5 shows the estimated slip up- and down-ice from the ELA on the Big Timber glacier. Slip becomes the dominant part (>90%) of the flow in the lower 4.0 km of the glacier. Because Amelong Creek was supplying meltwater from Amelong Glacier (Fig. 18c) to the bed of Big Timber glacier at this point, a substantial increase in basal slip is logical. Even with the accepted error in the deformation mass flux on this glacier (see next section), continuity theory shows that basal slip was the dominant part of flow in this part of the glacier. Slip is also required above the ELA, and was responsible for at least 60% of the total flow (Fig. 22, Table 5).

Sensitivity and Error Analysis

The calculations of τ_b, u_c and mass balance are only as good as the data and assumptions on which they were based. All values of surface slope, ice thickness and cross-sectional area were analyzed from topographic maps, using air photos and published documentation as aids in the analysis. Limited field work was done to check whether the valley floor was bedrock or fill. Using Big Timber as the test case, sensitivity of the model to changes in surface slope and thickness was performed to determine the error limits of the model.

Table 5. Mass balance and basal slip results for Big Timber glacier.

	Point of Maximum Shear Stress (ELA)
Ice surface elevation (m)	2240
Centerline ice velocity (u_c) (m a^{-1})	44.5
Deformation mass flux (m^3 a^{-1})	8.8×10^6

Mass Balance

Accumulation Gradient = 1.0 ± .20 mm/m
Ablation Gradient = 3.0 ± .60 mm/m
Net Winter Precipitation = .42 ± .08 m

Basal Slip Calculations

(1) Ice Elevation (m)	(2) Mass Gain(+) /Loss(-) (10^6 m^3)	(3) Continuity Mass Flux (10^6 m^3 a^{-1})	(4) Cross Sectional Area[1] (10^5 m^2)	(5) Average Velocity (3)/(4) (m a^{-1})	(6) Creep Velocity ($\bar{u}$) (m a^{-1})	(7) Slip Velocity (5)-(6) (m a^{-1})	(8) % Slip
2560-3170	+7.88	7.9	2.86	27.6	11.0	16.6	60
2438-2560	+ .518	8.4	1.90	44.2	14.6	29.6	67
2316-2438	+ .314	8.7	1.55	56.1	18.5	37.6	67
2240-2316	+ .104	8.8	3.17	28.1	28.1	0.0	0
2195-2240	- .067	8.7	3.11	28.0	24.3	3.7	13
2073-2195	-1.20	7.5	2.37	31.8	16.7	15.1	48
1951-2073	-1.58	5.9	1.41	42.2	13.4	28.8	68
1829-1951	-1.68	4.2	0.86	49.8	7.7	42.1	85
1707-1829	-3.40	0.80	0.47	18.4	1.2	17.2	93
1615-1707	-0.82	0					

[1]Cross sections are taken at the lowest elevation in each area.

The accuracy of the topographic maps may well be the most important question when determining error. Thompson (1979) shows that for statistical purposes, the allowable root mean square error (RMSE) for a topographic map of scale 1:24,000 is:

$$\text{allowable RMSE} = 0.3CI + 24(\tan a) \qquad (9)$$

where CI = contour interval and a = slope angle. In the Big Timber

study, the maps that were used had contour intervals of 20, 40 and 80 ft (6.1, 12.2, 24.4 m). Most of the glacier surface that was calculated from ice marginal features lay within the 40 ft (12.2 m) contour map. Slope angles along the moraine crests were well below 20°; thus tan a is almost negligible. For this map, the allowable RMSE (one standard deviation) is ± 20 ft (6.1 m) assuming a slope of 18°. However, this is the allowable two-tailed vertical error for any single point on a map; thus the probability of the point elevation being greater than or less than this limit is 0.16. Calculations of slope and thickness are determined from multiple points, thus the probabilities of errors being at the extremes are multiplicative. Table 6 shows the calculations of slope, thickness, average effective basal shear stress and centerline velocity based on the maximum errors for 0.5, 0.83 and 1.0 times the RMSE (σ) along with the probabilities of these events occurring. These results show that even for .5 σ (± 3.0 m) with a maximum accumulated calculation error of ± 20%, the probability that compounding errors of thickness and slope estimation will occur is only 0.0092. Based on these probabilities, it is likely ($p > 99\%$) that the calculated values of τ_b, u_c and mass flux using the topographic map data are valid ± 20%.

Ice surface slope produced the most variance in calculations of average effective basal shear stress (Table 6). Because glacier velocity is not affected by local changes in surface slope (Raymond, 1980), ice surface slope was averaged over 8-20(H) (2.4 km for Big Timber glacier). Inherent errors from the topographic maps are also

Table 6. Error and probability analysis of map-induced errors on basal shear stress and velocity calculations at the ELA for Big Timber glacier.

Error	none	$.5\sigma$ [1] (± 3.0 m)			$.83\sigma$ (± 4.6 m)			σ (± 6.1 m)		
		High	Low[2]	p[3]	High	Low	p	High	Low	p
Slope ($\sin\alpha$)	.055	.057	.052	.096	.059	.051	.044	.060	.050	.026
τ_b (bar)	1.15	1.19	1.09		1.23	1.07		1.25	1.05	
Thickness (m)	351	357	344	.096	360	341	.044	363	338	.026
τ_b (bar)	1.15	1.17	1.13		1.18	1.12		1.19	1.11	
τ_b using combined worst error	1.15	1.21	1.07	.0092	1.26	1.04	.0019	1.29	1.01	.0006
Centerline Velocity ($m\ a^{-1}$)	44.5	52.8	35.2	.0092	60.1	32.1	.0019	65.0	29.1	.0006

[1] σ = root mean square error (RMSE). See text for explanation.
[2] High and Low refer to the highest and lowest values using the maximum combined error in each column.
[3] Probability of these errors occurring.

reduced when a longer step length is used. The percentage errors in vertical rise are diminished by longer lengths of horizontal distance.

Ice thickness also affected the calculations of τ_b and u_c but was less of a control than surface slope (Table 6). The errors induced from reading the topographic maps are shown in Table 6, but another error in determining ice thickness comes from the assumption that the centerline elevation equals the ice marginal elevation. As stated earlier, comparison to modern glaciers (Fig. 12) shows that centerline elevation is generally slightly higher than the ice margin below the ELA and generally much lower above the ELA. Because the average variation below the ELA is minor and shows no constant trend, no correction factor was added to the ice thickness and therefore values

of τ_b may be low by about 0.04 bar. Above the ELA, most of the centerline elevations are based on the theoretical profile which was lower than the observed features (Table 2), which agrees with the observations on modern glaciers (Fig. 12).

Another error in calculating thickness is induced by assuming that the valley floor is bedrock. In Big Timber Canyon, field survey showed that most of the upper part of the valley is bedrock. In the lower reaches, the valley bottom was covered with alluvium and till; thus the ice thicknesses here are probably underestimated. Because some bedrock outcrops also occur in this region, the till covering is probably thin and thus does not produce much error.

Errors in ice thickness will also affect the calculations of the shape factor (F), which is determined from the ratio of the glacier half-width to centerline thickness (Nye, 1965b). Due to the generally large thicknesses and glacier widths, errors in calculated ice thickness only change the shape factor by approximately .01. The shape factors used in calculating average effective basal shear stress were averaged over the same distance as slope (2.4 km) and should thus reflect the smoother profile of glacier velocity shown on modern glaciers (Raymond, 1980).

An error in mass flux can be produced in the calculation of the cross-sectional areas. Successive planimetry of several cross-sectional areas produced a standard deviation of 1% or less. Therefore, error from the planimeter is negligible. Talus, alluvium and till will affect the shape of the cross-section and induce some

error. However, given the size of the cross-sections, it is felt that this error is also negligible (1%).

For a given glacier length and valley shape, more mass must flow through the ELA on a maritime glacier than a continental glacier to offset the higher accumulation (Fig. 11). Surface slope is largely dependent on valley slope, thus only an increase in thickness and or basal sliding can account for this change in velocity. The estimated thicknesses are accurate ± 20%. Calculated mass balances should be reflective of actual conditions on these paleoglaciers, unless basal slip was greatly increased.

The least likely assumption in this model is that basal slip is zero where deformation velocity is at a maximum. While this assumption may not be true, relative changes in slip from one point to another on the glacier are well modelled using the continuity equation. This is better than assuming a constant slip across the glacier, which is clearly not the case for the Big Timber Glacier (Table 5).

Results from other Valleys

Lemhi Range

The Lemhi Range of east-central Idaho was extensively glaciated during the Pleistocene as evidenced by the many U-shaped valleys. Based on the valley selection criteria, four valleys in this range (Fig. 6) were chosen to be used in this study. Two adjacent valleys (Stroud Creek and Everson Creek) were selected to test the

reproducibility of the model between adjacent valleys of similar size and shape.

Stroud Creek Glacier. Stroud Creek lies in the northern end of the Lemhi Range and flows northeastward through a U-shaped valley (Fig. 24a). The valley splits into two cirques at its head and has a relatively constant gradient (Fig. 25). Glacial trimlines are easily identifiable in air photographs and on the topographic maps as are several moraine crests (Fig. 24b). No field survey was performed in this valley. Because the glacial evidence is well preserved in Stroud Creek valley, it was assumed that field checking would not significantly alter the results. Published documentation (Ruppel, 1980) does not distinguish the relative ages of the moraines, so the largest, well-defined moraines were assumed to correlate with the last glacial maximum.

Bedrock is well exposed in the valley floor except near the terminal moraine area. One large Holocene landslide (Ruppel, 1980) produced some modification of the valley approximately 2 km up the valley from the glacier terminus (Fig. 24b), however, the areal extent of this modification is minimal. Therefore, values of ice thickness are accurate except in the area near the paleoglacier terminus.

The paleoglacier was approximately 7.5 km long and reached a maximum thickness of 158 m at 3.6 km up valley from the terminus (Fig. 24c,25). The highest average effective basal shear stress (1.02 bar) occurred on the glacier at a surface elevation of 2609 m (3.9 km from the terminus). Ice surface slope was averaged over 4000 ft (1.3 km). A theoretical profile using an average effective basal shear

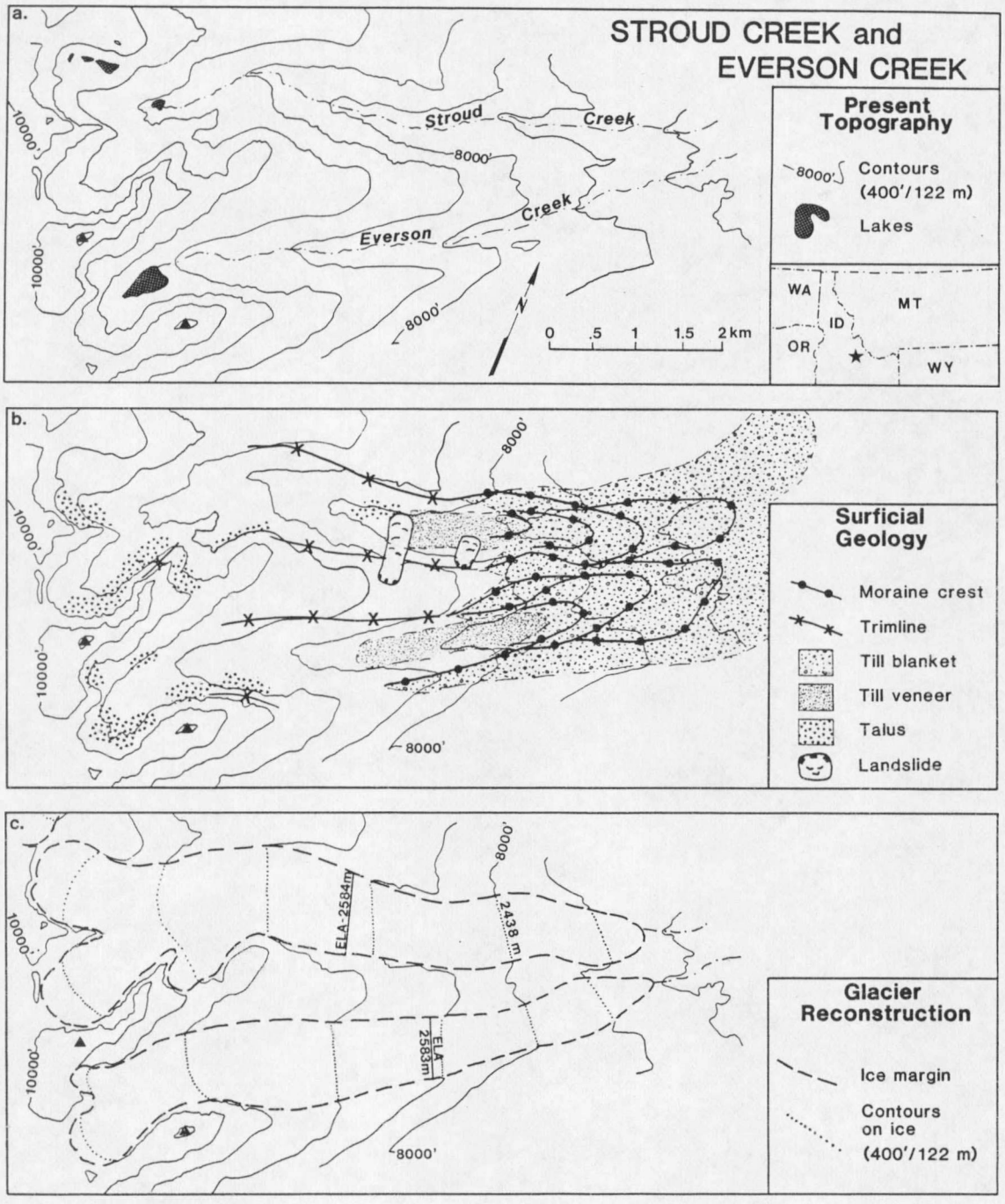

Figure 24. Map of Stroud and Everson Creek valleys and the glacier reconstructions.

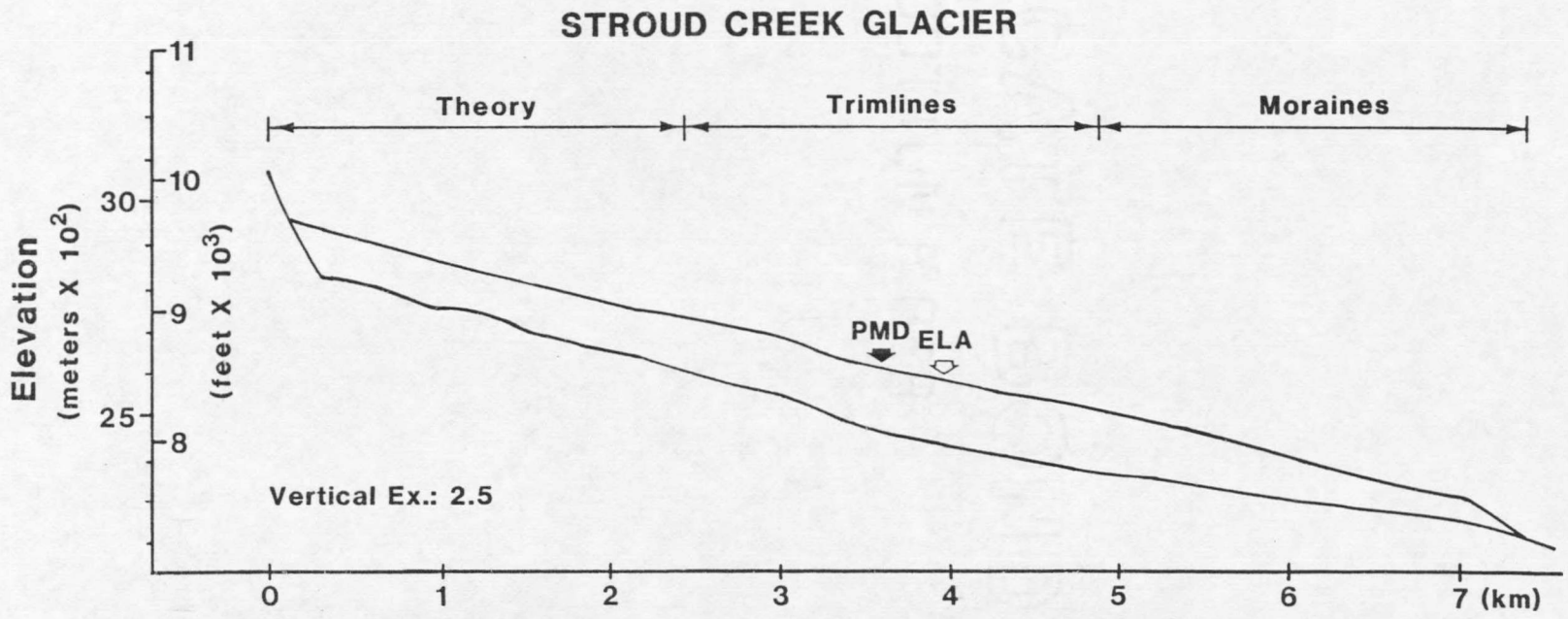

Figure 25. Longitudinal profile of Stroud Creek glacier. PMD is the point of maximum deformation flux.

stress of .80 bar produced the best correlation to the geologic evidence and was used to estimate ice surface elevation in the cirque area. The ELA was estimated at 2584 m (Table 7).

Table 7. Mass balance and basal slip results for Stroud Creek Glacier.

	Point of Maximum Shear Stress	ELA
Ice surface elevation (m)	2609	2584
Centerline ice velocity (u_c) (m a^{-1})	13.5	7.3
Deformation mass flux (m^3 a^{-1})	7.59 x 10^5	4.11 x 10^5

Mass Balance

Accumulation Gradient = 0.8 ± .16 mm/m
Ablation Gradient = 2.4 ± .48 mm/m
Net Winter Precipitation = .17 ± .03 m

Basal Slip Calculations

(1) Ice Elevation (m)	(2) Mass Gain(+) /Loss(-) (10^6 m^3)	(3) Continuity Mass Flux (10^5 m^3 a^{-1})	(4) Cross Sectional Area (10^4 m^2)	(5) Average Velocity (3)/(4) (m a^{-1})	(6) Creep Velocity ($\bar{u}$) (m a^{-1})	(7) Slip Velocity (5)-(6) (m a^{-1})	(8) % Slip
2682-3048	+.684	6.84	9.23	7.4	5.9	1.5	20
2609-2682	+.030	7.14	8.93	8.0	8.5	0	0
2585-2609	+.003	7.17	8.91	8.0	4.6	3.4	43
2560-2585	-.007	7.10	7.15	9.9	3.8	6.1	62
2438-2560	-.230	4.80	6.25	7.7	3.3	4.4	57
2316-2438	-.349	1.31	2.18	6.0	.15	5.9	98
2219-2316	-.142	0					

The point of assumed no-slip occurred above the ELA, and an accumulation gradient of 0.8 ± .16 mm/m produced the best (within limits of resolution) balance between net accumulation up to that point (7.1 x 10^5 m^3 a^{-1}) and the deformation mass flux through the glacier cross-section at that point (7.6 x 10^5 m^3 a^{-1}). Using this gradient, the total net accumulation above the ELA was 7.2 x 10^5

$m^3\ a^{-1}$. Comparison of the deformation mass flux at the ELA (4.1×10^5 $m^3\ a^{-1}$) and the total net accumulation, which equals the actual mass flux through the ELA, shows that basal slip accounted for 43 percent of the velocity at the ELA (Table 7). An ablation gradient of 2.4 ± .48 mm/m produced a balance between total net ablation over the glacier surface below the ELA and the average annual mass flux at the ELA. Basal slip accounts for approximately 60 percent of the mass flux below the ELA except in the very terminus where slip is clearly dominant (Table 7). Above the ELA, deformation flux is dominant.

Everson Creek Glacier. Everson Creek runs through the valley immediately south of Stroud Creek (Fig. 24a). The valley is similar in size to Stroud Creek valley with a little straighter and more northerly trending channel. No field survey was performed in this valley either; however, trimlines and moraine crests show up well on both the air photographs and the topographic maps. Published documentation on this valley (Ruppel, 1980) does not distinguish between the ages of the moraines, and moraines with a similar morphology to the ones used in Stroud Creek were assumed to correlate to the same advance (Fig. 24b). There is evidence that prior to the last glacial maximum, the two glaciers merged at their distal ends and flowed further down the valley. There has been some post-glacial modification of the valley shape especially in the lower 1.5 km of the valley.

The paleoglacier was approximately 7.2 km long and reached a maximum thickness of 149 m at 4.3 km up valley from the terminus (Fig. 24c,26). The highest average effective basal shear stress

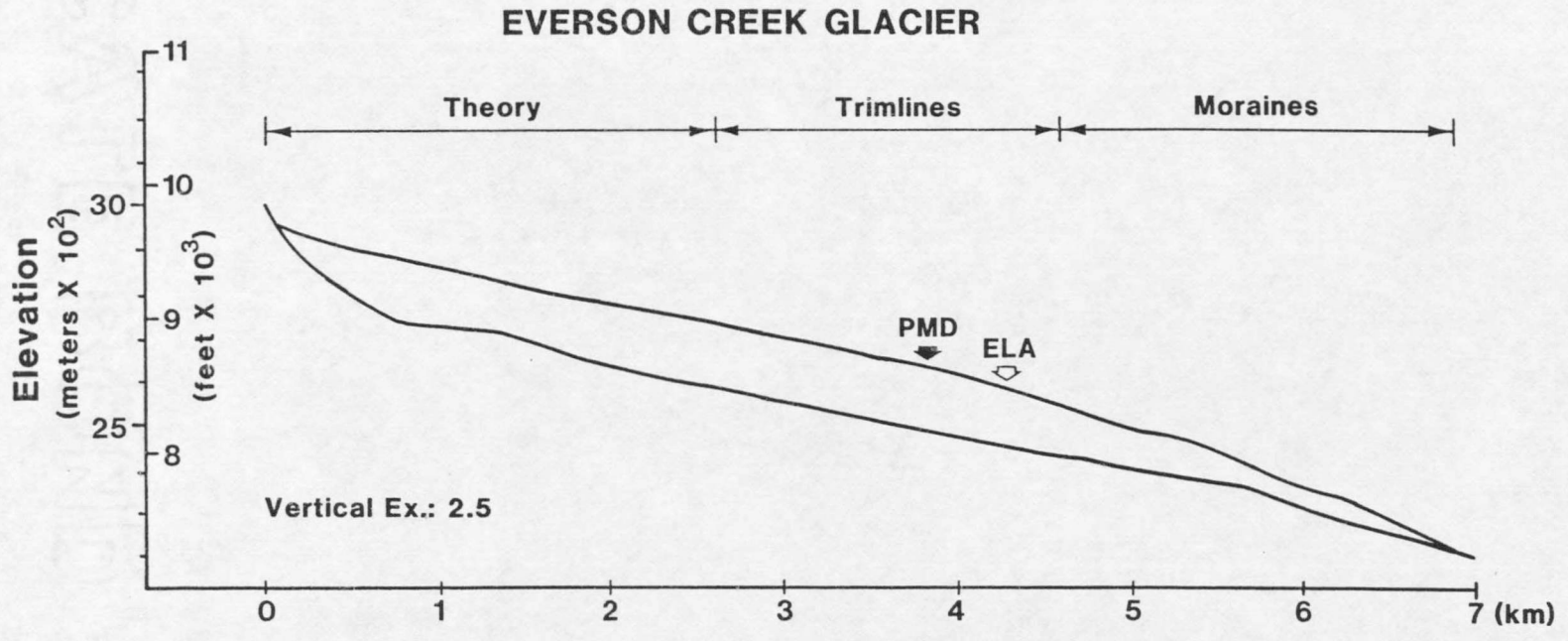

Figure 26. Longitudinal profile of Everson Creek glacier.

(.94 bar) occurred 3.0 km up the valley where the surface elevation was 2633 m. Ice surface slope was averaged over 4000 ft (1.3 km). A theoretical profile using an average effective basal shear stress of .80 bar produced the best agreement with the geologic evidence. The ELA was estimated at 2583 m (Table 8).

Table 8. Mass balance and basal slip results for Everson Creek Glacier.

	Point of Maximum Shear Stress	ELA
Ice surface elevation (m)	2633	2583
Centerline ice velocity (u_c) (m a^{-1})	10.2	8.1
Deformation mass flux (m^3 a^{-1})	4.02×10^5	2.77×10^5

Mass Balance

Accumulation Gradient = 0.7 ± .14 mm/m
Ablation Gradient = 1.9 ± .38 mm/m
Net Winter Precipitation = .12 ± .02 m

Basal Slip Calculations

(1) Ice Elevation (m)	(2) Mass Gain(+) /Loss(-) (10^6 m^3)	(3) Continuity Mass Flux (10^5 m^3 a^{-1})	(4) Cross Sectional Area (10^4 m^2)	(5) Average Velocity (3)/(4) (m a^{-1})	(6) Creep Velocity ($\bar{u}$) (m a^{-1})	(7) Slip Velocity (5)-(6) (m a^{-1})	(8) % Slip
2804-3048	+.235	2.36	7.27	3.3	3.8	0	0
2682-2804	+.149	3.85	7.84	4.9	3.5	1.4	29
2633-2682	+.015	4.00	6.54	6.1	6.3	0	0
2585-2633	+.007	4.07	5.44	7.5	5.1	2.4	32
2560-2585	-.005	4.02	4.85	8.3	5.2	3.1	37
2438-2560	-.091	3.11	1.79	17.4	.62	16.8	96
2316-2438	-.193	1.18	1.31	9.0	.56	8.4	93
2219-2316	-.108						

An accumulation gradient of 0.7 ± .14 mm/m produced the best balance between net accumulation up to 2633 m (4.0×10^5 m^3 a^{-1}) and the deformation mass flux through the cross-section at this point

(4.2×10^5 m^3 a^{-1}). The total net accumulation above the ELA using this gradient was 4.1×10^5 m^3 a^{-1}. Basal slip accounted for 32 percent of the total motion at the ELA and became the dominant part of the motion in the lower 1.5 km of the glacier (Table 8). An ablation gradient of 1.9 ± .38 mm/m provided the balance between net ablation below the ELA and average annual mass flux through the ELA.

The calculated values of mass balance gradients and average annual net accumulation (Table 8) for Everson Creek glacier compare favorably with those for Stroud Creek glacier (Table 7). Both glaciers appear to have been sluggish, slow-moving glaciers sustained by low moisture.

Mill Creek Glacier. Mill Creek, located two valleys to the north of Stroud and Everson Creeks, flows northeastward through a glacially sculpted, U-shaped valley (Fig. 27a). At the eastern end of the valley, the stream is diverted northward by a large right-lateral moraine. The valley heads in a two-tiered northeast facing cirque with several tarns. Several nested moraines (Fig. 27b) can be identified on the air photographs and in the field, however published documentation (Ruppel, 1980) does not distinguish between the relative ages of the moraines, so the largest, well-defined terminal moraine was assumed to correlate with the last glacial maximum.

The valley has been subjected to post-glacial modification, especially in its lower reaches. Two large landslides have obliterated the right lateral moraine at its proximal end. Numerous recessional and re-advance moraines cover the valley floor in the lower reaches. Thus, reconstructed ice thicknesses in the lower

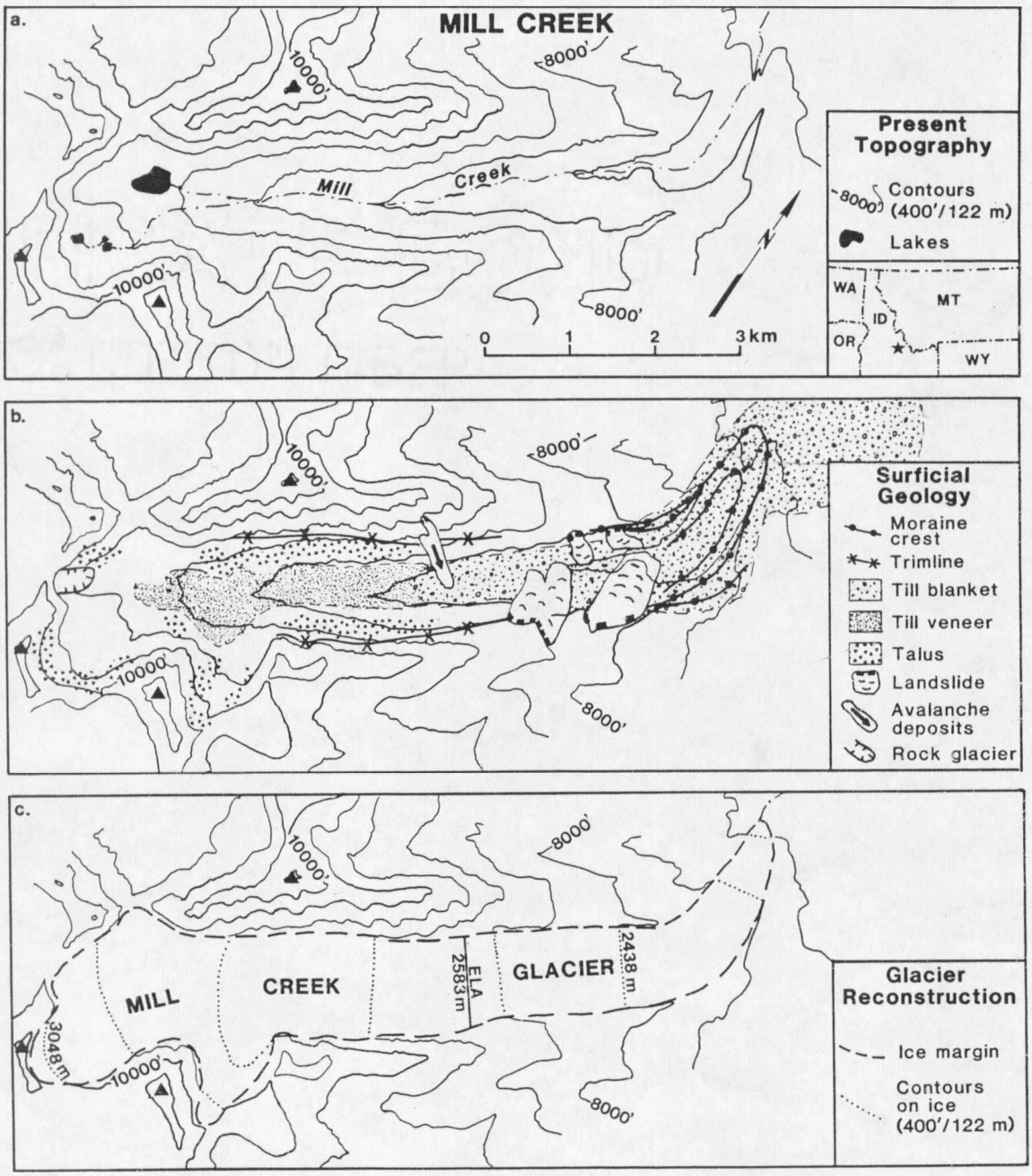

Figure 27. Map of Mill Creek valley and the glacier reconstruction.

portions of the valley (0-4 km from the terminus) are most likely minimum values. Talus and avalanche deposits line the base of the slopes along the valley walls. Because there are also bedrock outcrops along the valley floor from midway up the valley to the cirque, these deposits do not contribute appreciable error to the valley cross-section area calculations.

The reconstructed glacier was approximately 10.3 km long and reached a maximum thickness of 232 m at 5.5 km from the terminus (Fig. 27c,28). The maximum average effective basal shear stress of 1.09 bars was reached at 7.9 km (2780 m elevation), just below the confluence with a tributary cirque. A theoretical profile using an average basal shear stress of .90 bar provided the best match with the geomorphic evidence and was used to estimate ice surface elevation in the cirque. The ELA was estimated at 2583 m.

An accumulation gradient of 1.9 ± .38 mm/m produced the best match between net accumulation above 2780 m (2.69×10^6 m^3 a^{-1}) and the deformation mass flux at 2780 m (2.76×10^6 m^3 a^{-1}). Continuity mass flux at the ELA using this gradient was 3.29×10^6 m^3 a^{-1}, with basal slip accounting for 27 percent of the velocity at this point (Table 9). An ablation gradient of 5.6 ± 1.1 mm/m produced a balance between total net ablation and the average annual mass flux at the ELA. As in the other glaciers, basal slip accounts for most of the mass flux in the lowest portions of the glacier.

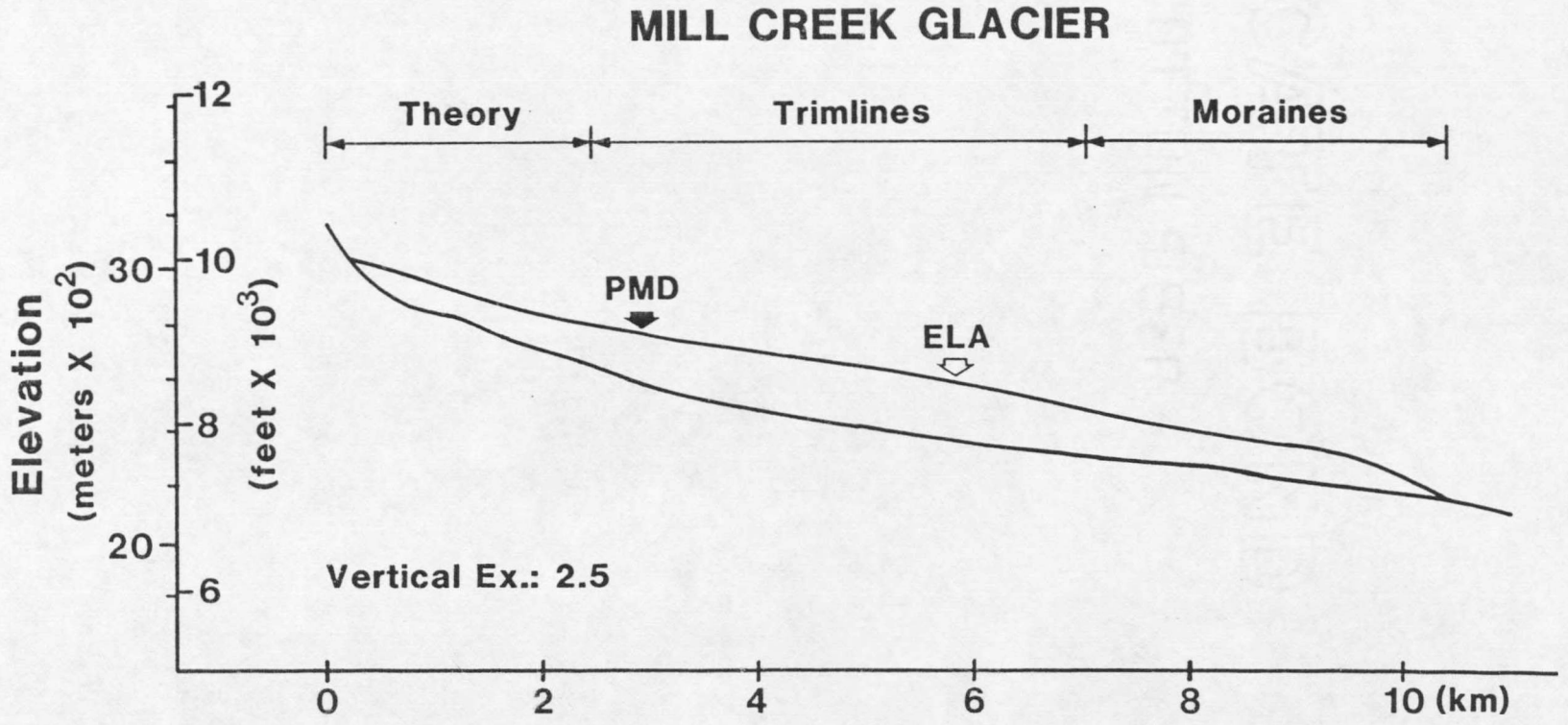

Figure 28. Longitudinal profile of Mill Creek glacier.

Table 9. Mass balance and basal slip results for Mill Creek Glacier.

	Point of Maximum Shear Stress	ELA
Ice surface elevation (m)	2780	2583
Centerline ice velocity (u_c) (m a^{-1})	23.7	23.9
Deformation mass flux (m^3 a^{-1})	2.76×10^6	2.40×10^6

Mass Balance

Accumulation Gradient = 1.9 ± .38 mm/m
Ablation Gradient = 5.6 ± 1.1 mm/m
Net Winter Precipitation = .42 ± .08 m

Basal Slip Calculations

(1) Ice Elevation (m)	(2) Mass Gain(+) /Loss(-) (10^6 m^3)	(3) Continuity Mass Flux (10^5 m^3 a^{-1})	(4) Cross Sectional Area (10^4 m^2)	(5) Average Velocity (3)/(4) (m a^{-1})	(6) Creep Velocity ($\bar{u}$) (m a^{-1})	(7) Slip Velocity (5)-(6) (m a^{-1})	(8) % Slip
2780-3169	+2.69	2.69	1.85	14.5	14.9	0	0
2682-2780	+ .464	3.15	1.68	18.8	11.0	7.8	41
2585-2682	+ .145	3.29	1.59	20.7	15.1	5.6	27
2560-2585	- .017	3.27	1.38	23.7	13.0	10.7	45
2438-2560	- .727	2.55	.956	26.7	2.3	24.4	91
2316-2438	-1.81	0.73	.449	16.3	2.4	13.9	85
2194-2316	- .634	0.10	.0054	18.5	.19	18.3	99
2164-2194	- .091	0.01					

Meadow Lake Glacier. Meadow Lake Canyon, located in the east-central portion of the Lemhi Range, has a well developed U-shape and heads in a bowl shaped cirque, occupied by a tarn (Meadow Lake) (Fig. 29a). The valley is relatively straight and trends northeastward. Knoll (1977) investigated the glacial history of the valley and identified thirteen distinct glacial advances. The deposits and scouring features of the first glacier of Glaciation III (Knoll, 1977) have subsequently been correlated to the last glacial

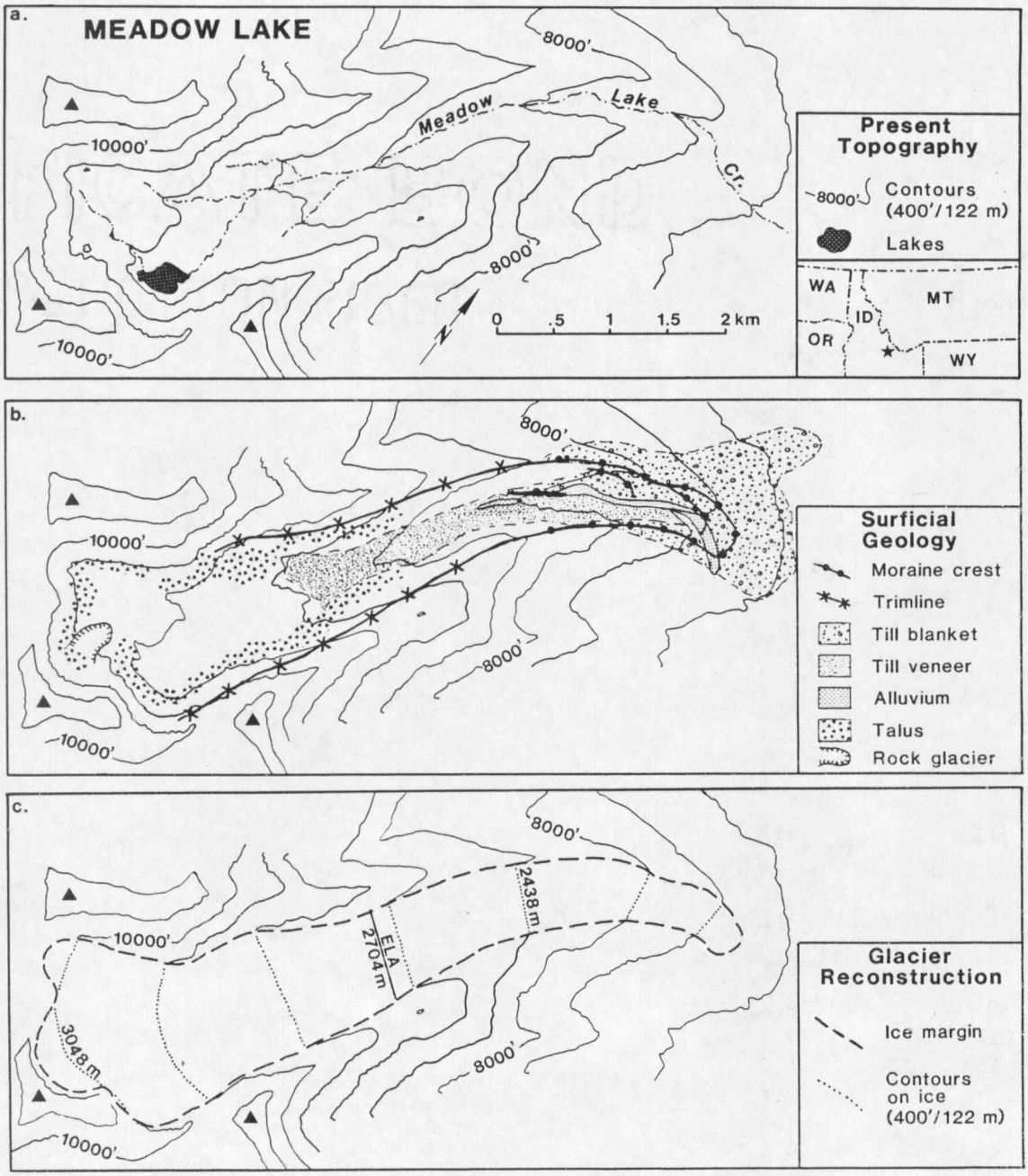

Figure 29. Map of Meadow Lake Canyon and the glacier reconstruction.

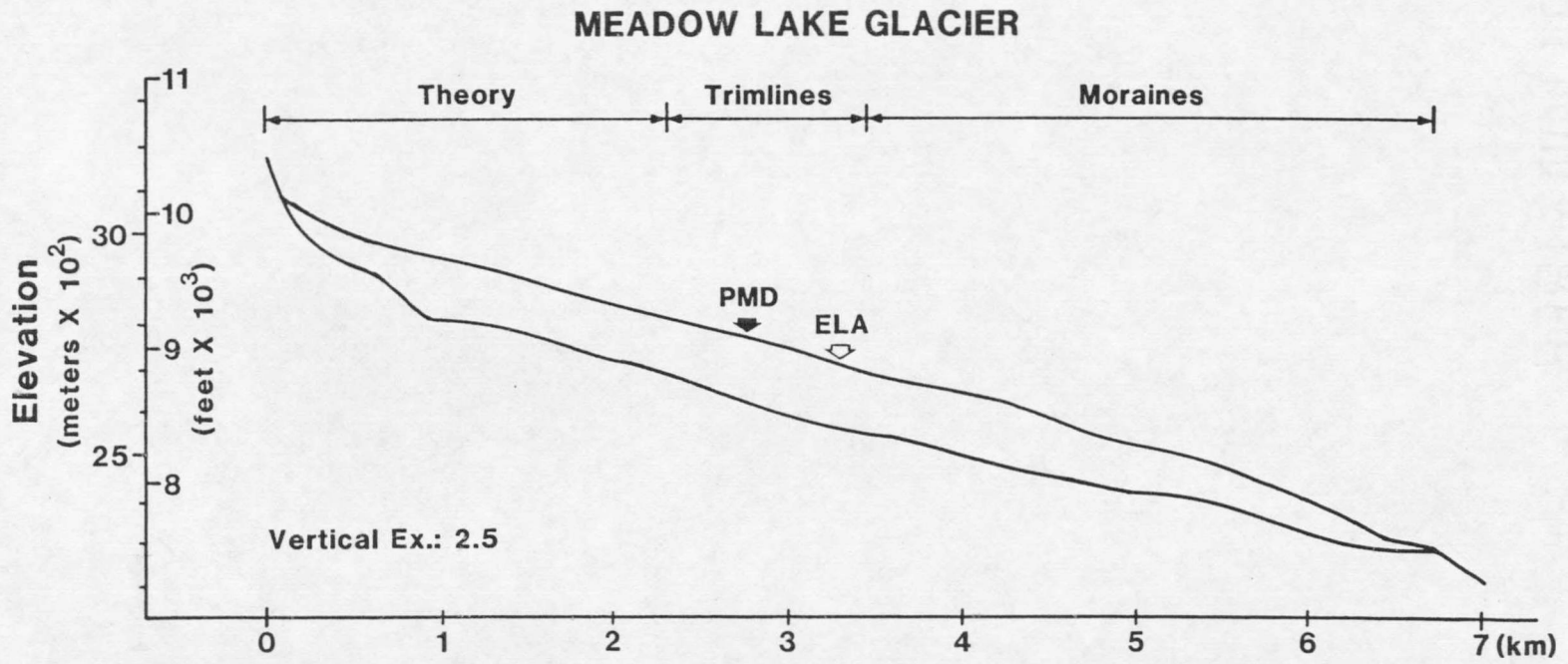

Figure 30. Longitudinal profile of Meadow Lake glacier.

maximum (Ruppel and Lopez, 1981; Richmond, 1986) and were used as the glacial limits in the present study.

The reconstructed glacier was approximately 7.0 km long and reached its maximum thickness 3.6 km from the terminus (Figs. 29c,30). A maximum average effective basal shear stress of 1.09 bars was reached at this point (2768 m) also. A theoretical profile using an average effective basal shear stress of .90 bar provided the best match with the geomorphic evidence. The ELA was estimated at 2704 m.

An accumulation gradient of 1.3 ± .26 mm/m provided the balance between the net accumulation up to the point of assumed no-slip (2768 m) and the deformation mass flux through the glacier cross-section at that point (9.4×10^5 m^3 a^{-1}). Comparison of the deformation mass flux at the ELA (3.6×10^5 m^3 a^{-1}) to the total net accumulation using the gradient (9.3×10^5 m^3 a^{-1}), which should equal the actual flux at the ELA, shows that 63% of the motion at the ELA was due to basal slip (Table 10). Basal slip varied along the length of the glacier and accounted for most of the motion near the terminus. An ablation gradient of 2.9 ± .58 mm/m provided a balance between total net ablation over the glacier surface and the average annual mass flux through the ELA.

Beaverhead Range

The Beaverhead Range lies to the north of the Lemhi Range along the Montana-Idaho border (Fig. 4). Several glaciers flowed down the eastern side of the range into the Big Hole Valley leaving beautifully sculpted U-shaped canyons and large moraine complexes. Many of the valleys have several tributary cirques and most of the paleoglaciers

Table 10. Mass balance and basal slip results for Meadow Lake Glacier.

	Point of Maximum Shear Stress	ELA
Ice surface elevation (m)	2768	2704
Centerline ice velocity (u_c) (m a^{-1})	15.8	7.7
Deformation mass flux (m^3 a^{-1})	9.50×10^5	3.7×10^5

Mass Balance

Accumulation Gradient = 1.4 ± .28 mm/m
Ablation Gradient = 3.1 ± .62 mm/m
Net Winter Precipitation = .27 ± .05 m

Basal Slip Calculations

(1) Ice Elevation (m)	(2) Mass Gain(+) /Loss(-) (10^6 m^3)	(3) Continuity Mass Flux (10^5 m^3 a^{-1})	(4) Cross Sectional Area (10^4 m^2)	(5) Average Velocity (3)/(4) (m a^{-1})	(6) Creep Velocity ($\bar{u}$) (m a^{-1})	(7) Slip Velocity (5)-(6) (m a^{-1})	(8) % Slip
2926-3109	+.637	6.37	14.1	4.5	3.5	1.0	22
2865-2926	+.186	8.23	9.90	8.3	6.5	1.5	22
2804-2865	+.108	9.31	10.8	8.6	6.7	1.9	22
2768-2804	+.046	9.77	9.54	10.2	10.0	0.2	2
2743-2768	+.019	9.96	8.91	11.2	7.0	4.2	38
2704-2743	+.007	10.0	7.54	13.3	4.9	8.4	63
2682-2704	-.005	9.97	6.78	14.7	3.8	10.9	74
2621-2682	-.088	9.09	6.03	15.1	7.5	7.6	50
2560-2621	-.102	8.07	4.95	16.3	2.9	13.4	82
2499-2560	-.208	5.99	3.35	17.9	2.2	15.7	88
2438-2499	-.172	4.27	1.55	27.5	1.5	26.0	95
2377-2438	-.150	2.77	1.28	21.6	1.2	20.4	94
2286-2377	-.262	0					

were interconnected with each other with ice flowing over the divides between valleys. Although there was extensive glaciation in this range, only one or two of the valleys meets the selection criteria.

Miner Lakes Glacier. Miner Lakes valley is one of the valleys in the Beaverhead Range without a complex cirque configuration or ice flowing over the valley divides. The valley trends northeastward from

its head, where it is split into two cirques. Large moraines are clearly evident on the topographic maps (Fig. 31a) and air photographs. Published documentation on the glacial history is limited (Alden, 1953), and no ages are assigned to any of the moraines. As in the other valleys without documented histories, the largest, well-defined moraines were assumed to correlate with the last glacial maximum.

The distal end of the valley is covered with recessional and re-advance moraines and post-glacial alluvium. The valley floor is flat with almost no change in elevation for the first 6.6 km up valley from the terminus (Fig. 32). Valley fill is extensive here. As a result, estimated ice thicknesses are minima. Bedrock outcrops are found on the valley floor approximately 10 km up valley from the terminus. From this point on, there is little or no post-glacial fill on the valley floor (Fig. 31b). Talus cones line the sides of the valley in the upper reaches; however, due to the large width and depth of the valley, the effect of these deposits on cross-sectional area calculations is minimal.

The paleoglacier was approximately 18 km long and reached a maximum thickness of 338 m at 10 km up valley from the terminus (Figs. 31c,32). The highest average effective basal shear stress (1.26 bars) was located at this point, at an ice surface elevation of 2518 m. Ice surface slope was averaged over 8000 ft (2.4 km) in calculating τ_b. A theoretical profile using an average basal shear stress of .80 bar matched the observed features well and was used to

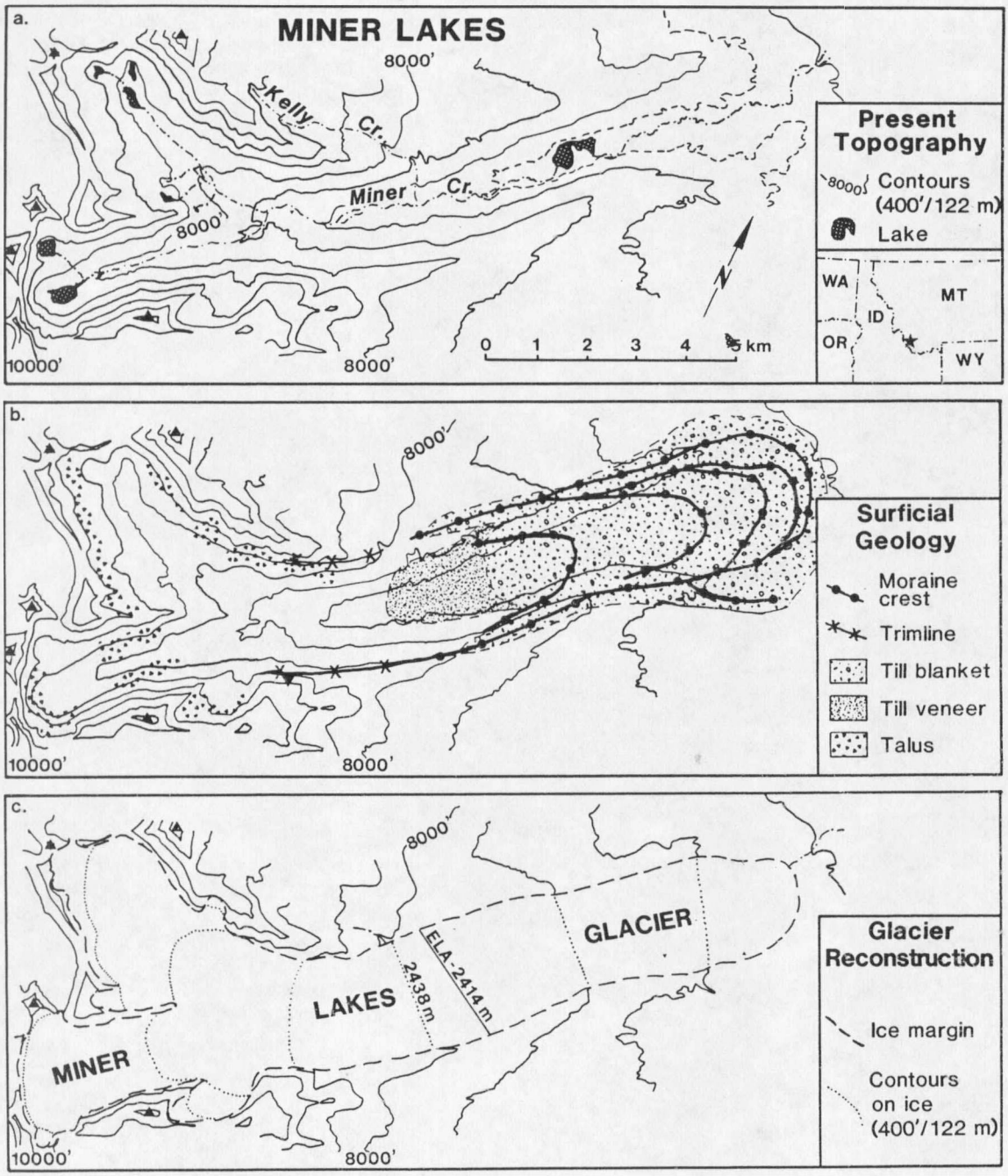

Figure 31. Map of Miner Lakes valley and the glacier reconstruction.

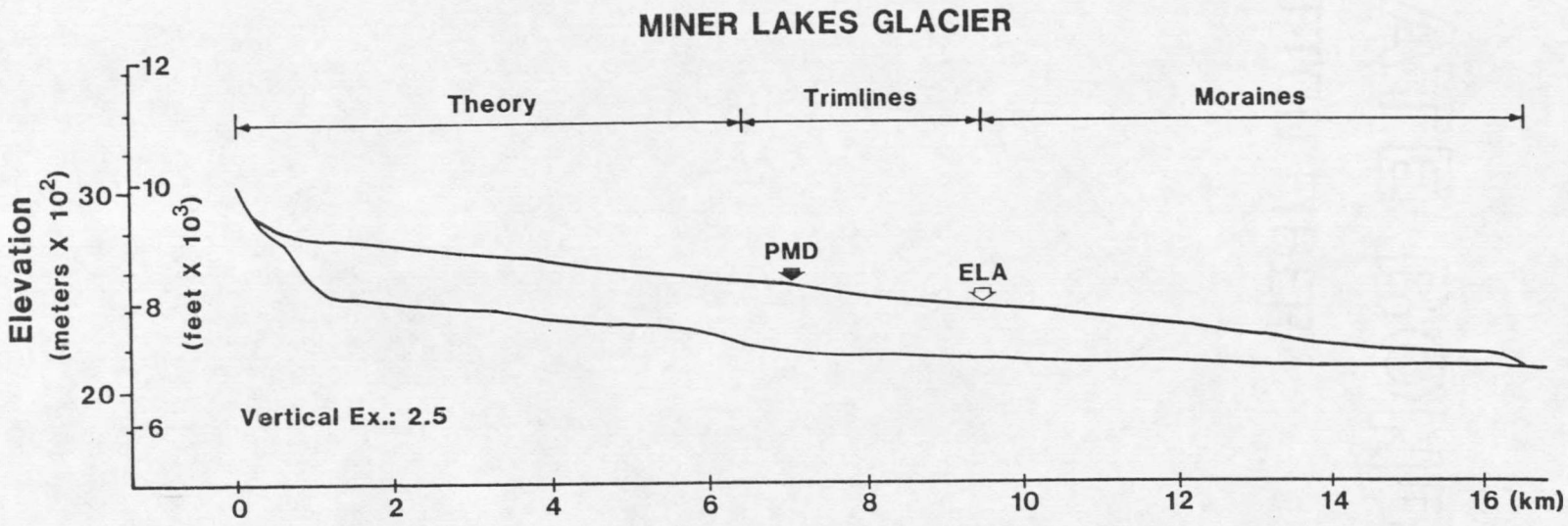

Figure 32. Longitudinal profile of Miner Lakes glacier.

estimate ice surface elevations in the cirques. The ELA was estimated at 2414 m (Table 11) using highest lateral moraine, THAR and AAR.

Table 11. Mass balance and basal slip results for Miner Lakes Glacier.

	Point of Maximum Shear Stress	ELA
Ice surface elevation (m)	2518	2414
Centerline ice velocity (u_c) (m a^{-1})	55.8	5.9
Deformation mass flux (m^3 a^{-1})	1.65×10^7	1.38×10^6

Mass Balance

Accumulation Gradient = 2.7 ± .54 mm/m
Ablation Gradient = 8.7 ± 1.7 mm/m
Net Winter Precipitation = .63 ± .12 m

Basal Slip Calculations

(1) Ice Elevation (m)	(2) Mass Gain(+) /Loss(-) (10^6 m^3)	(3) Continuity Mass Flux (10^5 m^3 a^{-1})	(4) Cross Sectional Area (10^4 m^2)	(5) Average Velocity (3)/(4) (m a^{-1})	(6) Creep Velocity ($\bar{u}$) (m a^{-1})	(7) Slip Velocity (5)-(6) (m a^{-1})	(8) % Slip
2560-2926	+15.6	15.6	4.59	34.0	21.7	12.3	36
2517-2560	+ .688	16.3	4.69	34.8	35.2	0	0
2438-2517	+ .581	16.9	3.53	47.9	7.7	40.2	83
2414-2438	+ .066	17.0	3.74	45.5	3.7	41.7	92
2316-2414	- 2.23	14.8	2.33	63.5	3.0	60.5	95
2194-2316	- 7.55	7.22	1.59	45.4	-	-	-
2103-2194	- 7.22	0.0					

An accumulation gradient of 2.7 ± .54 mm/m produced the best match between net accumulation (1.64×10^7 m^3 a^{-1}) above 2518 m and the deformation mass flux through the cross-section at this point (1.65×10^7 m^3 a^{-1}). Total net accumulation above the ELA was 1.7×10^7 m^3 a^{-1} which, when compared to the deformation mass flux at the ELA (1.38×10^6 m^3 a^{-1}), shows that basal slip accounts for more than 90 percent of the motion at the ELA (Table 11). An ablation gradient

of 8.7 ± 1.7 mm/m produced a balance between average annual mass flux at the ELA and total net ablation below the ELA.

Summary

Application of glacial flow theory to reconstructed paleoglaciers provides information on the dynamics of these glaciers. Values for velocity, mass balance gradients and basal slip are produced in the process and can now be compared from glacier to glacier. Analysis of two adjacent valleys of similar form and length shows that the model provides consistent results. These results can now be compared with the other valleys to assess the utility of the model.

DISCUSSION

The Model

The model developed in this study determines the dynamics of a paleoglacier (mass balance, thickness, rate of flow and length) using simple glacial flow theory. Several underlying assumptions affect the accuracy of the results. Before the results are analyzed, it is necessary to examine the relative merit of these assumptions. The model consists of 1) glacier reconstruction, 2) calculation of average effective basal shear stress using the reconstructed glacier geometry, 3) calculation of glacier velocity and mass flux using these shear stresses and 4) calculation of paleoglacier mass balance using the calculated mass fluxes. Each step in the model builds upon the assumptions made in the previous step. The assumptions underlying each step are addressed in this section.

Glacier Reconstruction

The reconstruction of each paleoglacier represents the geometry of the glacier at its maximum late Pleistocene extent. It was assumed that all glaciers reached their maximum extent at approximately the same time during the last glacial maximum (20,000 years ago). Because each glacier was assumed to maintain a steady state, the calculated dynamics of each glacier would represent full-glacial, equilibrium conditions.

The geologic evidence that was used to determine the areal extent of each glacier was either represented in published literature as correlative with the last glacial maximum or was morphologically similar to evidence in other valleys in the region which was correlated with the last glacial maximum (Porter and others, 1983; Richmond, 1986). As discussed in Methods, the largest, well-defined terminal moraines and the lowest lateral moraine that graded to the terminal moraine were used to delineate the glacial extent in the ablation area. Because the lateral moraines always graded into the trimlines that were used to delineate the glacial extent in the accumulation area, the trimlines were thought to be time-correlative with the moraines. In some valleys, there was more than one terminal moraine that fit the description of the "largest, well-defined moraine." Using any of these other moraines did not appreciably change the size or shape of the glacier, except in the very terminal area. A change in area affected the ELA estimates (AAR, THAR) and the balance gradients, but because the size of the change was small, changes in the reconstructed dynamics were minimal.

The assumption that all the glaciers reached and maintained their maximum extent at approximately the same time can be questioned. While the last glacial maximum is usually modelled as 18,000 years B.P. (CLIMAP, 1976; Porter and others, 1983), Barry (1983) notes that land evidence supporting this date is limited. Most "absolute" ages for moraines of alpine glaciers in the northern Rocky Mountains place the last maximum in the time period of 22,000 to 20,000 years B.P. (Porter and others, 1983; Richmond, 1986). Presumably, minor

fluctuations in extent also occurred between 22,000 and 20,000 years B.P. (Davis and Osborn, 1988), but the evidence is usually lost within the deposits representative of larger climatic fluctuations. In any event, the results from this model are time-averaged, usually over centuries or millennia, and are acceptable for the purposes of this study.

Each glacier was assumed to reach a steady state. Paterson (1981, p. 45) notes that "this is an important theoretical concept, but one that is never encountered in practice." Glaciers are constantly adjusting their geometries to yearly changes in mass balance, so an actual balance between ablation and accumulation does not usually occur over a yearly period of measurement. Positive balance years should result in an advance of the glacier, however, the response time of these changes is dependent on the size of the glacier and ranges from several years for small cirque glaciers to centuries for ice sheets (Paterson, 1981). Attempts to calculate the annual mass balance from the terminal positions of modern glaciers showed considerable discrepancies from measured balances, however, when averaged over a 10-year running mean, the differences were small (Nye, 1965a). The largest terminal and lateral moraines were used in this study and must reflect a long term average position. As a result, calculated mass balance reflects an averaged "steady state" condition.

Reconstructed glacier geometries used in this study are time-averaged, thus calculations of glacier dynamics using these reconstructions are also time-averaged. On the geologic time scale, general climatic changes are also averaged over centuries or

millennia. As a result, these calculated values are indicative of the glacier response to general climatic trends, namely the regional climate of the last glacial maximum.

Basal Shear Stresses

Basal shear stresses calculated by equation 1 were assumed to equal the average effective basal shear stress of the glacier. The narrow range of shear stress values (0.5 to 1.5 bars) is due to the adjustments a glacier makes for increases in slope or thickness (Mathews, 1967). If thickness or surface slope became so great that this shear stress range was greatly exceeded, the basal ice would deform easily until its thickness or slope was significantly reduced. Conversely, if the ice was thin and flat because basal shear stress was low, movement would virtually cease. After a period of time, accumulation of more ice would increase the thickness or slope or both until the yield stress was reached, and the ice would flow again (Mathews, 1967). The reconstructions in this study produced time and space averaged values of thickness and slope, therefore equation 1 produced average basal shear stresses.

Equation 1 also implies that the bedrock friction exactly balances the down-slope component of the weight of the overlying ice (Paterson, 1981). In regions of extending and compressing flow, this is not the case, and longitudinal components of stress must be added to obtain the total effective shear stress (Paterson, 1981). These components can be induced by longitudinal variations in bed slope and channel cross-section shape, bends in valleys, and confluence of tributaries (Raymond, 1980). In this study, valley selection criteria

minimized longitudinal stresses induced by these factors. Furthermore, fluctuations of thickness and slope over distances that are small compared with the ice thickness cannot influence the overall behavior of the glacier. When surface slope and valley shape are averaged over 8-20(H), the longitudinal components of stress are negligible and the average effective basal shear stress is approximated by equation 1 (Raymond, 1980; Paterson, 1981).

Another assumption made when calculating average effective basal shear stress was that values of thickness and surface slope were accurate. The limitations of estimating ice surface elevation (and therefore ice surface slope) have already been discussed in Results. Because thickness was determined from the difference of ice surface elevation and bedrock elevation, values of estimated thickness were low in areas where the valley floor is not bedrock (mostly near the terminus). Accurate values of estimated thickness are most critical at the point of maximum shear stress and the ELA. In this study, the valley floor is bedrock at these points in all valleys. In the terminal area, the low values of thickness underestimated average effective basal shear stress and produced an underestimate of the deformation velocity in this area.

Average effective basal shear stress was also used to calculate theoretical profiles of each paleoglacier. This slab approximation (Schilling and Hollin, 1981) assumes a constant shear stress along the entire glacier length. In reality, shear stress varies along the length of a glacier, but within the narrow range of 0.5 to 1.5 bars.

As a result, the assumption of an average shear stress is a good first approximation.

The profile that best matched the geologic evidence in the lower portions of the glaciers was used to estimate ice surface elevations in the cirque areas, where geologic evidence was lacking. Schilling and Hollin (1981) note that the iterative scheme tends to overestimate ice thickness. With the step length used in this study (0.3 km), ice thicknesses in the cirque regions would be overestimated by approximately 10 m (Schilling and Hollin, 1981).

This study accurately models the average effective basal shear stresses of these paleoglaciers. Longitudinal stresses were minimized by the valley selection criteria and by averaging of ice slope and valley shape over 8-20(H). These average effective basal shear stresses were used to calculate the velocity and mass flux along each paleoglacier.

Glacier Velocity - Ice Deformation

As explained in Methods, glacier velocity has components of ice deformation and basal slip. Ice centerline velocities due to deformation were calculated using equation 3. The dependence of equation 3 on ice thickness and surface slope has been examined in previous chapters. The effects of the other constants in the ice flow equation (A and n) must also be examined.

In this study, A is assumed to be constant. In reality A varies with the ice temperature. Ice temperatures for paleoglaciers cannot be measured and an approximation must be made. The value of A used in this study (0.167 bar^{-3} a^{-1}) assumes a uniform temperature (0°C)

throughout the glacier, which is a reasonable approximation for a temperate valley glacier. In a subpolar or polar glacier, lower air and ice temperatures are encountered and the value of A varies through the ice thickness and with elevation. Paterson (1981, Table 3.3) calculated values for A using n = 3 and some of the results are presented in Table 12. These values indicate that as temperature decreases, A decreases and the rate of ice deformation therefore decreases. By using a constant, maximum value of A (at 0°C), ice deformation velocities may be overestimated. Most of the ice deformation takes place at the base of the glacier where temperatures are at or near the pressure melting point in temperate and subpolar glaciers. Unless the climate in the study area was extremely polar during the last glacial maximum, ice deformation rates in this study are reasonable, but may be overestimated by as much as an order of magnitude. Because calculated mass balances in this study were dependent on the calculation of maximum deformation velocity, which is dependent on the value of A, they may be maxima.

Table 12. Values of the flow law constant A (after Paterson, 1981).

Temperature (°C)	A (bar^{-3} a^{-1})
0	.167
-5	.054
-10	.016
-20	.0098

The value of n is derived from the slope of the line of effective shear stress plotted against effective strain rate and is dependent on the orientation of the ice crystals. In polycrystalline glacier ice,

there is a preferred orientation of the crystals which does not change under local stress. In steady-state creep tests of polycrystalline ice at temperatures above 10°C, n varied from 2.8 to 3.2 (Weertman, 1973). An average value of n = 3 is normally applied to valley glaciers and was used in this study. Because the preferred orientation of the ice crystals is realized early on in the formation of glacier ice (in the accumulation area), it was deemed reasonable to use an average value across the glacier. Deformation velocities vary as H^n and $\sin\alpha^n$, so small changes in n would affect the calculated velocities. The actual value of n cannot be determined for paleoglaciers and whether it should be higher or lower than 3 cannot be determined. Therefore, an assumed value of n = 3 is reasonable.

The value of A used in this study may have overestimated the actual deformation. If n were actually greater than 3, deformation rates were underestimated. Because of this conflict, equation 3 provides a good estimate of paleoglacier deformation velocity using the parameters chosen in this study.

Glacier Velocity - Basal Slip

As noted previously, basal slip is not easily modelled either in existing glaciers or paleoglaciers. Basal slip must occur because diurnal or seasonal changes in observed velocities occur on modern glaciers. These changes cannot be accounted for by changes in deformation rates, because ice thickness and surface slope do not change that rapidly. Some change must take place at the bed of the glacier to account for this increased motion (Raymond, 1980).

Field Observations. The major problem in understanding the mechanics of basal sliding is the difficulty in observing it, because by definition, basal sliding occurs at the base of a glacier. Sliding motion has been observed in some ice tunnels. These observations are not indicative of normal subglacial conditions because they were made near the edge of glaciers where ice is thin, or in icefalls where the ice is relatively thin and steep (Raymond, 1980; Paterson, 1981). Boreholes drilled into the central parts of glaciers provide more typical conditions for examining the processes involved in basal sliding. Measurement of the tilting of boreholes can be used to estimate slip if the surface velocity is known and the borehole reaches the base of the glacier. Television cameras placed in the boreholes can be used to accurately measure the amount of slip (Paterson, 1981). The problem with borehole measurements is that thermal drills rarely reach the base of the glacier. If they do, water flowing up into the borehole obscures the bed from the camera (Raymond, 1980; Paterson, 1981). Estimations of basal sliding can also be made by subtracting actual surface velocity from the calculated deformation velocity. Because the valley shape factor and ice thickness cannot always be adequately measured for accurate calculations of deformation velocity, this method can lead to erroneous results.

Observations made using these methods show that basal sliding can account for 3-90% of total surface velocity (Paterson, 1981, Table 5.2). The sliding component varies along the length of a glacier and the highest slip percentages were observed where the ice was not in

contact with the bedrock (Paterson, 1981). Meier (1967) showed that there was no clear relationship between effective basal shear stress and sliding velocity on the Blue Glacier in Washington and the data summarized by Paterson (1981, Table 5.1) for other glaciers agrees with this observation. If basal sliding cannot even be accurately modelled in modern glaciers, how can assumptions be made about the component of basal sliding to the total velocity in paleoglaciers?

We do know that total mass flux (average velocity x cross-sectional area) varies smoothly along the length of a glacier (Raymond, 1980). Balance flux is a maximum at the ELA, thus maximum speed is expected in the central reach of a glacier (Raymond, 1980). The ratio of basal sliding to total velocity can vary along the length of a glacier (Paterson, 1981). Methods used by other workers (Haeberli and Penz, 1985; Leonard and others, 1986; McCalpin, 1987; Holmlund, 1988) were examined in the light of this information and are discussed below.

Other Methods. Haeberli and Penz (1985) and McCalpin (1986) assumed a constant slip rate at the ELA (50%) to calculate mass balances for the paleoglaciers they studied. A value of 50% represents the mean of the data in Paterson (1981, Table 5.2). However as noted above, the actual range was 3-90%, and this range occurred on the same glacier! The assumption that all glaciers had 50% slip at the ELA seems unreasonable. Leonard and others (1986) calculated minimum mass balances assuming no slip at the ELA on paleoglaciers in the Colorado Front Range. The method of assuming no slip at the ELA was attempted on Big Timber glacier. Deformation fluxes were also

calculated at discrete points above and below the ELA. The difference between an upstream flux and the next downstream flux (Δ Q) was divided by the surface area between the two points. The result should define the average specific net balance between those points, and successive iterations should define the mass balance gradients. However, the plot of these values against elevation showed no linearity whatsoever (Fig. 33). If 50% slip was assumed along the glacier length, the values only increased in magnitude (Fig. 33), with no clear relation of mass balance to elevation.

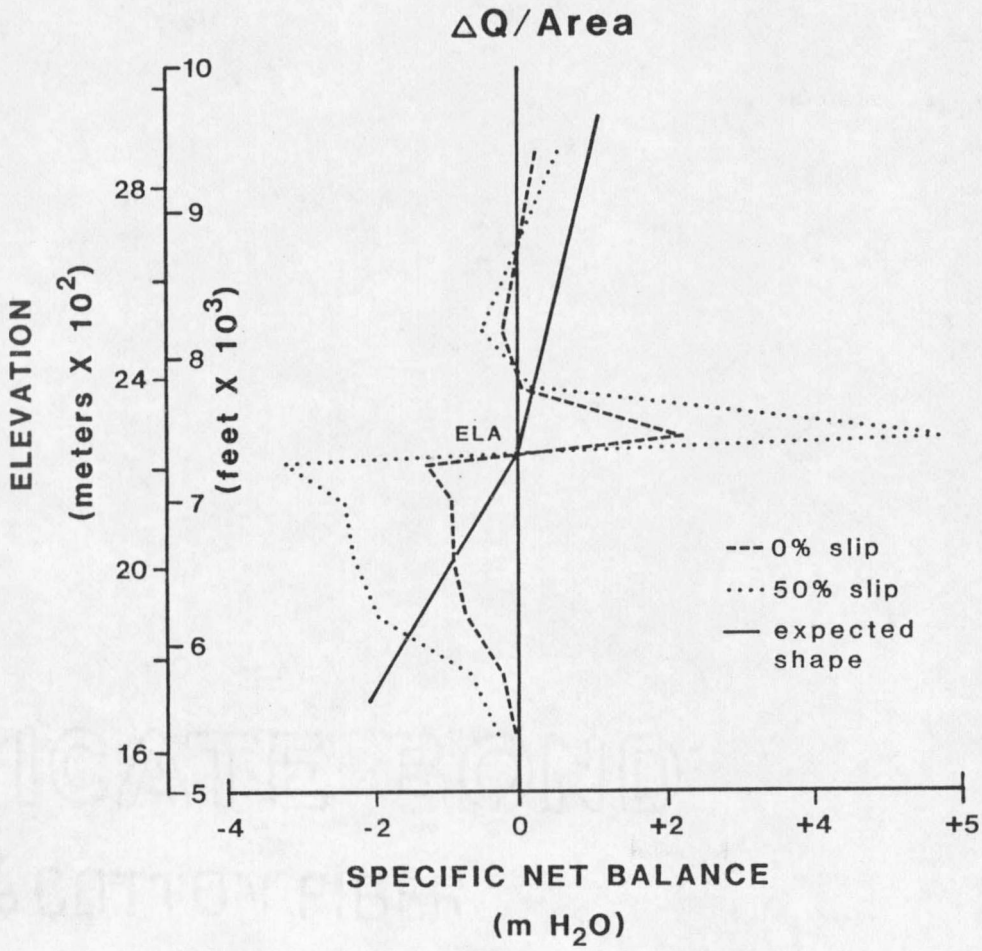

Figure 33. An attempt to model mass balance gradients using mass flux and area.

On a steady state glacier, the net mass exchange at the ELA is balanced by net ablation below the ELA. Using the model of Pierce (1979) (Fig. 15), a linear ablation gradient was calculated that matched the net ablation to the net mass exchange at the ELA (Fig. 23). Here slip was again assumed to be zero at the ELA. Any amount of slip can be assumed at the ELA and a corresponding balance gradient can be calculated. Using the continuity model described in Methods, it became evident that the difference between deformation flux and continuity flux could be accounted for by basal slip. Therefore, in addition to mass balance gradients, the model provided estimates of basal slip along the length of the glacier, which no one had been able to do before on paleoglaciers. Basal slip was still assumed to be a fixed value at the ELA, and this problem needed to be addressed.

This study. Because mass flux on a glacier changes slowly along the length of a glacier (Pierce, 1979; Raymond, 1980), maximum deformation flux has to be offset by minimum slip flux. This provided an additional assumption upon which estimates of basal sliding could be made on the paleoglacier. Highest deformation flux occurred in this study where the maximum average effective basal shear stress occurred. Conceivably, a lower deformation velocity (calculated from a less-than-maximum shear stress) can be offset by a large cross-sectional area to produce the maximum deformation flux. At the point of highest deformation flux, slip flux should be lowest. However, it still may account for part of the total motion, and the actual value for a paleoglacier cannot be determined. In this study, basal sliding

was assumed to be zero at the point of maximum deformation flux. This assumption has merit in that it sets a lower limit for estimations of mass flux in the model. It also provides minimum estimates of basal sliding along the length of the glacier using the continuity equation.

McCalpin (1987) noted that deformation velocities calculated in areas of strongly extending or compressing flow would either overestimate or underestimate deformation velocities. Most of the maximum shear stresses in this study (upon which total flux for the glacier was based) occurred in uniform reaches of flow. Also, areas of strongly extending or compressing flow were minimized by the valley selection criteria.

Mass Balance

In this study, the point of maximum deformation flux occurred at or above the ELA in all valleys. Annual net accumulation above the ELA was calculated from the accumulation gradient that produced a balance of net accumulation up to the point of maximum deformation and the mass flux through the point of maximum deformation, extrapolated to the ELA where necessary. In the steady state system, this net accumulation is equivalent to the net mass exchange through the ELA and the net ablation below the ELA. As stated above, values of mass balance calculated in this model are minima. However, it will be shown below that the values calculated in this model are still acceptable.

The Results

Stroud Creek versus Everson Creek

The model was originally developed and refined in Big Timber Canyon, yet there were no appropriate adjacent valleys with which to compare the Big Timber results. Two adjacent valleys in the Lemhi Range, Stroud Creek and Everson Creek (Fig. 24), were chosen to test the reproducibility of the model from valley to valley. These valleys were selected because the paleoglaciers were of similar size, shape and orientation.

Both glaciers covered the same altitudinal range from 2316 to 3048 m (Appendices F and G). Equilibrium line altitudes for the two glaciers were estimated to be within 1 m of each other (Tables 6,7). The glaciers had comparable valley slopes (Figs. 25,26) and maximum thicknesses were also similar (Stroud = 158 m; Everson = 149 m). An average effective basal shear stress of .80 bar produced the best fit theoretical profiles for both glaciers. Stroud Creek glacier had a larger area (6.51 km^2) than Everson Creek glacier (4.67 km^2). In terms of reconstruction the two paleoglaciers were similar, and the glacier dynamics should have also been similar.

The average velocities along the length of Stroud Creek glacier and Everson Creek glacier were 7.8 m a^{-1} and 8.1 m a^{-1}, respectively. These low velocities are comparable to those of modern glaciers in the cold, low-moisture polar environments (Andrews, 1975; Paterson, 1981). On Everson Creek glacier, there was an anomalously high value of average velocity at the 2316 m cross-section (Table 8). The reconstructed cross-sectional area at this point is inaccurate because

recessional moraines and post-glacial alluvial fill have modified the valley (Fig. 24b), thereby producing this high value.

Mass balance estimates based on the flow rates are also similar. Calculated accumulation and ablation gradients for the two glaciers (Table 7,8) are the same (within the limits of error). Average annual net accumulation values also indicate similar local climates. For two adjacent valleys of similar form, the model produced similar results, indicating that the results from other valleys that are not adjacent can be assumed to be comparable.

Comparison to Mill Creek

Mill Creek lies 2 km to the north of Stroud Creek in the Lemhi Range. The Mill Creek glacier was a larger glacier (total area = 11.56 km^2) than Stroud and Everson glaciers. Average velocity on Mill Creek glacier was 19.9 m a^{-1}, more than twice that of the other two. Average effective basal shear stresses were higher on Mill Creek which would account for the higher velocities (Appendix H). A theoretical profile using an average effective basal shear stress of .90 bar produced the best match to the geologic profile. Only the ELA (2583 m) was similar among the three glaciers.

Mass balance estimates (Table 9) were much higher for Mill Creek than for the other two. While the balance gradients were still low, they were more than double those of Stroud and Everson glaciers. One explanation is that the mass balance estimates produced by this model reflect the local glacier climate. Meier (1966) found that two adjacent, parallel branches of the Klawatti Glacier in the North Cascades of Washington experienced differences in volume over a period

of 14 years. The thickness of the north branch decreased by an average of 8.3 m, while the thickness of the south branch increased an average of 5.8 m. Values of accumulation and ablation must have differed on these two branches, reflecting differences in local climate. Possible factors that would cause differences in local climate include shading differences, wind-drifted snow accumulation, and increased avalanching adding to the accumulation. There were no obvious differences in the causes of these factors between Mill Creek, Stroud Creek and Everson Creek glaciers.

Another possible explanation for the difference in the mass balances is that basal slip was not zero at the point of maximum deformation flux on Stroud and Everson glaciers. Incorporating a basal sliding component into the mass flux at this point would increase the mass balances of these glaciers. Average basal slip percentages were 55% on Mill Creek glacier in comparison to 47% and 41% on Stroud and Everson glaciers respectively. Stroud Creek was used to test the effect an assumed slip percentage at the point of maximum deformation would have on the mass balance (Table 13). These results show that even with an assumed basal slip of 50% at the point of maximum deformation, mass balance values for Stroud Creek would still be lower than those for Mill Creek. Also, average basal slip along the glacier would have been 74%, which seems unlikely, especially in the cirque areas where the glacier was probably frozen to its bed.

Table 13. Mass balance estimates for Stroud Creek assuming 0, 10, 20, and 50 % basal slip at the point of maximum deformation flux.

	Assumed Slip (%)	Mass flux ($\times 10^5$ m^3 a^{-1})	Mass Balance Gradients Accumulation (mm/m)	Ablation (mm/m)
Stroud Creek	0	7.6	0.8 ± .16	2.4 ± .48
	10	8.4	0.9 ± .18	2.7 ± .54
	20	9.5	1.1 ± .22	3.2 ± .64
	50	15.2	1.7 ± .34	5.0 ± 1.0
Mill Creek	0	27.6	1.9 ± .38	5.6 ± 1.1

The mass balance values provided by the model are minima, therefore the values for Stroud and Everson may be low. Using increased values for basal sliding would raise the mass balance values, but basal sliding would have to be the primary factor in flow across the glaciers to bring mass balance values up to those of Mill Creek. Because the variations in mass balance between these glaciers cannot be explained completely by basal sliding, it was assumed these mass balances reflect local climatic differences. Meier (1966) noted that in order to determine regional climatic trends from glacier mass balances, it is important to obtain a valid statistical sample of glacier behavior in any given region. This model provides the means to make minimum mass balance calculations for paleoglaciers and can be used to determine the general regional climate if a statistically valid sample of results can be obtained.

Comparison of all Valleys

Table 14 summarizes the dynamics of the glaciers that were examined in this study. There is no correlation between the size of the glacier and the mass balance values. Big Timber glacier was the second largest glacier, but has mass balance gradients less than Mill Creek and Meadow Lake glaciers which are only one-fifth as big. Average velocities generally increased with increasing size. Larger glaciers have larger accumulation areas and therefore overall larger net accumulation values. This mass must be moved down the glacier and can be achieved through higher velocities. Equilibrium line altitudes were highest in the Lemhi Range and lowest in the Crazy Mountains. Comparisons of basal sliding and mass balance estimates are discussed in detail in the following sections.

Table 14. Mass balance summary for all the glaciers.

Glacier Name	Total Area (km^2)	ELA (m)	Average Velocity ($m\ a^{-1}$)	Average Slip (%)	Slip at ELA (%)	Mass Balance Gradients Accumulation (mm/m)	Ablation (mm/m)
Big Timber	32.9	2240	33.1	56	0	1.0 ± 0.2	3.0 ± 0.6
Miner Lakes	41.4	2414	45.2	61	92	2.7 ± .54	8.7 ± 1.7
Mill Creek	11.5	2583	19.9	55	27	1.9 ± .38	5.6 ± 1.1
Stroud Creek	6.51	2584	7.8	47	43	0.8 ± .16	2.4 ± .48
Everson Creek	4.67	2583	8.1	41	32	0.7 ± .14	1.9 ± .38
Meadow Lake	5.76	2704	14.1	54	63	1.4 ± .28	3.1 ± .62

Basal Slip

Average basal slip on all the glaciers was close to 50% showing the prevalence of this average value in basal sliding studies. Basal slip on these paleoglaciers generally increases from an assumed value of zero at the point of maximum deformation to values greater than 90% in the terminal areas. Therefore, an average value of 50% is to be expected.

In all the glaciers, basal sliding became the dominant form of motion near the termini. One explanation is inherent in the way basal slip is calculated in the model. Because slip is determined by the difference between deformation flux and continuity flux, an error in the calculation of deformation flux leads to error in the slip flux. In the terminal areas of these valleys, post-glacial modification of the valley shape could lead to underestimates of average effective basal shear stress, cross-sectional area and deformation flux; thus overestimates of basal slip. One example is Meadow Lake Canyon, where recessional moraines and outwash have filled in the valley in the lowest 1.5 km and valley cross-sections are more V-shaped than U-shaped. Basal slip estimates are high (Table 10) in this region of the glacier and average velocity does not show the expected decrease in the terminal area (Raymond, 1980).

Another explanation is that there is an actual increase in the amount of basal sliding in the terminal regions of the glaciers. On Big Timber glacier, basal slip increased dramatically in the lowest 4 km of the glacier (Table 5) and average effective basal shear stresses were unusually low in this portion of the glacier (Table 2). It is

thought that one of the principal factors in the cause of basal sliding is the presence of water at the bed (Raymond, 1980). Meltwater from Amelong glacier (Fig. 18a) added significant amounts of water to the base of Big Timber glacier and could have induced basal sliding. The same situation occurred on Miner Lakes glacier (Fig. 31). A small cirque glacier on the north side of the valley added meltwater to the main valley at about the 2438 m level (the general location of present day Kelly Creek (Fig. 31a)). High values of basal slip were found on this part of the valley along with unusually low values of average effective basal shear stress. However, there is also a great deal of fill in the valley from this point to the terminus which can also account for the low values of shear stress.

A third explanation is that the till at the base of the glacier was deforming (Boulton and Jones, 1979) instead of the ice and this was causing high velocities in the terminal areas. Because errors in the calculation of the ice thickness and cross-sectional areas would have to be very large (50-100%) in some cases to appreciably decrease the amount of basal slip, and because meltwater streams do not enter all the valleys, this mechanism may be the cause for the increased sliding in some of these glaciers. Subglacial till is deposited in the terminal area mainly through pressure melting beneath active moving ice (Sugden and John, 1976). Meltwater percolates down through the glacier in the ablation area, and these subglacial tills can become saturated. Pressure from the overlying ice can induce flow within the till, and this would add to the total velocity of the

glacier. Normally, water is squeezed out of the till by the ice pressure, but if the glacier was moving over shale or the till was comprised chiefly of clays, these formations could create an impermeable boundary for the water (Boulton and Jones, 1979). Big Timber glacier flowed over shales in the Cretaceous Livingston Group in its lower regions (Aten, 1974), and this mechanism could account for the high basal slip values near the terminus.

Whatever the mechanism for basal sliding in these paleoglaciers, it is clear that sliding did occur and that the amount of sliding varied along the length of the glacier. Slip velocities on the parts of the glaciers where the valley cross-sectional areas and average effective basal shear stress were well modelled were assumed to be minimal, yet reasonable values. Basal sliding may be overestimated in the regions where post-glacial modification of the valley has occurred.

Paleoclimatic Interpretations

Mass balance gradients

Calculated mass balance gradients for paleoglaciers have been used by other workers (Haeberli and Penz, 1985; Leonard and others, 1986) as proxies for paleoclimate. On modern glaciers, ablation gradients generally decrease with increasing continentality and decreasing moisture availability (Meier and Post, 1962; Meier and others, 1971). There has been no change in the continentality of the northern Rocky Mountains since the last glacial maximum and the calculated gradients should therefore reflect a continental

environment. The dominant source of moisture for the northern Rocky Mountains at present is the Pacific Ocean with some additional moisture along the Rocky Mountain front from the Gulf of Mexico (Mitchell, 1969; Harding, 1982).

It should be noted that there are exceptions to the trend of higher gradients in maritime areas. The Blue glacier in the Olympic Range of Washington has an anomalously low ablation gradient of 5 mm/m (Meier and others, 1971), most likely reflecting the microclimate of its locality. If low values of ablation gradients can be found in maritime regions, it would be reasonable to assume that high gradients can be found in continental regions where local microclimates result in large amounts of accumulation. Indeed, the Grasshopper glacier in the Beartooth mountains has an ablation gradient of 22 mm/m (Alford and Clark, 1968).

This study. Ablation gradients for the paleoglaciers in this study ranged from 1.9 to 8.7 mm/m (± 20%) (Table 14). Except for Miner Lakes and Mill Creek, the gradients were much lower than those observed on most modern glaciers (Meier and others, 1971; Pierce, 1979). It must be remembered that the values derived from this model are minima, and the actual values may have been higher.

Miner Lakes is an exception to the general trend of very low ablation gradients. As stated previously, ablation gradients can reflect a local climate particular to the glacier rather than the general climate. In this study, the gradient could also be reflective of the way in which it was derived. On Miner Lakes glacier, the maximum average effective basal shear stress was 1.26 bars. This

relatively high shear stress could reflect an area of extensive flow (Pierce, 1979). Looking at the longitudinal profile of the glacier (Fig. 32), the point of maximum deformation occurs where the ice flows over a step in the bedrock topography, and the slope is steeper than above or below. This step would create a high value of average effective shear stress and could overestimate the actual net mass exchange for the glacier. Whether the gradient is reflective of local climate or the method cannot be determined.

For Stroud Creek, a 50% slip rate at the point of maximum deformation doubled total mass flux, hence the ablation gradient (Table 13). Because the point of maximum deformation is not always at the ELA, net accumulation (and net ablation) for the whole glacier would be slightly more than double. If 50% slip is assumed at the point of maximum deformation on the glaciers in this study, then ablation gradients would effectively double for each glacier. With the exception of Miner Lakes and Mill Creek, the gradients would still be lower than most found on modern glaciers (Meier and others, 1971; Pierce, 1979).

However, the assumption of 50% slip at the point of maximum deformation is not reasonable for these paleoglaciers. Average basal slip on Big Timber is already 56% and basal sliding accounts for over 60% of the flux above the ELA already. Perhaps basal slip was 10% at the ELA, but the ablation gradient would only change by 11% and would still be a very low value. Although the ablation gradients in this study are minima, they are also reasonable estimates. They are considered to be especially representative of actual conditions when

the average basal slip in the accumulation area is greater than 50% (e.g. Big Timber).

Other studies. The ablation gradient of Big Timber glacier (3.0 mm/m) is in contrast to the higher ablation gradient (9.0 mm/m) that Pierce (1979) determined for the Yellowstone ice cap which lay to the south of the Crazy Mountains (Fig. 6). Pierce (1979) based his gradient on modern glaciers located in areas which he assumed to have similar climates to the Yellowstone area during the last glacial maximum. However, in order to balance the ablation with the net mass exchange, 90% basal slip at the ELA was required. Pierce (1979) assumed climate and then forced glacial flow theory to that gradient. In the present study, the gradient (climate) is implied by the flow, which is more in line with the standard glacier-climate relationships (Fig. 1). Using a model similar to the one in this study, Leonard and others (1986) calculated very low ablation gradients (0.7-1.9 mm/m) for late Pleistocene glaciers in the Colorado Front Range. Their results show that those glaciers were also sustained by a cold and dry climate, in contrast to the modern glacier climates that have been used as analogs for late Pleistocene climates.

Net Accumulation

The mass balance gradients provided values of annual net accumulation volume on each paleoglacier. An estimate of the average annual net accumulation (in m H_2O a^{-1}) above the ELA was determined by dividing the annual net accumulation volume ($m^3 \cdot a^{-1}$) by the accumulation area (m^2) (Table 15). This value is an average for the

entire accumulation area, with the actual net accumulation at the ELA being zero and the net accumulation at each elevation above the ELA being determined by the accumulation gradient. It also represents the net accumulation at an elevation approximately halfway between the ELA and the headwall, with the exact elevation being determined by the accumulation gradient (Table 15).

Table 15. Net accumulation.

Glacier Name	Mass Exchange (10^6 m^3 a^{-1})	Accumulation Area (10^6 m^2)	Average Net Accumulation (m H_2O a^{-1})	Elevation (m)
Big Timber	8.8	21.2	.42	2660
Miner Lakes	17.0	27.0	.63	2647
Mill Creek	3.29	7.85	.42	2804
Stroud Creek	0.72	4.24	.17	2797
Everson Creek	0.40	3.34	.12	2754
Meadow Lake	1.00	3.75	.27	2897

At that point on the glacier, the calculated annual net accumulation should be approximately equal to the total annual accumulation. Average annual temperatures above the ELA are below zero (Andrews, 1975), and any snow that does melt would percolate back down into the glacier and refreeze. Sublimation does occur, but would be low because of the enormous amount of energy (640 calories cm^{-3}) that is required for this process (Andrews, 1975). Some of the accumulation may fall in the form of rain, which will freeze to the surface or percolate into the snow and add to the total water content.

Thus, calculated annual net accumulation at this elevation closely approximates annual precipitation. It must also be reiterated that these calculated values are minima.

The calculated average annual net precipitation values for each paleoglacier were plotted on the graph with the modern precipitation gradients for each mountain range (Fig. 34). In all cases, the calculated values of precipitation were less than those predicted by the gradients. The graph shows that even if the calculated late Pleistocene net accumulation and the modern winter precipitation represent minimum values, the annual precipitation during the last glacial maximum on these glaciers was as much as 20-75% less than present. The small number of glaciers that were examined in this study do not allow any statistically valid regionalization of paleo-precipitation patterns. However, the mountain ranges that have higher precipitation today (Beaverhead, Crazy) had the higher total paleoprecipitation amounts.

Comparison to other studies. Locke and Kemph (1987) modelled the late Pleistocene winter precipitation patterns in western Montana. The results of this study agree well with their results. In the Beaverhead Range, they calculated a 30 cm decrease from present (Locke, personal communication) in winter precipitation compared to a minimum decrease in annual precipitation of 15 cm in this study. Net precipitation decrease in the Crazy Mountains was 50 cm in this study compared with 75 cm estimated by Locke and Kemph (1987). Because the values in the present study reflect the difference between calculated

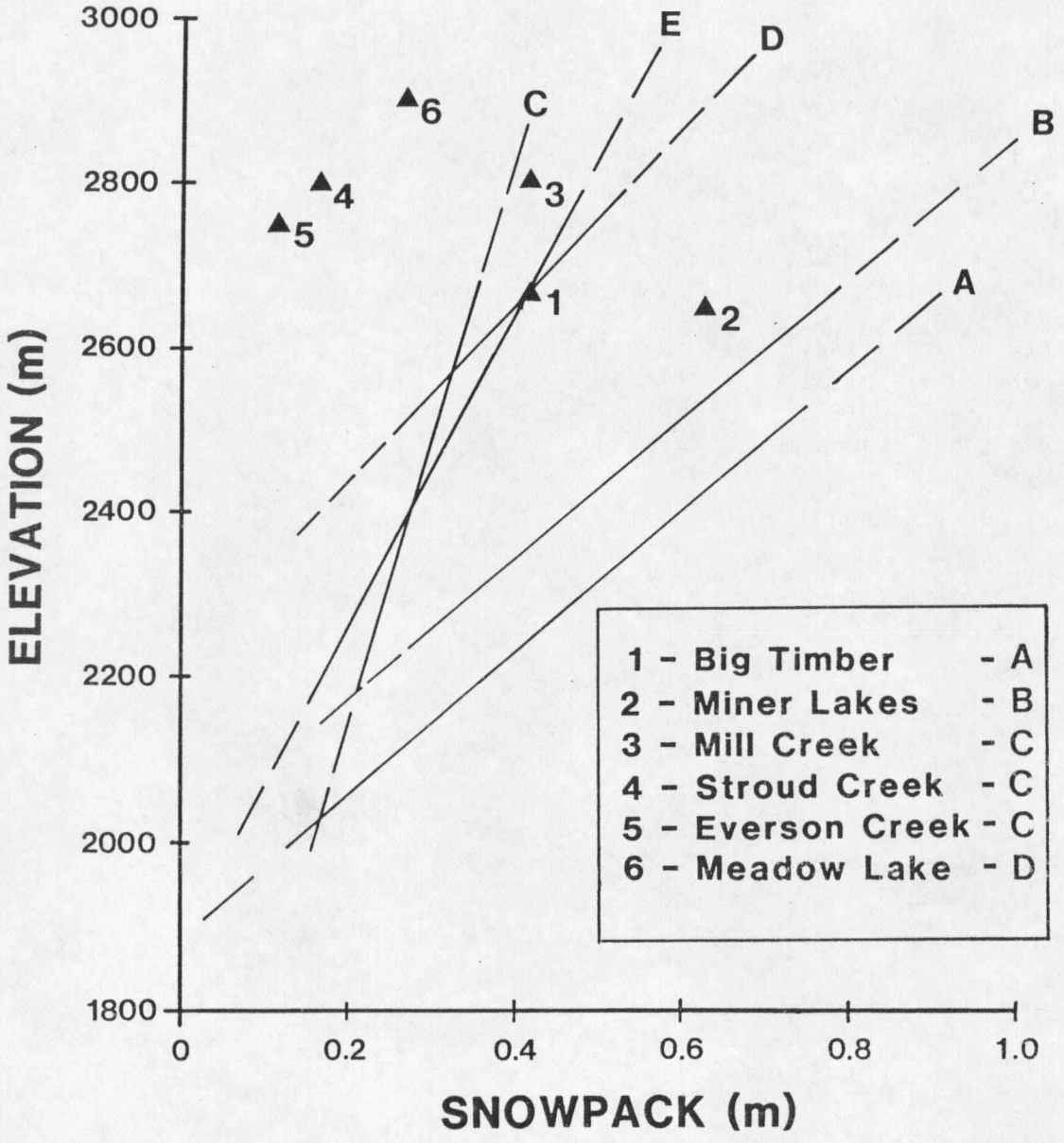

Figure 34. Comparison of calculated net accumulation (solid triangles) to modern snowpack accumulation gradients for the mountain ranges in this study (same labels as Figure 9: A = Crazy; B = Beaverhead; C = Lemhi north; D = Lemhi south; E = Lemhi combined).

annual precipitation and modern net winter accumulation, the actual decrease was probably greater and therefore closer to the values of Locke and Kemph (1987). In general, there was a greater difference in the Crazy Mountains than in the Beaverhead Range which is consistent with the findings of Locke and Kemph (1987). Expansion of the work of Locke and Kemph (1987) to Idaho (Locke and others, 1989) suggests that paleoprecipitation there was also lower than present, consistent with the results of this study in the Lemhi Range.

General Circulation Models (Kutzbach and Wright, 1985; Manabe and Broccoli, 1985) have interpreted a weaker westerly airflow over the study area during the last glacial maximum. A weaker jet stream over this area would reduce the frequency of storms through the area and therefore reduce the total annual precipitation. The results of this study are consistent with that interpretation. Kutzbach and Wright (1985) also interpreted a 25-30% decrease in total annual precipitation over the region. While this is an average value for the northwestern United States, results from this study and others (Locke and Kemph, 1987; Locke and others, 1989) indicate that the average decrease may have been up to 50% less than present.

CONCLUSIONS

A reliable reconstruction of the areal extent of late Pleistocene glaciers can be made using topographic maps and aerial photographs if evidence such as moraines and trimlines are preserved. From this reconstruction, calculations of average effective basal shear stress, ice velocity and mass balance can be made. Allowable error in the topographic maps affects the precision of the calculations, but the probability of a 20% error in calculated velocity (thus mass flux) is only 1%. Field survey is useful in determining the extent and amount of post-glacial modification of the glaciated valleys.

Calculations of average effective basal shear stress using the data derived from the maps can be used as a check on the validity of the reconstruction. Normal effective basal shear stresses should range from 0.5 to 1.5 bar if the reconstruction is valid. Unusually low values of basal shear stress in the terminal areas of paleoglaciers can be induced by error in reconstruction. These values may also reflect increased basal sliding in the terminal area from the addition of meltwater to the bed or from basal till deformation.

Sensitivity of the flow law equations to changes in ice slope can be minimized by selecting valleys with constant or slowly varying slope and by averaging slope and valley shape factors over a distance of 8-20 times the ice thickness. Local variations in surface slope do not affect the glacier velocity over short distances. This averaging also reduces the effect of error in the topographic maps by making the

vertical error a smaller percentage of the distance over which slope is averaged.

For a valley with a floor of constant or slowly varying slope, the mass balance of a paleoglacier can be calculated assuming no basal sliding occurs at the point where the highest deformation mass flux occurs. This point should occur at or near the ELA where lower temperatures should reduce the amount of basal meltwater and where thicknesses and valley cross-sectional areas are generally greatest. If this point occurs at a point other than the ELA, net mass exchange at the ELA can be calculated from the continuity equation and an appropriate mass balance gradient. Net mass exchange is equal to the net accumulation and net ablation on a steady state glacier.

Use of the continuity equation also provides an estimation of basal slip along the length of the glacier. Previous studies (Haeberli and Penz, 1985; Leonard and others, 1986; McCalpin, 1986) assumed a constant slip percentage at the ELA but could not model the variation in slip along the rest of the glacier. This study provides the first estimation of the variation of slip along the length of paleoglaciers. The actual values are minima. However, they do show that basal slip varies from glacier to glacier and that the assumption of a constant slip percentage at the ELA for all glaciers is inaccurate.

Comparison of calculated mass balance gradients to modern analogs provides an estimation of the climate that occurred when the glaciers were at their peak. Calculated mass balance gradients in this study were similar to modern gradients found in the Brooks Range of Alaska

(McCall Glacier: 2 mm/m; Meier and others, 1971). This indicates that the climate of the last glacial maximum in southwestern Montana and northwestern Idaho was much drier and probably colder than present.

Mass balance estimates also provide paleoprecipitation values for the glacier accumulation areas. The average annual net accumulation at a point above the ELA can be calculated and compared to modern average precipitation values. Results of this study show that the local paleoprecipitation on these glaciers was less than modern values for the same elevation. Deflection of the westerly jetstream around the massifs of the Laurentide and Cordilleran ice sheets (Kutzbach and Wright, 1985; Manabe and Brocolli, 1985) potentially caused a decreased frequency of storms in the area, which might be reflected in decreased precipitation. The results of this study also confirm the independent findings of Locke and Kemph (1987) and Locke and others (1989) which yielded paleoprecipitation values roughly 50% of modern values.

Suggestions for Future Study

Dynamics Modelling

The main assumption in the model is that basal sliding is a minimum at the point of maximum deformation flux. The result of this assumption is that all values of velocity, mass flux and mass balance are minima. A method of determining a reasonable maximum to these values must be found. It is reasonable to assume some slip at the point of maximum deformation. The actual amount must still be determined, within limits. If the amount of slip at this point can be

determined, then more precise calculations of mass balance and precipitation can be made.

The temperature dependent constant A can vary with elevation and thickness in the glacier. The constant A can change by an order of magnitude with a 10°C change in temperature. Using paleotemperature estimates from other models (e.g. GCMs - Kutzbach and Wright, 1985), variations in temperature through the glacier can be modelled. This information could be used in the calculation of deformation velocity which would lead to more accurate calculations of mass flux, mass balance and precipitation.

Paleoclimatic Modelling

The extensive glaciation of the mountains of southwestern Montana and adjacent Idaho provide numerous valleys in which this model can be applied. If more valleys are studied in this area, regional paleoprecipitation patterns could be determined. The effects of the continental ice sheets on windflow patterns could be better defined by the results from further study.

The mass balance of the glacier is a combination of the input through accumulation and the output through ablation. These are usually investigated as functions of winter precipitation and summer temperature respectively (Sugden and John, 1975). For paleoglaciers, this represents one equation with two unknowns. This model provides values of paleoprecipitation, eliminating one of the unknowns. If paleoprecipitation values are calculated for enough valleys, an estimation of regional paleotemperature may also be possible.

The model can be used in other regions as well. Care must be taken to select valleys with constant or slowly varying slope to minimize the modelling errors induced by compressive or extensive flow. Also valleys with well defined glacial geologic features are desirable to facilitate and enhance the accuracy of the glacier reconstruction.

REFERENCES CITED

Alden, W.C., 1953, Physiography and glacial geology of western Montana and adjacent areas: U.S. Geological Survey Professional Paper 231, 200 p.

Alford, D., and Clark, R., 1968, The 1967 mass balance of the Grasshopper Glacier, Montana: Northwest Science, v. 42, p. 115-123.

American Geographical Society, 1960, Nine glacier maps: AGS Special Publication No. 34.

Andrews, J.T., 1975, Glacial systems: North Scituate, Massachusetts, Duxbury Press, 191 p.

Aten, R.E., 1974, Geomorphology of the east flank of the Crazy Mountains, Montana [Ph.D. thesis]: Lafayette, Indiana, Purdue University, 136 p.

Barry, R.G., 1981, Mountain weather and climate: New York, Meuthen, 313 p.

Barry, R.G., 1983, Late Pleistocene climatology, in Porter, S.C., ed., Late Quaternary environments of the United States: Volume 1, The Late Pleistocene: Minneapolis, University of Minnesota Press, p. 390-407.

Blair, T.A., and Fite, R.C., 1965, Weather elements, a text in elementary meteorology: Englewood Cliffs, New Jersey, Prentice-Hall, 364 p.

Boulton, G.S., and Jones, A.S., 1979, Stability of temperate ice caps and ice sheets resting on beds of deformable sediment: Journal of Glaciology, v. 24, p. 29-43.

CLIMAP Project Members, 1981, Seasonal reconstructions of the earth's surface at the last glacial maximum: Geological Society of America Map Chart Series, MC-36.

Critchfield, H.J., 1974, General climatology: Englewood Cliffs, New Jersey, Prentice-Hall, 446 p.

Davis, P.T., and Osborn, G., 1988, Preface, Holocene glacier fluctuations: Quaternary Science Reviews, v. 7, p. 113-114.

Echelmeyer, K., and Zhongxiang, W., 1987, Direct observation of basal sliding and deformation of basal drift at subfreezing temperatures: Journal of Glaciology, v. 33, p. 83-98.

Field, W.O., ed., 1975, Mountain glaciation in the northern hemisphere: Hanover, New Hampshire, U.S. Army Corps of Engineers, Cold Regions Research and Engineering Laboratories, 698 p.

Flint, R.F., 1971, Glacial and Quaternary geology: New York, John Wiley and Sons, 892 p.

Fullerton, D.S., and Colton, R.B., 1986, Stratigraphy and correlation of the glacial deposits on the Montana plains, in Sibrava, V., Bowen, D.Q., and Richmond, G.M., eds., Quaternary Glaciations in the Northern Hemisphere: Quaternary Science Reviews, v. 5, p. 69-82.

Glen, J.W., 1952, Experiments on the deformation of ice: Journal of Glaciology, v. 2, p. 111-114.

Graf, W.L., 1970, The geomorphology of the glacial valley cross section: Arctic and Alpine Research, v. 2, p. 303-312.

Graf, W.L., 1976, Cirques as glacier locations: Arctic and Alpine Research, v. 8, p. 79-90.

Haeberli, W., and Penz, U., 1985, An attempt to reconstruct glaciological and climatological characteristics of 18 ka ice age glaciers in and around the Swiss Alps: Zeitschrift für Gletscherkunde und Glazialgeologie, v. 21, p. 351-361.

Harding, W.G., 1982, Foreword, in Cunningham, C., ed., Montana Weather: Helena, Montana, Montana Magazine, p. 1-10.

Holmlund, P., 1988, Is the longitudinal profile of Storglaciaren, northern Sweden, in balance with the present climate?: Journal of Glaciology, v. 34, p. 269-273.

Kutzbach, J.E., and Wright, H.E., Jr, 1985, Simulation of the climate of 18,000 years BP; Results for the North American/North Atlantic/European Sector and comparison with the geologic record of North America: Quaternary Science Reviews, v. 4, p. 147-187.

Leonard, E.M., 1984, Late Pleistocene equilibrium-line altitudes and modern accumulation patterns, San Juan Mountains, Colorado, U.S.A: Arctic and Alpine Research, v. 16, p. 65-76.

Leonard, E.M., Huston, M.M., and Manley, A.E., 1986, Ice dynamics modelling of Rocky Mountain paleoglaciers - methods, results, and paleoclimatic inferences: Geological Society of America Abstracts with Programs, v. 18, p. 671.

Locke, W.W., and Kemph, T.S., 1987, Paleo-equilibrium line altitudes and paleoclimate of Montana during peak glacial times: Geological Society of America, Rocky Mountain Section, Abstracts with Programs, v. 19, p. 315.

Locke, W.W., 1989, Present climate and glaciation of western Montana, U.S.A.: Arctic and Alpine Research, v. 21, p. 234-244.

Locke, W.W., Murray, D.R., and Slaughter, K.W., 1989, Peak-glacial environments of the Rocky Mountains of Montana and Idaho: Abstracts, CANQUA 1989, Edmonton, Alberta.

Mathews, W.H., 1967, Profiles of late Pleistocene glaciers in New Zealand: New Zealand Journal of Geology and Geophysics, v. 10, p. 146-163.

Manabe S., and Broccoli, A.J., 1985, The influence of continental ice sheets on the climate of an ice age: Journal of Geophysical Research, v. 90, no. D1, p. 2167-190.

McCalpin, J., 1986, written communication, Utah State University, Logan, Utah.

Meier, M.F., and Post, A.S., 1962, Recent variations in mass net budgets of glaciers in North America: IASH Commission of Snow and Ice, Publication 58, p. 63-77.

Meier, M.F., 1966, Some glaciological interpretations of remapping programs on South Cascade, Nisqually, and Klawatti Glaciers, Washington: Canadian Journal of Earth Sciences, v. 3, p. 811-818.

Meier, M.F., 1968, Calculations of slip of Nisqually glacier on its bed: no simple relation of sliding velocity to shear stress: IASH General Assembly of Bern - Commission of Snow and Ice, Publication 79, p. 49-57.

Meier, M.F., Tangborn, W.V., Mayo, L.R., and Post, A., 1971, Combined ice and water balances of Gulkana and Wolverine Glaciers, Alaska, and South Cascade Glacier, Washington, 1965 and 1966 hydrologic years: U.S. Geological Survey Professional Paper 715-A, 23 p.

Meierding, T.C., 1982, Late Pleistocene glacial equilibrium-line altitudes in the Colorado Front Range: A comparison of methods: Quaternary Research, v. 18, p. 289-310.

Mitchell, V.L., 1969, The regionalization of climate in the western United States [Ph.D. thesis]: Madison, Wisconsin, University of Wisconsin, 147 p.

NOAA, 1985a, Climatological data, annual summary, Idaho, v. 88, no. 13: Asheville, North Carolina, National Climatic Data Center.

NOAA, 1985b, Climatological data, annual summary, Montana, v. 88, no. 13: Asheville, North Carolina, National Climatic Data Center.

Nye, J.F., 1952, The mechanics of glacier flow: Journal of Glaciology, v. 2, p. 82-93.

Nye, J.F., 1965a, A numerical method of inferring the budget history of a glacier from its advance and retreat: Journal of Glaciology, v. 5, p. 589-607.

Nye, J.F., 1965b, The flow of a glacier in a channel of rectangular, elliptic or parabolic cross-section: Journal of Glaciology, v. 5, p. 661-690.

Paterson, W.S.B., 1981, The physics of glaciers. [2nd edition]: Oxford, Pergamon Press, 380 p.

Pierce, K.L., 1979, History and dynamics of glaciation in the northern Yellowstone National Park area: U.S. Geological Survey, Professional Paper 729-F, 90 p.

Porter, S.C., 1975, Equilibrium-line altitudes of late Quaternary glaciers in the southern Alps, New Zealand: Quaternary Research, v. 5, p. 27-47.

Porter, S.C., ed., 1983, Late Quaternary environments of the United States: Volume 1, The Late Pleistocene: Minneapolis, University of Minnesota Press, 407 p.

Porter, S.C., Pierce, K.L., and Hamilton, T.D., 1983, Late Wisconsin mountain glaciation in the western United States, in Porter, S.C., ed., Late Quaternary environments of the United States: Volume 1, The Late Pleistocene: Minneapolis, University of Minnesota Press, p. 71-111.

Price, L.W., 1981, Mountains & man: Berkeley, University of California Press, 506 p.

Raymond, C.F., 1980, Temperate valley glaciers, in Colbeck, S.C., ed., Dynamics of snow and ice masses: New York, Academic Press, p. 80-141.

Richmond, G.M., 1965, Glaciation of the Rocky Mountains, in Wright, H.E., and Frey, D.G., eds., The Quaternary of the United States: Princeton, New Jersey, Princeton University Press, p. 217-230.

Ross, C.P, Andrews, D.A., and Witkind, I.J., 1955, Geologic map of Montana: U.S. Geological Survey.

Ruppel, E.T., 1980, Geologic map of the Patterson quadrangle, Lemhi County, Idaho: U.S. Geological Survey Map GQ-1529.

Ruppel, E.T., and Lopez, D.A., 1981, Geologic map of the Gilmore quadrangle, Lemhi and Custer Counties, Idaho: U.S. Geological Survey Map GQ-1543.

Schilling, D.H., and Hollin, J.T., 1981, Numerical reconstruction of valley glaciers and small ice caps, in Denton, G.H., and Hughes, T.J., eds., The last great ice sheets: New York, John Wiley and Sons, p. 207-221.

Soil Conservation Service, 1986a, Idaho annual data summary, water year 1986 - Idaho Cooperative Snow Survey Data of Federal-State-Private Cooperative Snow Surveys: Boise, Idaho, Soil Conservation Service.

Soil Conservation Service, 1986b, Montana annual data summary, water year 1986 - Montana Cooperative Snow Survey Data of Federal-State-Private Cooperative Snow Surveys: Bozeman, Montana, Soil Conservation Service.

Sugden, D.E., and John, B.S., 1976, Glaciers and Landscape: London, Halsted Press, 376 p.

Taylor, R.L., and Ashley, J.M., 1986, Geologic map of Montana: Bozeman, Montana, Department of Earth Sciences, Montana State University.

Thompson, M.M., 1979, Maps for America: Washington, D.C., U.S. Government Printing Office, 265 p.

Waitt, R.B., Jr, and Thorson, R.M., 1983, The Cordilleran ice sheet in Washington, Idaho, and Montana, in Porter, S.C., ed., Late Quaternary Environments of the United States, Volume 1: The Late Pleistocene: Minneapolis, University of Minnesota Press, p. 53-70.

Weertman, J. 1973. Creep of ice, in Whalley, E., Jones, S.J., and Gold, L.W., eds., Physics and Chemistry of Ice: Ottawa, Royal Society of Canada, p. 320-337.

Weertman, J. 1979. The unsolved general glacier sliding problem: Journal of Glaciology, v. 23, p. 97-115.

APPENDICES

APPENDIX A

TOPOGRAPHIC MAPS AND AIR PHOTOS

Table 16. Topographic maps and aerial photographs used for glacier reconstruction.

Glacier	Topographic Maps (Year)	Aerial Photographs Line	Roll/Exposures	Date
Big Timber	Crazy Peak, MT (1972)	49	680/122-125	8-11-81
	Amelong Creek, MT (1972)	50	680/142-146	8-11-81
	Battleship Butte, MT (1972)	51	480/19-21	7-18-81
			680/152-154	8-11-81
		52	480/5-9	7-18-81
Miner Lakes	Homer Youngs Peak, MT (1966)	9	287/49-53	8-3-87
	Miner Lakes, MT (1966)	10	387/115-121	8-3-87
		11S	387/99-102	8-3-87
		12S	387/141-143[5]	8-3-87
			487/2-4[5]	8-3-87
		13S	487/31-35[5]	8-3-87
		14S	487/70-73[5]	8-3-87
		15C	487/79-82[5]	8-3-87
Meadow Lake	Gilmore, ID (1987)[2]	31	680/83-87	7-23-81
	Gilmore, ID[3]	32	680/50-54	7-23-81
	Gilmore SE, ID[4]			
Mill Creek	Paterson NW, ID[4]	25	480/119-122	7-15-81
	Paterson NE, ID[4]	26	480/148-151	7-15-81
	Paterson, ID[3] (1956)			
Stroud Creek/	Paterson NE, ID[4]	25	480/121-123	7-15-81
Everson Creek	Paterson SE, ID[4]	26	480/151-154	7-15-81
	Paterson, ID[3] (1956)	27	480/174-177	7-15-81

[1]Scale 1:24000 unless noted otherwise
[2]Provisional Edition
[3]Scale 1:62500 (15' map)
[4]Orthophoto quadrangle (scale 1:24000) produced from 15' map
[5]Scale 1:15840

APPENDIX B

PROGRAM FOR CALCULATING THEORETICAL GLACIER PROFILES

Figure 35. FORTRAN program for calculating theoretical glacier profiles.

```
C ***************************************************************************
C
C   PROGRAM: ICETOPO.FOR
C
C   PURPOSE: This program calculates the ice surface elevations for
C            a valley glacier using a perfectly plastic flow law.
C
C   WRITTEN: 09-OCT-88 (modified from BASIC)
C
C   LANGUAGE: MS-FORTRAN VER. 3.10
C
C   AUTHOR:  Donald R. Murray (after Schilling and Hollin, 1981)
C
C   MODIFIED: 21-OCT-88 DRM: Modified the input so that basal shear
C                            stress is input from terminal ratherthan
C                            from the file.
C
C   INPUT FILES: 1 - File with values of distance from terminus,
C                    bedrock elevation, and shape factor. Values must
C                    be separated by a space and all values for one
C                    step located on the same line in the order listed
C                    above.
C
C   INPUT VARIABLES: DIST     - distance (in feet) from ice terminus.
C                    GROUND   - bedrock elevation at each step (feet).
C                    SHAPE    - shape factor (F) as defined by Nye.
C                    TAU      - basal shear stress (bars).
C                    ICE      - ice surface elevation at initial
C                               point (feet).
C
C   OUTPUT:          Printout or file with the input variables and
C                    the calculated ice surface elevation at each
C                    step. If the output is to a file, the file must
C                    exist or an error will occur.
C ***************************************************************************
C
C    DECLARATION OF VARIABLES
C
      INTEGER DIST(100),GROUND(100),ICE(100)
      INTEGER THICK,YFILE,METRIC
      REAL*4  SHAPE(100)
      REAL*4  MTAU,MGRND,MTHICK,CNST,INCR,RHO,G,TAU
      CHARACTER*40 CASE
      CHARACTER*14 FNAME,OUTFILE
      CHARACTER*1 YORN,PORF,NEWRUN,SI
C
C   LET'S INITIALIZE SOME VARIABLES
C
```

```
      RHO = 910.
      G   = 9.810001
C
C   PRINT OUT THE INSTRUCTIONS FOR RUNNING THE PROGRAM
C
      WRITE (*,10) 'This program calculates ice surface elevations'
10    FORMAT (5X,A)
      WRITE (*,10) 'iteratively for valley glaciers using a perfectly'
      WRITE (*,10) 'plastic approximation'
      WRITE (*,10)
      WRITE (*,10) 'The following information must be supplied from a'
      WRITE (*,10) 'data file:'
      WRITE (*,10)
      WRITE (*,10) '     - Distance (in feet) from the ice terminus'
      WRITE (*,10) '     - Bedrock elevation (in feet)'
      WRITE (*,10) '     - Shape factor (dimensionless)'
      WRITE (*,10)
      WRITE (*,10) ' with each variable separated by a space.'
      WRITE (*,10)
C
C  CHECK TO SEE IF WE SHOULD CONTINUE OR NOT
C
      WRITE (*,'(1X,A\)') 'Do you wish to continue? '
      READ (*,'(A)') YORN
      IF ((YORN .EQ. 'n') .OR. (YORN .EQ. 'N')) STOP
C
C   CONTINUE ON WITH THE PROGRAM AND GET INITIAL INFORMATION
C
 12   WRITE(*,'(/,/,1X,A,/)')'First we need some initial information.'
      WRITE (*,'(1X,A\)') 'What is the name of this run? '
      READ (*,'(A)') CASE
C
C   GET THE NAME OF THE INPUT FILE
C
      WRITE (*,15) 'What is the name of the input file? '
      READ (*,'(A)') FNAME
      OPEN (1,FILE=FNAME)
 15   FORMAT (/,1X,A\)
 16   FORMAT (/,1X,A,A\)
C
C   CHECK TO SEE IF OUPUT GOES TO THE PRINTER OR A FILE AND IF THE
C   OUTPUT IS IN ENGLISH OR METRIC UNITS.
C
      YFILE = 0
      WRITE (*,16) 'Do you wish the output to go to a file or to ',
     +   'the printer (P=printer/F=file)? '
      READ (*,'(A)') PORF
      IF ((PORF .EQ. 'F') .OR. (PORF .EQ. 'f')) THEN
         WRITE (*,'(/,1X,A\)') 'What is the name of the ouput file? '
         READ (*,'(A)') OUTFIL
         OPEN (2,FILE=OUTFIL)
         YFILE = 1
```

```
      ELSE
         OPEN (2,FILE='LPT1')
      ENDIF
      METRIC = 0
      WRITE (*,16) 'Do you wish the output to be in English (E) or ',
     +   'SI (S) units? '
      READ (*,'(A)') SI
      IF ((SI .EQ. 'S') .OR. (SI .EQ. 's')) METRIC = 1
C
C   GET THE INITIAL ICE SURFACE ELEVATION
C
      WRITE(*,16) 'What is the ice surface elevation at the starting',
     +  ' point (in feet)? '
      READ (*,'(I5)') ICE(1)
C
C   GET THE BASAL SHEAR STRESS VALUE
C
      WRITE (*,16) 'What is the basal shear stress for this run (in ',
     +  'bars)? '
      READ (*,'(F4.2)') TAU
C
C   READ THE DATA FROM THE INPUT FILE
C
      DO 40, I=1,100
        READ (1,30,END=50) DIST(I), GROUND(I), SHAPE(I)
 30     FORMAT(BN,7X,I5,7X,I5,5X,F4.2)
 40   CONTINUE
C
 50   K = I-1
      THICK = ICE(1) - GROUND(1)
C
C   Print out the header and the data for step 1.
C
      WRITE (2,'(1X,A,//)') CASE
C
      IF (METRIC .NE. 1) THEN
        WRITE (2,60)
 60     FORMAT (1X,'Distance from',2X,'Bedrock',3X,'Ice Surface',4X,
     +  'Ice',5X,'Shape',6X,'Basal',/,3X,'Terminus',4X,'Elevation',
     +  3X,'Elevation',2X,'Thickness',2X,'Factor',2X,'Shear Stress',/,
     +  4X,'(ft)',9X,'(ft)',8X,'(ft)',8X,'(ft)',15X,'(bar)',/,1X,
     + '----------',4X,'---------',2X,'-----------',1X,'---------',2X,
     +  '------',2X,'------------',/)
        WRITE (2,65) DIST(1), GROUND(1), ICE(1), THICK, SHAPE(1), TAU
 65     FORMAT (3X,I6,6X,I6,7X,I6,5X,I6,6X,F3.2,6X,F4.2)
      ELSE
        WRITE (2,66)
 66     FORMAT (1X,'Distance from',2X,'Bedrock',3X,'Ice Surface',4X,
     +  'Ice',5X,'Shape',6X,'Basal',/,3X,'Terminus',4X,'Elevation',
     +  3X,'Elevation',2X,'Thickness',2X,'Factor',2X,'Shear Stress',/,
     +  4X,'(m)',10X,'(m)',9X,'(m)',9X,'(m)',16X,'(bar)',/,1X,
     + '----------',4X,'---------',2X,'-----------',1X,'---------',2X,
```

```
     +  '------',2X,'------------',/)
        WRITE (2,65) INT(DIST(1)*.3048), INT(GROUND(1)*.3048),
     +    INT(ICE(1)*.3048), INT(THICK*.3048), SHAPE(1), TAU
      ENDIF
C
      DO 75, I=2,K
C
C   Compute the distance from this step to the next/convert to metric.
C
         MLEN = (DIST(I) - DIST(I-1))*.3048
C
C   Convert the other values to metric for the calculations.
C
         MGRND = GROUND(I) * .3048
         MTAU  = TAU * 10**5
         MTHICK = THICK * .3048
C
C   Start calculations
C
         CNST = MTAU/(SHAPE(I) * RHO * G)
         INCR = MLEN/MTHICK
         ICE(I) = ICE(I-1) + (CNST * INCR * 3.2808)
C
C   Check out the new ice thickness
C
         THICK = ICE(I) - GROUND(I)
         IF (THICK .LE. 30) THEN
            WRITE (2,'(1X,A,/)') 'Nunatak or cirque headwall.'
            GOTO 100
         ENDIF
C
C   Print out the data, check to see if it should be English or Metric
C
         IF (METRIC .NE. 1) THEN
            WRITE (2,70) DIST(I), GROUND(I), ICE(I), THICK, SHAPE(I)
  70        FORMAT (3X,I6,6X,I6,7X,I6,5X,I6,6X,F3.2)
         ELSE
            WRITE (2,70) INT(DIST(I)*.3048), INT(MGRND),
     +        INT(ICE(I)*.3048), INT(THICK*.3048), SHAPE(I)
         ENDIF
  75  CONTINUE
C
C   If the data was written to a printer, send a form feed at the end.
C
 100  IF (YFILE .NE. 1) WRITE (2,'(/,A)') '1'
C
C  If the output was to a file, send a message to the console
C   saying that the printing has been completed.
C
      IF (YFILE .EQ. 1) WRITE (*,125) 'The data has been written to ',
     +  OUTFIL
 125  FORMAT (1X,/,1X,A30,A14)
```

```
C
C       See if another run is wanted
C
        WRITE (*,15) 'Do you wish to make another run (Y/N)? '
        READ (*,'(A)') NEWRUN
        IF ((NEWRUN .EQ. 'Y') .OR. (NEWRUN .EQ. 'y')) GOTO 12
C
C    End the program
C
        END
```

APPENDIX C

PROGRAM FOR CALCULATING SHEAR STRESS

Figure 36. FORTRAN program for calculating average effective basal shear stress.

```
C ***************************************************************************
C
C   PROGRAM: TAU.FOR
C
C   PURPOSE: This program calculates the theoretical basal shear
C            stress at a point on the glacier using the relation:
C
C                TAU = RHO*G*THICK*SIN ALPHA
C
C            where:  TAU  = average basal shear stress
C                    RHO  = ice density (910 kg/m**3)
C                    G    = acceleration due to gravity (9.81m/sec**2)
C                    THICK  = ice thickness
C                    SIN ALPHA = ice surface slope
C
C            Average basal shear stress (TRUTAU) is calculated by
C            multiplying TAU by SHAPE. SHAPE is a valley shape factor
C            that accounts for the frictional effects of the valley
C            walls.
C
C   WRITTEN: 14-OCT-88 (modified from BASIC)
C
C   LANGUAGE: MS-FORTRAN VER. 3.10
C
C   AUTHOR:  Donald R. Murray
C
C   MODIFIED:  21-OCT-88 DRM: Added a feature whereby the user can
C                        determine the step length over which to
C                        average the ice surface slope.
C
C   INPUT FILES: 1 - File with values of distance from terminus,
C                    bedrock elevation, ice surface elevation and
C                    shape factor at each iterative step.  Values must
C                    be separated by a space and all values for one
C                    located on the same line in the order listed.
C
C   INPUT VARIABLES: DIST  - distance (in feet) from the iceterminus.
C                    GROUND - bedrock elevation at each step (feet).
C                    ICE    - ice surface elevation (feet).
C                    SHAPE  - shape factor (F) as defined by Nye.
C
C   OUTPUT:          Printout or file with the input variables and the
C                    calculated shear stresses at each step. If the
C                    output is to a file, the file must exist or an
C                    error will occur.
C***************************************************************************
C
C    DECLARATION OF VARIABLES
```

```
C
      INTEGER DIST(100),GROUND(100),ICE(100)
      INTEGER THICK,YFILE,METRIC,AVSTEP,STEP
      REAL*4  SHAPE(100)
      REAL*4  CNST,RATIO,ANGLE
      REAL*4  MTHICK,SLOPE,TAU,TRUTAU
      CHARACTER*40 CASE
      CHARACTER*14 FNAME,OUTFILE
      CHARACTER*1 YORN,PORF,NEWRUN,SI,AVE
C
C   LET'S INITIALIZE SOME VARIABLES
C
      RHO = 910.
      G   = 9.810001
C
C   PRINT OUT THE INSTRUCTIONS FOR RUNNING THE PROGRAM
C
      WRITE (*,10) 'This program calculates basal shear stresses'
10    FORMAT (5X,A)
      WRITE (*,10) 'along the centerline of a glacial valley.'
      WRITE (*,10)
      WRITE (*,10) 'The following information must be supplied from a'
      WRITE (*,10) 'data file:'
      WRITE (*,10)
      WRITE (*,10) '     - Distance (in feet) from the ice terminus'
      WRITE (*,10) '     - Bedrock elevation (in feet)'
      WRITE (*,10) '     - Ice surface elevation (in feet)'
      WRITE (*,10) '     - Shape factor (dimensionless)'
      WRITE (*,10)
      WRITE (*,10) ' with each variable separated by a space.'
      WRITE (*,10)
      WRITE (*,10) ' In calculating the shear stress, ice surface '
      WRITE (*,10) ' slope can be averaged over several steps.'
      WRITE (*,10)
C
C  CHECK TO SEE IF WE SHOULD CONTINUE OR NOT
C
      WRITE (*,'(1X,A\)') 'Do you wish to continue? '
      READ (*,'(A)') YORN
      IF ((YORN .EQ. 'n') .OR. (YORN .EQ. 'N')) STOP
C
C   CONTINUE ON WITH THE PROGRAM AND GET INITIAL INFORMATION
C
 12   WRITE(*,'(/,/,1X,A,/)')'First we need some initial information.'
      WRITE (*,'(1X,A\)') 'What is the name of this run? '
      READ (*,'(A)') CASE
C
C   GET THE NAME OF THE INPUT FILE
C
      WRITE (*,15) 'What is the name of the input file? '
      READ (*,'(A)') FNAME
      OPEN (1,FILE=FNAME)
```

```
 15   FORMAT (/,1X,A\)
 16   FORMAT (/,1X,A,A\)
C
C   CHECK TO SEE IF OUPUT GOES TO THE PRINTER OR A FILE AND IF THE
C   OUTPUT IS IN ENGLISH OR METRIC UNITS.
C
      YFILE = 0
      WRITE (*,16) 'Do you wish the output to go to a file or to ',
     +   'the printer (P=printer/F=file)? '
      READ (*,'(A)') PORF
      IF ((PORF .EQ. 'F') .OR. (PORF .EQ. 'f')) THEN
         WRITE (*,'(/,1X,A\)') 'What is the name of the ouput file? '
         READ (*,'(A)') OUTFIL
         OPEN (2,FILE=OUTFIL)
         YFILE = 1
      ELSE
         OPEN (2,FILE='LPT1')
      ENDIF
      METRIC = 0
      WRITE (*,16) 'Do you wish the output to be in English (E) or ',
     +   'SI (S) units? '
      READ (*,'(A)') SI
      IF ((SI .EQ. 'S') .OR. (SI .EQ. 's')) METRIC = 1
C
C  See if the ice surface slope should be averaged over several steps.
C
      STEP = 1
      WRITE (*,15) 'Do you wish to use an average surface slope? '
      READ (*,'(A)') AVE
      IF ((AVE .EQ. 'y') .OR. (AVE .EQ. 'Y')) THEN
        WRITE (*,16) 'How many steps do you wish it to be averaged ',
     +      'over? '
        READ (*,'(I5)') AVSTEP
        STEP = AVSTEP/2
      ENDIF
C
C   READ THE DATA FROM THE INPUT FILE
C
      DO 40, I=1,100
        READ (1,30,END=50) DIST(I), GROUND(I), ICE(I), SHAPE(I)
 30     FORMAT(BN,7X,I5,7X,I5,7X,I5,5X,F4.2)
 40   CONTINUE
C
 50   K = I-1
C
C   Print out the header.
C
      WRITE (2,'(1X,A,//)') CASE
C
      IF (METRIC .NE. 1) THEN
        WRITE (2,60)
 60     FORMAT (1X,'Distance from',2X,'Bedrock',3X,'Ice Surface',4X,
```

```
     +  'Ice',5X,'Surface',2X,'Theo',2X,'Shape',3X,'True',/,3X,
     +  'Terminus',4X,'Elevation',3X,'Elevation',2X,'Thickness',3X,
     +  'Slope',3X,'Tau',3X,'Factor',2X,'Tau',/,
     + 4X,'(ft)',9X,'(ft)',8X,'(ft)',8X,'(ft)',13X,'(bar)',9X,'(bar)',
     +  /,1X,'----------',4X,'---------',2X,'----------',1X,
     +  '---------',2X,'-------',2X,'----',2X,'------',2X,'----',/)
      ELSE
        WRITE (2,65)
 65     FORMAT (1X,'Distance from',2X,'Bedrock',3X,'Ice Surface',4X,
     +  'Ice',5X,'Surface',2X,'Theo',2X,'Shape',3X,'True',/,3X,
     +  'Terminus',4X,'Elevation',3X,'Elevation',2X,'Thickness',3X,
     +  'Slope',3X,'Tau',3X,'Factor',2X,'Tau',/,
     +  5X,'(m)',10X,'(m)',9X,'(m)',8X,'(m)',14X,'(bar)',9X,'(bar)',
     +  /,1X,'----------',4X,'---------',2X,'----------',1X,
     +  '---------',2X,'-------',2X,'----',2X,'------',2X,'----',/)
      ENDIF
C
      DO 75, I=1,K
C
C   Compute the thickness of the ice at each point.
C
         THICK = ICE(I) - GROUND(I)
C
C   Compute the step factor.
C
         J = I - STEP
         IF (J .LE. 0) J = 1
         L = I + STEP
         IF (L .GT. K) L = K
C
C    Compute the ice surface slope.
C
         CNST  = FLOAT((ICE(L)-ICE(J))**2 + (DIST(L)-DIST(J))**2)
         SLOPE = (ICE(L)-ICE(J))/SQRT(CNST)
C        RATIO = FLOAT((ICE(L)-ICE(J))/(DIST(L)-DIST(J)))
C        ANGLE = ATAN(RATIO)
C        SLOPE = SIN(ANGLE)
C
C  Compute the ice shear stresses
C
         TAU = RHO*G*THICK*.3048*SLOPE/10**5
         TRUTAU = TAU * SHAPE(I)
C
C   Print out the data, check to see if it should be English or Metric
C
         IF (METRIC .NE. 1) THEN
            WRITE (2,70) DIST(I), GROUND(I), ICE(I), THICK, SLOPE,
     +              TAU, SHAPE(I), TRUTAU
  70        FORMAT (3X,I6,6X,I6,7X,I6,4X,I6,5X,F5.3,4X,F4.2,4X,F3.2,
     +             3X,F4.2)
         ELSE
            WRITE (2,70) INT(DIST(I)*.3048), INT(GROUND(I)*.3048),
```

```
     +        INT(ICE(I)*.3048), INT(THICK*.3048), SLOPE, TAU,
     +        SHAPE(I), TRUTAU
          ENDIF
  75  CONTINUE
C
C   If the data was written to a printer, send a form feed at the end.
C
 100  IF (YFILE .NE. 1) WRITE (2,'(/,A)') '1'
C
C  If the output was to a file, send a message to the console
C   saying that the printing has been completed.
C
      IF (YFILE .EQ. 1) WRITE (*,125) 'The data has been written to ',
     +  OUTFIL
 125  FORMAT (1X,/,1X,A30,A14)
C
C       See if another run is wanted
C
      WRITE (*,15) 'Do you wish to make another run (Y/N)? '
      READ (*,'(A)') NEWRUN
      IF ((NEWRUN .EQ. 'Y') .OR. (NEWRUN .EQ. 'y')) GOTO 12
C
C   End the program
C
      END
```

APPENDIX D

PROGRAM FOR CALCULATING ABLATION GRADIENTS

Figure 37. BASIC program for calculating ablation gradients.

```
10 REM************************************************************
20 REM Program: ABLATE.BAS
30 REM
40 REM Purpose: This program calculates the corresponding volumes of
50 REM          ablation for altitudes below the ELA.
60 REM
70 REM Author: Donald R. Murray
80 REM
90 REM Written: May 23, 1988
100 REM
110 REM Modified:
120 REM
130 REM Input: File containing data (in ft) of of elevation below the
140 REM         ELA and the surface area (km**2) that this elevation
150 REM         represents.
160 REM
170 REM Output: Printout of the elevation, the specific net balance
180 REM         there and the volume of ice that is ablated.
190 REM
200 REM************************************************************
210 DIM ELEVATION(15),AREA(15)
220 I = 1
230 INPUT "What is the name of the file"; F$
240 FILE$ = "B:"+F$
250 INPUT "What is the ELA elevation"; ELA
260 INPUT "What is the initial ablation gradient (mm/m)"; AG
270 INPUT "What is the incremental change"; AGSTEP
280 INPUT "How many iterations do you want"; ITER
290 OPEN FILE$ FOR INPUT AS 1
300 INPUT #1, ELEVATION (I),AREA(I)
310 IF EOF(1) THEN CLOSE:GOTO 340
320 I = I + 1
330 GOTO 300
340 X = I
350 FOR K = 1 TO ITER
360 TOTAL = 0
370 LPRINT " ELA =",ELA
380 LPRINT " ABLATION GRADIENT = ",AG
390 LPRINT
400 LPRINT "ELEVATION   SPECIFIC BALANCE    VOLUME LOST"
410 LPRINT "  (ft)            (m)          ( x 10**6 m**3)"
420 LPRINT "---------   ---------------  ---------------"
430 FOR I = 1 TO X
440 LOWER = (ELA - ELEVATION(I))*.3048
450 NETBAL = LOWER*AG/1000
460 VOLUME = NETBAL * AREA(I)
470 TOTAL = TOTAL + VOLUME
480 LPRINT USING "  #.###        ";ELEVATION(I),NETBAL,VOLUME
490 NEXT I
```

```
500 LPRINT "                                                    --------"
510 LPRINT USING "                                                   ##.### "; TOTAL
520 LPRINT
530 AG = AG - AGSTEP
540 NEXT K
550 END
```

APPENDIX E

PROGRAM FOR CALCULATING ACCUMULATION GRADIENTS

Figure 38. BASIC program for calculating accumulation gradients.

```
10 REM************************************************************
20 REM Program: ACCUM.BAS
30 REM
40 REM Purpose: This program calculates the corresponding volumes of
50 REM          accumulation for altitudes above the ELA.
60 REM
70 REM Author: Donald R. Murray
80 REM
90 REM Written: June 14, 1988
100 REM
110 REM Modified:
120 REM
130 REM Input:  File containing data (in ft) of elevation above the
140 REM         ELA and the surface area (km**2) that this elevation
150 REM         represents.
160 REM
170 REM Output: Printout of the elevation, the specific net balance
180 REM         there and the volume of ice that is accumulated.
190 REM
200 REM************************************************************
210 DIM ELEVATION(15),AREA(15)
220 I = 1
230 INPUT "What is the name of the file"; F$
240 FILE$ = "B:"+F$
250 INPUT "What is the ELA elevation"; ELA
260 INPUT "What is the initial accumulation gradient (mm/m)"; AG
270 INPUT "What is the incremental change"; AGSTEP
280 INPUT "How many iterations do you want"; ITER
290 OPEN FILE$ FOR INPUT AS 1
300 INPUT #1, ELEVATION (I),AREA(I)
310 IF EOF(1) THEN CLOSE:GOTO 340
320 I = I + 1
330 GOTO 300
340 X = I
350 FOR K = 1 TO ITER
360 TOTAL = 0
370 LPRINT " ELA =",ELA
380 LPRINT " ACCUMULATION GRADIENT = ",AG
390 LPRINT
400 LPRINT "ELEVATION   SPECIFIC BALANCE    VOLUME GAINED"
410 LPRINT "  (ft)            (m)         ( x 10**6 m**3)"
420 LPRINT "---------   ---------------  ---------------"
430 FOR I = 1 TO X
440 HIGHER = (ELEVATION (I) - ELA)*.3048
450 NETBAL = HIGHER*AG/1000
460 VOLUME = NETBAL * AREA(I)
470 TOTAL = TOTAL + VOLUME
480 LPRINT USING "  #.###       ";ELEVATION(I),NETBAL,VOLUME
490 NEXT I
```

```
500 LPRINT "                                                    --------"
510 LPRINT USING "                                                   ##.### "; TOTAL
520 LPRINT
530 AG = AG - AGSTEP
540 NEXT K
550 END
```

APPENDIX F

DATA FOR STROUD CREEK

Table 17. Stroud Creek paleoglacier morphology and rheology interpreted from topographic maps and comparison with theoretical values.

Distance from Terminus (ft)	Bedrock Elevation (ft)	Ice Elevation (ft)	Ice Thickness (ft)	Shape Factor	Calc. τ_b[1] (bar)	Theoretical Ice Elevation[2] (ft)	Diff. (Theo.-Calc.) (ft)
0	7280	7280	0				
1000	7400	7580	180	0.84			
2000	7440	7640	200	0.84	0.39	7640	0
3000	7500	7760	260	0.80	0.54	7823	63
4000	7540	7840	300	0.77	0.69	7940	100
5000	7590	7960	370	0.76	0.76	8036	76
6000	7660	8080	420	0.75	0.85	8123	43
7000	7720	8160	440	0.74	0.79	8208	48
8000	7760	8240	480	0.71	0.74	8292	52
9000	7840	8320	480	0.71	0.74	8369	49
10000	7900	8400	500	0.72	0.78	8445	45
11000	7960	8480	520	0.73	0.82	8518	38
12000	8060	8560	500	0.75	1.02	8588	28
13000	8160	8640	480	0.77	1.00	8660	20
14000	8360	8800	440	0.79	0.94	8734	-66
15000	8440	8880	440	0.79	1.00	8833	-47
16000	8520	8960	440	0.80		8926	-34
17000	8680			0.81		9015	
18000	8740			0.81		9123	
19000	8840			0.81		9217	
20000	9000			0.81		9313	
21000	9040			0.81		9428	
22000	9200			0.81		9521	
23000	9280			0.81		9633	
24000	10080			0.81			

[1]Calculated from Equation (2).
[2]Calculated from Equation (3) assuming τ_b = .80 bar.

APPENDIX G

DATA FOR EVERSON CREEK

Table 18. Everson Creek paleoglacier morphology and rheology interpreted from topographic maps and comparison with theoretical values.

Distance from Terminus (ft)	Bedrock Elevation (ft)	Ice Elevation (ft)	Ice Thickness (ft)	Shape Factor	Calc. τ_b[1] (bar)	Theoretical Ice Elevation[2] (ft)	Diff. (Theo.-Calc.) (ft)
0	7280	7280	0				
1000	7400	7440	40	0.87			
2000	7480	7640	160	0.87	0.60		
3000	7600	7760	160	0.87	0.60		
4000	7760	7920	160	0.86	0.48		
5000	7800	8080	280	0.73	0.72	8080	0
6000	7880	8160	280	0.73	0.66	8223	63
7000	7960	8280	320	0.73	0.69	8340	60
8000	8000	8400	400	0.72	0.93	8447	47
9000	8080	8520	440	0.72	0.90	8538	18
10000	8160	8640	480	0.72	0.94	8626	-14
11000	8230	8700	470	0.73	0.84	8712	12
12000	8320	8800	480	0.74	0.77	8794	-6
13000	8390	8880	490	0.76	0.87	8875	-5
14000	8490	8960	470	0.78	0.80	8952	-8
15000	8560			0.79		9032	
16000	8620			0.80		9109	
17000	8720			0.80		9183	
18000	8880			0.80		9262	
19000	8920			0.80		9357	
20000	8960			0.80		9440	
21000	9200			0.80		9516	
22000	9520			0.80		9631	
22500	9840			0.80			

[1]Calculated from Equation (2).
[2]Calculated from Equation (3) assuming τ_b = .80 bar.

APPENDIX H

DATA FOR MILL CREEK

Table 19. Mill Creek paleoglacier morphology and rheology interpreted from topographic maps and comparison with theoretical values.

Distance from Terminus (ft)	Bedrock Elevation (ft)	Ice Elevation (ft)	Ice Thickness (ft)	Shape Factor	Calc. τ_b[1] (bar)	Theoretical Ice Elevation[2] (ft)	Diff. (Theo.-Calc.) (ft)
0	7100	7100	0				
1000	7160	7280	120	0.80			
2000	7200	7460	260	0.74	0.54	7460	0
3000	7240	7600	360	0.74	0.75	7631	31
4000	7280	7680	400	0.74	0.73	7745	65
5000	7330	7760	430	0.74	0.78	7840	80
6000	7400	7800	400	0.76	0.64	7925	125
7000	7460	7900	440	0.77	0.64	8006	106
8000	7500	7920	420	0.78	0.62	8083	163
9000	7560	8000	440	0.79	0.66	8154	154
10000	7580	8080	500	0.78	0.79	8225	145
11000	7600	8160	560	0.76	0.84	8292	132
12000	7640	8240	600	0.74	0.96	8356	116
13000	7680	8320	640	0.73	1.01	8419	99
14000	7720	8400	680	0.72	1.06	8481	81
15000	7780	8480	700	0.71	1.01	8542	62
16000	7820	8560	740	0.70	1.05	8603	43
17000	7880	8640	760	0.70	1.05	8663	23
18000	7960	8720	760	0.70	1.01	8723	3
19000	8020	8760	740	0.71	1.00	8783	23
20000	8080	8840	760	0.72	1.04	8843	3
21000	8160	8900	740	0.73	1.03	8902	2
22000	8240	8960	720	0.73	1.00	8962	2
23000	8320	9040	720	0.73	1.07	9024	-16
24000	8400	9120	720	0.73	1.07	9088	-32
25000	8540	9200	660	0.74	1.02	9152	-48
26000	8680	9280	600	0.76	0.99	9222	-58
27000	8840	9360	520	0.79	0.89	9299	-61
28000	8920	9440	520	0.79	0.89	9389	-51
29000	9080			0.80		9476	
30000	9280			0.80		9580	
31000	9360			0.80		9717	
32000	9520			0.80		9832	
33000	9900			0.80		9964	
34000	10400			0.80			

[1]Calculated from Equation (2).
[2]Calculated from Equation (3) assuming τ_b = .90 bar.

APPENDIX I

DATA FOR MEADOW LAKE

Table 20. Meadow Lake paleoglacier morphology and rheology interpreted from topographic maps and comparison with theoretical values.

Distance from Terminus (ft)	Bedrock Elevation (ft)	Ice Elevation (ft)	Ice Thickness (ft)	Shape Factor	Calc. τ_b[1] (bar)	Theoretical Ice Elevation[2] (ft)	Diff. (Theo.-Calc.) (ft)
0	7509	7509					
1000	7520	7600	80	0.90			
2000	7580	7800	220	0.74	0.70	7800	0
3000	7720	7960	240	0.74	0.73	8002	42
4000	7840	8120	280	0.72	0.71	8164	44
5000	7920	8260	340	0.72	0.79	8305	45
6000	7960	8320	360	0.69	0.81	8429	109
7000	8040	8440	400	0.68	0.77	8532	92
8000	8120	8600	480	0.69	0.99	8629	29
9000	8200	8680	480	0.69	0.90	8722	42
10000	8320	8760	440	0.70	0.75	8812	52
11000	8380	8840	460	0.70	0.87	8907	67
12000	8480	8960	480	0.71	0.92	8995	35
13000	8600	9080	480	0.73	1.09	9082	2
14000	8720	9160	440	0.76	0.99	9172	12
15000	8880	9300	420	0.78	0.97	9265	-35
16000	8980	9400	420	0.79	1.08	9373	-27
17000	9100	9520	420	0.80	1.00	9477	-43
18000	9160			0.80		9586	
19000	9200			0.80		9682	
20000	9560			0.80		9767	
21000	9720			0.80		9966	
22000	10400			0.80			

[1]Calculated from Equation (2).
[2]Calculated from Equation (3) assuming τ_b = .90 bar.

APPENDIX J

DATA FOR MINER LAKES

Table 21. Miner Lakes paleoglacier morphology and rheology interpreted from topographic maps and comparison with theoretical values.

Distance from Terminus (ft)	Bedrock Elevation (ft)	Ice Elevation (ft)	Ice Thickness (ft)	Shape Factor	Calc. τ_b[1] (bar)	Theoretical Ice Elevation[2] (ft)	Diff. (Theo.-Calc.) (ft)
0	6800	6800	0				
1000	6900	7100	200	0.95			
2000	6920	7120	200	0.95	0.10		
3000	6930	7130	200	0.99	0.13		
4000	6940	7160	220	0.99	0.14		
5000	6955	7170	215	0.99	0.16		
6000	6965	7200	235	0.99	0.26		
7000	6955	7240	285	0.95	0.27		
8000	6955	7260	305	0.94	0.34		
9000	6955	7300	345	0.94	0.42		
10000	6955	7320	365	0.93	0.50		
11000	6960	7410	450	0.91	0.58		
12000	6965	7440	475	0.90	0.62		
13000	6965	7480	515	0.88	0.73		
14000	6970	7560	590	0.87	0.67	7560	0
15000	6970	7600	630	0.85	0.76	7618	18
16000	6970	7660	690	0.85	0.73	7671	11
17000	6990	7700	710	0.84	0.69	7720	20
18000	6990	7740	750	0.84	0.72	7767	27
19000	6990	7780	790	0.84	0.66	7811	31
20000	6990	7820	830	0.83	0.62	7854	34
21000	7000	7840	840	0.83	0.62	7894	54
22000	7040	7880	840	0.83	0.64	7933	53
23000	7040	7920	880	0.82	0.64	7973	53
24000	7060	7940	880	0.82	0.69	8011	71
25000	7080	7960	880	0.82	0.81	8048	88
26000	7080	8000	920	0.81	0.87	8085	85
27000	7100	8040	940	0.80	0.93	8121	81
28000	7120	8080	960	0.79	1.05	8157	77
29000	7130	8120	990	0.78	1.15	8193	73
30000	7140	8200	1060	0.76	1.26	8229	29
31000	7150	8260	1110	0.76	1.25	8264	4
32000	7200	8300	1100	0.76	1.25	8298	-2
33000	7260	8360	1100	0.76	1.09	8333	-27
34000	7380	8420	1040	0.76	1.05	8368	-52
35000	7520	8480	960	0.76	1.05	8407	-73
36000	7560	8520	960	0.76	1.01	8450	-70
37000	7600	8560	960	0.76	0.99	8493	-67
38000	7620			0.75		8536	
39000	7640			0.73		8579	
40000	7670			0.73		8621	
41000	7700	8760	1060	0.70		8665	-95

Table 21. (continued).

Distance from Terminus (ft)	Bedrock Elevation (ft)	Ice Elevation (ft)	Ice Thickness (ft)	Shape Factor	Calc. τ_b[1] (bar)	Theoretical Ice Elevation[2] (ft)	Diff. (Theo.-Calc.) (ft)
42000	7800	8840	1040	0.68		8709	-131
43000	7870	8880	1010	0.68	0.77	8756	-124
44000	7900	8920	1020	0.68	0.78	8804	-116
45000	7910	8960	1050	0.67	0.72	8852	-108
46000	7950	9020	1070	0.67		8898	-122
47000	7970			0.67		8944	
48000	8010			0.67		8988	
49000	8030			0.68		9032	
50000	8030	9100	1070	0.69		9074	
51000	8360			0.71		9113	
52000	9000			0.73		9166	
53000	9300			0.75		9401	
54000	10000			0.78			

[1]Calculated from Equation (2).
[2]Calculated from Equation (3) assuming τ_b = .80 bar.

MONTANA STATE UNIVERSITY LIBRARIES

3 1762 10108883 7